Fall October 7, 2016

Janecke and Markowski, 2013 (2016 revised) Revised SCEC Final report on the NEW East Shoreline strand of the San Andreas fault.pdf

Susanne U. Janecke
Daniel K. Markowski

Three parts: Original proposal (2011), provisional report (Janecke, 2013), and a final summary in the form of the MS thesis of Daniel Markowski (2016). The abstract herein is the abstract of Janecke's provisional report except that I updated the name of the fault to East Shoreline strand of the SAF. A different "Shoreline fault" is already in the Quaternary fault and fold database. See Markowski (2016) and Janecke et al. 2016 for additional updates.

Summary:

In 2013 Janecke submitted a provisional report to SCEC about our research along the newly identified East Shoreline strand of the San Andreas fault. That report is included here as part two. This revised report includes two additional items: Janecke's original proposal and the MS thesis of Daniel Markowski. These three items are enumerated in the Table of contents. The original proposal was written in 2011 and documents that Janecke discovered the East Shoreline fault zone prior to 2011.

Table of contents

Janecke's initial SCEC-2012 proposal: PART ONE

This proposal was written and submitted in 2011, and shows that the East Shoreline fault zone was Janecke's original discovery dating back to before 2011. Sahakian, Kell, Harding, Driscoll, and Kent claim otherwise (Sahakian et al., 2016, BSSA). The author can provide additional written documentation at your request.

The submitted provisional report from 2013. PART TWO

Testing a step-over model of the southern San Andreas fault at Durmid Hill. 8 p.

The MS thesis by Daniel Markowski: PART THREE

The MS thesis of Daniel Markowski was partly support by this SCEC grant, and we include it here in our final, revised report for SCEC grant. Janecke cowrote this work with Daniel Markowski.

Markowski, Daniel K., 2016, Confirmation of a New Geometric and Kinematic Model of the San Andreas Fault at Its Southern Tip, Durmid Hill, Southern California: MS thesis, Utah State University, 133 p. two plates. http://digitalcommons.usu.edu/etd/4987/

2012 SCEC Proposal
Testing a step-over model of the southern San Andreas fault at Durmid Hill
Susanne U. Janecke, Utah State University
$26,845 $26,845
Special Fault Study Areas
Start Date: February 1, 2012
SCEC science objectives: *4a, 4b, 4c*

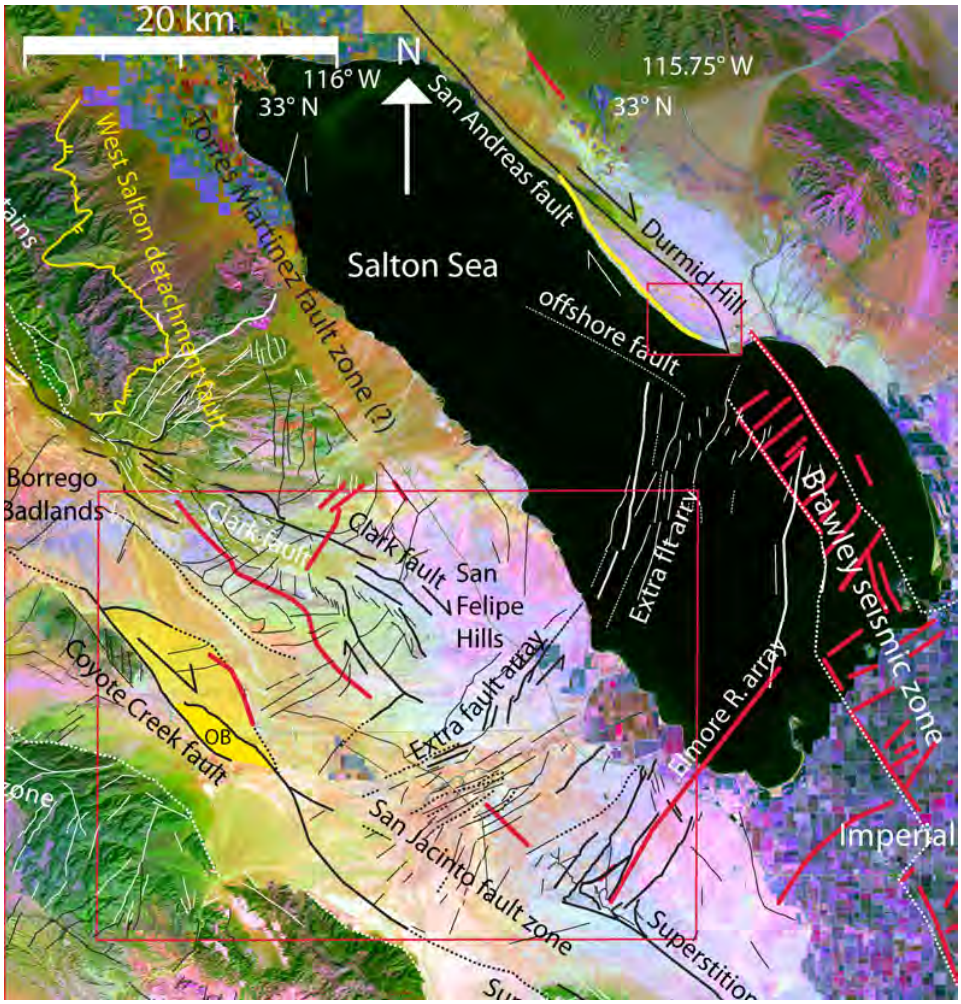

Figure 1. Simplified map of active strike-slip faults around the Salton Sea (modified from Janecke et al., 2010). Notice that NE to NNE-striking cross faults of the Extra-Elmore fault arrays are conspicuous and pervasive from the San Jacinto fault to the "offshore fault" in the NE. This proposal will investigate why there is no northeastward continuation of the Extra fault array in the Durmid Hill area. Durmid Hill may instead have formed as a left-stepping fault zone, like the greater Ocotillo Badlands along the Coyote Creek fault zone (in the SW corner of the map, the area OB in yellow as well as ~10 km north). Yellow=hypothesized SW strand of San Andreas fault, Red=selected aligned earthquakes from Haukkson et al., 2011 and Lin et al., 2007.

Written and submitted Nov 2011

Summary of Prior SCEC-funded research:

In 2010 and 2011 Janecke was awarded the SCEC grants to investigate the interaction of the Clark strand of the San Jacinto fault and the crossing left-lateral faults SE of its tip (Fig. 1). These are part of the Extra and Elmore Ranch fault arrays (Fig. 2). We hypothesized that the Clark fault does not terminate NW of the crossing fault arrays (e.g. as in Kirby et al., 2007), but instead continues at depth beneath the crossing faults, has a complex mutually interfering relationship at the surface or produces enough distributed strain to rotate the Extra fault array in a clockwise direction. Seven weeks of fieldwork and in depth analysis suggests that our hypotheses are correct. The Clark fault connects in the subsurface with the Superstition Hills fault and is expressed in aligned microseismicity directly along the projected trace of the largest strand of the Clark fault (Fig. 2), rotated left-lateral faults, and nascent dextral faults along strike (red faults within the yellow study area in Fig. 2). This work will be synthesized in the MS thesis of Steve Thornock. The first rounds of results were presented at the SCEC annual meeting and in our progress report (Janecke and Thornock, 2011; Janecke, 2011).

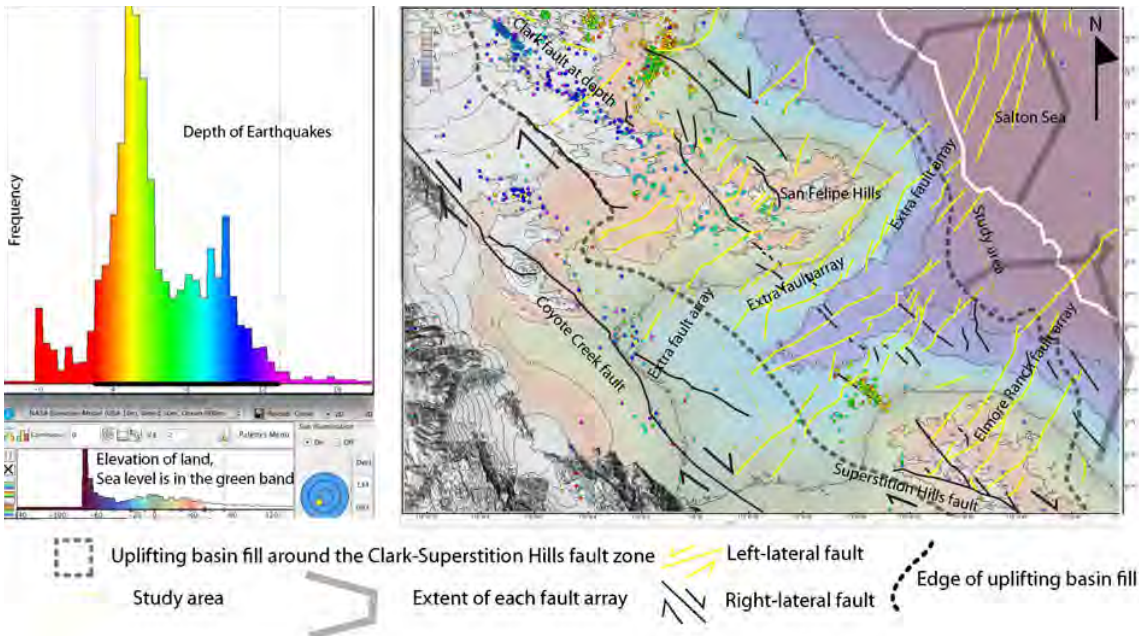

Fig. 2. Colored digital elevation model of strike-slip faults along with earthquakes since 2006 colored by their depth. NE-striking sinistral faults are yellow and NW-striking dextral fault of the San Jacinto fault zone are black. Notice the NW-trending uplift centered on the Clark-Superstition Hills fault. Faint yellow outline is the study area.

Updated Abstract: We mapped between the tip of the Clark fault and the Superstition Hills to assess the possible SE continuation of the Clark fault that appears in InSAR-based inversions. One field season, extensive mapping on imagery, landscape analysis, and correlation of mapped fault traces with of published InSAR, gravity and magnetic data suggest that NE-striking left-lateral faults dominate in the shallow crust whereas the nascent Clark fault persists under or through the crossing left-lateral network at deeper levels (Fig. 2). There is more evidence for active NE-striking left-lateral faults than of NW-striking dextral faults at the surface. NE-striking faults form a continuous, curving and dense array between the Coyote Creek fault zone and the Salton Sea and are in line with previously mapped faults beneath the Sea. Most ENE to NNE-striking faults are steep, preserve more horizontal slickenlines than dip-slip slickenlines due to left- and left-oblique

slip. These numerous fault zones, which include the Extra, Elmore Ranch, and Kane Spring faults, produce small domal uplifts along their traces, and cut Holocene sediment of Lake Cahuilla. The main strand of the Extra fault zone cuts Holocene lakebeds, generated colluvial wedges, but is lapped by ~900 yrs. BP sand dunes and 1-2 deep lake cycles of Lake Cahuilla. Only one of the 4 larger strands of the Clark fault in the San Felipe Hills continues SE as small-offset dextral faults (Fig. 2). This strand projects to similar small offset dextral faults in the Superstition Hills, with a possible gap near San Sebastian Marsh. An alignment of earthquakes along trend of this fault documents the 6-8 km depth range of the Clark fault under the Extra fault array (Fig. 2). Despite the limited expression of the Clark fault zone at the surface, there is strong evidence that it persists SE to the Superstition Hills fault in the subsurface because the Clark fault is axial to a major hourglass-shaped uplift of basin fill that stretches from the SE tip of the Santa Rosa Mountains to the New River, in Imperial Valley (see its dashed outline in Fig. 2.). Major strands of the San Jacinto fault zone form the "spine" of this uplift except in its narrow waist around San Sebastian Marsh where a blind fault is likely. The uplift is so large and active that it has trapped all the sediment of the San Felipe and Carrizo Wash drainage basins in the west, starving the delta on its NE side 3Fig. 2).

Technical description:

The only section of the San Andreas fault that has been locked for most of the historic period (Sieh, 1986; Sieh et al., 1989; Philibosian et al., 2011) is the southern San Andreas fault in Coachella Valley. As a result, this section pose a higher than normal seismic hazard in southern California and it has been the model earthquake for some recent Shakeout exercises (Porter, et al., 2011) and the shaking resulting from both northward and southward propagating ruptures along this section is well understood (Olsen, et al., 2006, 2008, 2009; Aagaard, 2008). Building on a kinematic model by Hudnut et al. (1989) with high resolution shallow seismic reflection data of active normal oblique-slip faults beneath the Salton Sea, Brothers et al. (2009 and 2011) proposed that slip on NNE-striking faults triggers slip on the southern San Andreas fault. The high slip rates implied by their analysis may imply an overdue condition along the southern San Andreas fault at Durmid Hill. It may also indicate that a northward propagating rupture along the San Andreas fault in Coachella valley is more likely than a bilateral or southward propagating rupture.

Durmid Hill is a subtle rise at the southern end of the San Andreas fault on the northeast shore of the Salton Sea. It is 15 km long, up to 5 km wide, and rises 80 m above the Sea. The SE tip of the San Andreas fault cuts through the hill along a central spine of higher topography and there are very good exposure of folded and faulted Pleistocene sediment throughout the Hill (Fig. 3). Nearshore Holocene beach sediments, which cover some of Durmid Hill, provide a marker of young activity in the area. The Brawley seismic zone is the plate boundary south of the San Andreas fault (Fig. 1). The only somewhat detailed geologic map of Durmid Hills is ~ 40 years old (Babcock, 1974), with some detailed structural maps in small areas (Bürgmann, 1991).

The San Andreas fault in this area creeps (Lyons and Sandwell, 2003; http://cires.colorado.edu/~bilham/creepmeter.file/DurmidCreepmeters.htm) and there is a major SW down step in the basement at the San Andreas fault in Durmid Hill (Babcock, 1974). This vertical offset agrees with the topographic contrasts across the faults and suggest that there is a vertical component of slip in addition to the dominant strike-slip component.

Durmid Hill is famous for its impressive Quaternary contraction, transpression, and rapid uplift since the latest Pleistocene (~1-4 mm/yr), deformation of the 0.75 Ma Bishop tuff into isoclinal folds, boudins and thrust slices, and beveling by Lake Cahuilla (Fig. 3; Sylvester et al., 1988; Bilham and Williams, 1985; Babcock, 1974; Bürgmann, 1991; Wojtal et al., 2007). The deformation is equally intense in the Pliocene-Pleistocene Borrego Formation as the overlying Pleistocene Brawley Formation and shortening began in the latest Pleistocene (Bilham and Williams, 1985).

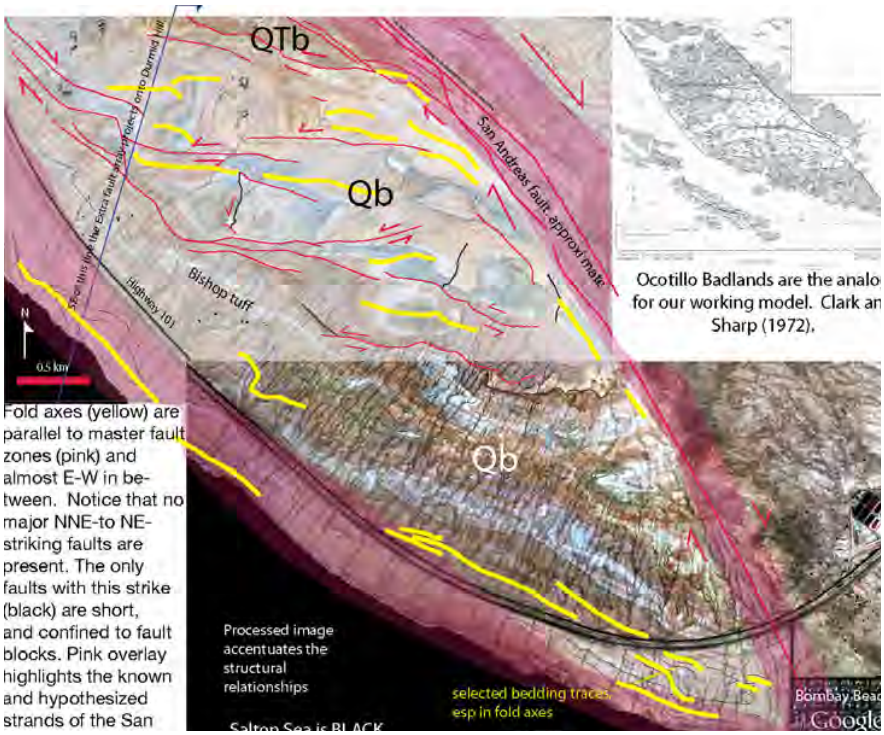

Figure 3. Preliminary map of southern part of Durmid Hill. Mapping was compiled in Google Earth imagery from July 22, 2005 due to their superior color, resolution and contrast. Janecke hypothesizes that there is a major strand of the San Andreas fault between the Sea and Hwy 111 (pink zone) that is currently less active than the NE strand, and may have blind sections. The central part of the field area shows numerous E-striking left-lateral faults (red) and folds (yellow), few NE-striking faults (black), and the main strand of the San Andreas fault zone in the NE (pink). Fieldwork will assess the lateral continuity of dextral faults in the SW fault zone (which were omitted here for clarity). Qb, Brawley Formation, QTb, Borrego Formation. Selected **black** bedding traces in the SW define the NW structural grain near the shoreline. There is no evidence for the Extra fault array in Durmid Hill.

One popular model of the contraction is that it is the result of slight counterclockwise rotation of the strike of the San Andreas fault in Durmid Hill relative to the plate-motion (Bilham and Williams, 1985). The contraction is the result of transpression in the damage zone of the San Andreas fault and some of this strain rotated folds axes clockwise about vertical axes (Bürgmann, 1991). All existing geometric models predict that the intensity of folding and rotation of fold axes would decrease away from the San Andreas fault and that there should be one consistent or gradually changing orientation of fold axes. Instead, the original mapping by Babcock (1974), Bürgmann (1991) and Janecke (unpublished) show a sigmoidal pattern of folding and faulting (Fig. 3). There is a tremendous amount of NE-SW shortening in the narrow strip of land between Highway 111 and the Salton Sea where folds verge SW (Babcock, 1974)(Fig. 3). From west to east, faults and folded parallel the shore of the Salton Sea (N40°W), trend E-W for about 1.5 to 2.5 km, and then bending back to the N45°W trend near the San Andreas fault in each of three structural domains. No existing model explains this pattern.

In stark contrast to this the field evidence for persistent transpression, consideration of cross faults beneath and SW of the Salton Sea predicts important normal faults or left-lateral strike-slip faults in Durmid Hill (Hudnut et al., 1989; Brothers et al., 2009, 2011). These two models further predict that release of fault-normal stresses by slip on cross faults initiated large earthquakes on the San Andreas fault at Durmid Hill in the past and is likely to recur in the future. The significant distance between the San Andreas fault and the newly imaged offshore strands of the Extra fault zone (Fig. 1; 6.5 to 8 km, Brothers et al., 2009, 2011) raise doubts about the these models and

suggest that there may be a buffer to coordinated, triggered, or simultaneous slip events on the Extra fault array and San Andreas fault.

Nevertheless, these cross-fault models spawned exciting analyses of ground shaking as a function of rupture directivity (Olsen et al., 2006, 2008, 2009; Aagaard, 2008) and contributed to the selection of an M 7.9 earthquake at Durmid Hill as the model earthquake for the ShakeOut Exercise in 2008 (Porter et al., 2011; Jones et al., 2008). Because a northward propagating rupture scenario was shown to be particularly destructive in the Los Angeles basin area (Olsen et al., 2006, 2008, 2009) we propose to investigate the past behavior of the southernmost San Andreas fault at Durmid Hill to test whether there is evidence for nucleation and northward rupture of prior large earthquakes along the San Andreas fault in accord with the trigger models.

Our field tests of these incompatible models will take a fresh detailed look at the structural geology of Durmid Hill and searching for evidence of the NNE to NE-striking cross faults predicted by the two cross-fault models. Our fieldwork will simultaneously test a third model: Janecke's hypothesis that the southern San Andreas fault is a breached left-stepping pair of dextral faults at Durmid Hill. It is currently impossible to accurately assess the likelihood of large earthquakes nucleating at Durmid Hill because there is no geometric model that successfully explains all the structures of the area.

Working hypothesis: We will test a geometric and kinematic model that is based on the well characterized left-step in the Coyote Creek fault in the greater Ocotillo Badlands area (Figs. 1 and 3, upper right; Sharp and Clark, 1972; Brown et al., 1991; Steely, 2006). This step-over provides an excellent match to the structural relationships in Durmid Hill and presents many testable predictions, with the modification of a breached NE edge. If the breached step-over model is correct, the San Andreas fault has two important strands: the well known one near the crest of Durmid Hill and another cryptic one near or under the Salton Sea. The latter fault may have localized the shoreline of the Salton Sea on its lower SW side if it has the same vertical component of slip as the main strand of the San Andreas fault. This strand should be easy to validate in the field as long as it is not underwater. An InSAR interferogram that captured creep on the main NE strand of the San Andreas fault strand (Lyons and Sandwell, 2003) is suggestive of creep on a ~2 km long piece of the SW strand west of Bombay Beach.

Tests and Questions: The field test proposed here will assess the relative presence, frequency, importance, and implications of NNE-striking steep faults of the Extra fault array in Durmid Hill, the existence and character of dextral faults near the shoreline of the Salton Sea, and the origin and activity of the contractional structures in Durmid Hill. Questions to be addressed in our field studies: 1) Does the geology of the southern tip of the San Andreas fault at Durmid Hill reflect branch points between the San Andreas fault and normal to left-oblique-slip faults of the Extra fault array-as predicted by several recent models? 2) Does the geology of the southern tip of the San Andreas fault reflect more indirect influence of offshore normal or oblique-slip faulting? 3) Does the southern San Andreas fault zone have an unrecognized major strand roughly 2 km to the southwest of the main central strand? 4) If so, is this strand active or inactive, or less active than the main strand? 5) Is there evidence for Holocene slip on this fault zone? Did the ~10 km of the San Andreas fault SE of Salt Creek formed after the more northerly striking parts, as predicted by the breached step-over model? 6) Does the geometry of Durmid Hill produce increasing fault-normal stress by contraction or decreased fault-normal stress from normal faults or strike-slip faults under the Salton Sea? 7) Does the gravity data in Durmid Hill reflect a strand along the shoreline? Janecke's ongoing collaboration with Vicki Langenheim will be critical in answering this question.

Methods: The main data set for our research will be structural analysis based on new field mapping on high-resolution enhanced false-color aerial photographs. The imagery is available for free in Google Earth (Fig. 3) and Janecke's research group just purchased a field-hardened

Toughbook computer in order to access and map directly on these images in the field. A GPS location program built into the computer will help us to locate ourselves within the nearly featureless landscape of Durmid Hill. We will map on images from July 22, 2005 and Jan 12, 2006 because these show the entire field area in incredible detail and particularly vivid color (Fig. 3). Calibration of the range of colors on the image with rock suggests that sands with different provenance, grain size, marl and mudstone produce the range of colors on the aerial photograph. These distinctive lithologies are exceptional marker for assessing the strain in the damage zone of the San Andreas fault at Durmid Hill. Janecke has already processed the highest resolution Landsat (15 m) data sets to highlight the lithologic units. The Pleistocene Bishop ash provides another key marker unit in this area is clearly visible in all imagery and in the field (Fig. 3) and will be used to subdivide the Brawley Formation into mappable subunits for more detailed analysis (Babcock, 1974; Bürgmann, 1991; Wojtal, 2007).

Schedule: Introductory analysis, image analysis and mapping on Google Earth and digital elevation models are underway. A new graduate student entering our program in fall of 2012 will prepare for the research by learning about transpression and transrotation, fault networks, so that field work can begin in the winter of 2013. That effort will produce the bulk of the new field measurements and mapping. Modeling during the following spring, summer and fall will reveal the main structural features of the area and show whether loading or unloading by faults beneath the Salton Sea has been important in this study area. A second field season in the winter of 2014 will be needed for a final field test of the resulting geometric and kinematic models.

Work plan and methods: A new incoming graduate student will map the field area using a combination of methods. Janecke will train the student and map those areas that are too complex for the graduate student, or are outside of the area she/he can reach in a reasonable field season. Image analysis, followed by fieldwork and then more image analysis in an interactive sequence is the best way to map such a complex area. One key task will be to locate any NE-striking faults in the area that may be part of the Extra fault array. The extreme SE tip of Durmid Hill appears to be the only area where such faults may be located and we plan a focused effort there. Products include: 1) A geologic and structural map of Durmid Hill SW of the San Andreas fault and NE of the Salton Sea; 2) A structural domain map; 3) Kinematic data showing the slip directions and sense of slip across the faults in the damage zone of the San Andreas fault, 4) An activity map highlighting structures with Holocene and Latest Pleistocene deformation. We will apply for NCALM LiDAR data to further constrain the off-fault areas adjacent to the main San Andreas fault, with the shoreline area as our first priority. Offset streams, ridges, and deflected drainages near the shore of the Salton Sea are very suggestive of Holocene slip on the hypothesized fault zone there.

Implications and future work: The hypothesized SW strand of the SAF at Durmid Hill fault may buffers the main NE strand of the San Andreas fault from cross faults and stress changes originating under the Salton Sea while also resisting the initiation of large ruptures there. The Extra fault array may terminate at the SW strand of the San Andreas fault and/or at an enigmatic NW-striking fault farther offshore (see fig. 1 and Brothers et al., 2009, 2011). Field tests are critical because the component of contraction across the main strand of the San Andreas fault implied by the step-over model makes the Durmid Hill area an unlikely nucleation point for future large ruptures. If the first year of fieldwork in Durmid Hill is promising we anticipate the need for trenching, detailed gravity and magnetic surveys, InSAR, GPS inversions, rupture modeling, and much more. **A WORKSHOP TO TALK ABOUT COLLABORATIVE RESEARCH STRATEGIES IS BEING DISCUSSED. IT WILL PROBABLY BE PROPOSED AND CONVENED WITHIN THE NEXT YEAR.**

References:

Aagaard, B., 2008. Southern California ShakeOut Scenario Ground Motion Animations, http://earthquake.usgs.gov/regional/nca/simulations/shakeout/, accessed 31 October 2011.

Babcock, E.A., 1974, Geology of the northeast margin of the Salton Trough, Salton Sea, California, Geol. Soc. Am. Bull., 85, 321-332, 1974.

Bilham, R., and P. Williams, 1985, Sawtooth segmentation and deformation processes on the southern San Andreas Fault, California, Geophys. Res. Lett., 12(9), 557-560.

Brothers, D.S., N. W. Driscoll, G. M. Kent, A. J. Harding, J. M. Babcock & R. L. Baskin, 2009, Tectonic evolution of the Salton Sea inferred from seismic reflection data. Nature Geoscience, 2, 581-584.

Brothers, D., D. Kilb, K. Luttrell, N. Driscoll and G. Kent, Loading of the San Andreas fault by flood-induced ruptures beneath the Salton Sea, Nature Geosciences, pp. 1-7, NGEO1184, DOI:10.1038, 2011

Brown, N. N.; Fuller, M. D.; and Sibson, R. H. 1991, Paleomagnetism of the Ocotillo Badlands, southern California, and implications for slip transfer throughan antidilational fault jog. Earth Planet. Sci. Lett. 102:277–288.

Bürgmann, R., 1991,Transpression along the Southern San Andreas fault, Durmid Hill, California. Tectonics, 10, pp. 1152–1163.

Dibblee, T. W., Jr., 1954, Geology of the Imperial Valley region, California, in Jahns, R. H., ed., Geology of southern California: California Division of Mines Bulletin 170, p. 21-28.

Hauksson E., W. Yang and P.M. Shearer, Waveform relocated earthquake catalog for southern California (1981 - 2011), manuscript in preparation, 2011.

Hudnut, K., Seeber, L., Rockwell, T., Goodmacher, J., Klinger, R., Lindvall, S., and McElwain, R., 1989, Surface ruptures on cross-faults in the 24 November 1987 Superstition Hills, California, earthquake sequence: Bulletin of the Seismological Society of America, v. 79, p. 282–296.

Janecke S.U., Dorsey, R.J., Forand, D., Steely, A.N., (Kirby et al., 2007), S.M., Lutz, A.T., Housen B.A., Belgarde, B., Langenhim, V.E., Rittenour, T.M., 2010, High Geologic Slip Rates since Early Pleistocene Initiation of the San Jacinto and San Felipe Fault Zones in the San Andreas Fault System: Southern California, USA: Geological Society of America Special Paper 475, 48 p., doi:10.1130/2010.2475.

Janecke, S.U., 2011, Progress report: Digital mapping of active interpenetrating faults within the San Jacinto fault zone, southern California: SCEC annual report. http://sceccore.usc.edu/proposalfiles/2010reports/Janecke_10134_report.pdf

Janecke, S.U., and Thornock, S.J., 2011, Interactions between the Clark strand of the San Jacinto fault zone and the Extra-Elmore fault arrays: 2011 SCEC Annual Meeting poster A-149.

Jones, L. M., Bernknopf, R., Cox, D., Goltz, J., Hudnut, K., Mileti, D., Perry, S., Ponti, D., Porter, K., Reichle, M., Seligson, H., Shoaf, K., Treiman, J., and Wein, A., 2008. The ShakeOut Scenario: USGS Open File Report 2008-1150 and California Geological Survey Preliminary Report 25, http://pubs.usgs.gov/of2008/1150 and http://conservation.ca.gov/cgs, Sacramento, CA.

Kirby, S.M., Janecke, S.U., Dorsey, R.J., Housen, B.A., McDougall, K., Langenheim, V., and Steely, A., 2007, Pleistocene Brawley and Ocotillo formations: Evidence for initial strike-slip deformation along the San Felipe and San Jacinto fault zones, California: The Journal of Geology, v. 115, p. 43–62, doi: 10.1086/509248.

Lin, G., Shearer, P.M., and Hauksson, E., 2007, Applying a three-dimensional velocity model, waveform cross correlation, and cluster analysis to locate southern California seismicity

from 1981 to 2005: Journal of Geophysical Research, v. 112, B12309, doi: 10.1029/2007JB004986.
Lyons, S. and D. Sandwell, 2003, Fault creep along the southern San Andreas from InSAR, permanent scatterers, and stacking, J. Geophys. Res . ,108 (B1), 2047, doi:10.1029/ 2002JB001831, 2003.
Olsen, K. B., Day, S. M., Dalguer, L., Mayhew, J., Cui, Y., Zhu, H., Cruz-Atienza, V. M., Roten, D., Maechling, P., Jordan, T. H., and Chourasia, A., 2009. ShakeOut-D: Ground motion estimates using an ensemble of large earthquakes on the southern San Andreas fault with spontaneous rupture propagation, Geophys. Res. Lett. 36, L04303
Olsen, K. B., Day, S. M., Minster, J. B., Cui, Y., Chourasia, A., Faerman, N., Moore, R., Maechling, P., and Jordan, T., 2006. Strong shaking in Los Angeles expected from southern San Andreas earthquake, Geophys. Res. Lett. 33, L07305.
Olsen, K. B., Day, S. M., Minster, J. B., Cui, Y., Chourasia, A., Okaya, D., Maechling, P., and Jordan T, 2008. TeraShake2: Spontaneous rupture simulations of Mw7.7 earthquakes on the southern San Andreas fault, Bull. Seism. Soc. Am. 98, 1162–1185.
Philibosian, B., T. E. Fumal, R. J. Weldon, K. J. Kendrick, K. M. Scharer, S. P. Bemis, R. J. Burgette, and B. A. Wisely (2009). Photomosaics and logs of trenches on the San Andreas Fault near Coachella, California, in U.S. Geol. Surv. Open-File Rept. 2009-1039.
Porter, K., Jones, L., Cox, D., Goltz, J., Hudnut, K., Perry, S., Ponti, D., Reichle, M., Rose, A.,Scawthorn, C., Seligson, H., Shoaf, K., Treiman, J., and Wein, A., 2011. The ShakeOut Scenario: A hypothetical Mw 7.8 earthquake on the southern San Andreas Fault, Earthquake Spectra 27, 239–261.
Sieh, K., 1986. Slip rate across the San Andreas fault and prehistoric earthquakes at Indio, California, Eos, Transactions, American Geophysical Union 67, 1200.
Sieh, K., Stuiver M., and Brillinger, D., 1989. A more precise chronology of earthquakes produced by the San Andreas Fault in southern California. Journal of Geophysical Research -Solid Earth 94, 603–623.
Sharp, R. V., and Clark, M.M., 1972, Geologic evidence of previous faulting neat the 1968 rupture of the coyote Creek fault: U. S. Geological Survey Professional Paper 787, pp. 131-140.
Steely, A.N., 2006, The evolution from late Miocene West Salton detachment faulting to cross-cutting oblique strike-slip faults in the southwest Salton Trough, California [M.S thesis]: Utah State University, 253 p., 3 plates, scale 1:24,000.
Sylvester, A. G., 1988, Strike-slip faults: Geological Society of America Bulletin, v. 100, p. 1666–1703.
Sylvester, A., R. Bilham, M. Jackson, and S. Barrientos (1993), Aseismic Growth of Durmid Hill, Southeasternmost San Andreas Fault, California, J. Geophys. Res., 98(B8), 14233-14243.
Wojtal, S.F., 2007, Assessing the long-term displacement field associated with deformation of the borderlands of the San Andreas fault, Durmid Hill, CA: GSA Annual Meeting Abstracts with program, Paper No. 138-11.

Final Report for 2012 SCEC Grant to Susanne Ursula Janecke

2012 SCEC Proposal

Testing a step-over model of the southern San Andreas fault at Durmid Hill

Susanne U. Janecke, Utah State University

$20,000

Special Fault Study Areas

Start Date: Nov. 30 1, 2012

SCEC science objectives: ***4a, 4b, 4c***

Main findings:

1. The southernmost San Andreas fault is experiencing contraction and strike slip strains and is therefore unlikely to be a future nucleation point for the next "BIG ONE".

2. The southern San Andreas fault has an additional, active strand that is near the shoreline of the Salton Sea. The San Andreas fault zone is thus at least 3 km wide in this area.

3. This **EAST** SHORELINE strand of the San Andreas fault was active in the Holocene, and may be continuous with an ~30 km-long northwest-striking deformation boundary detected in many INSAR datasets in the urban centers of Palm Springs, Palm Desert, Cathedral City, Rancho Mirage, and La Quinta (Martin, 2011; Tong et al., 2011).

4. There is little evidence for interactions with the NNE-striking left-oblique Extra fault zone on the northeast shore of the Salton Sea.

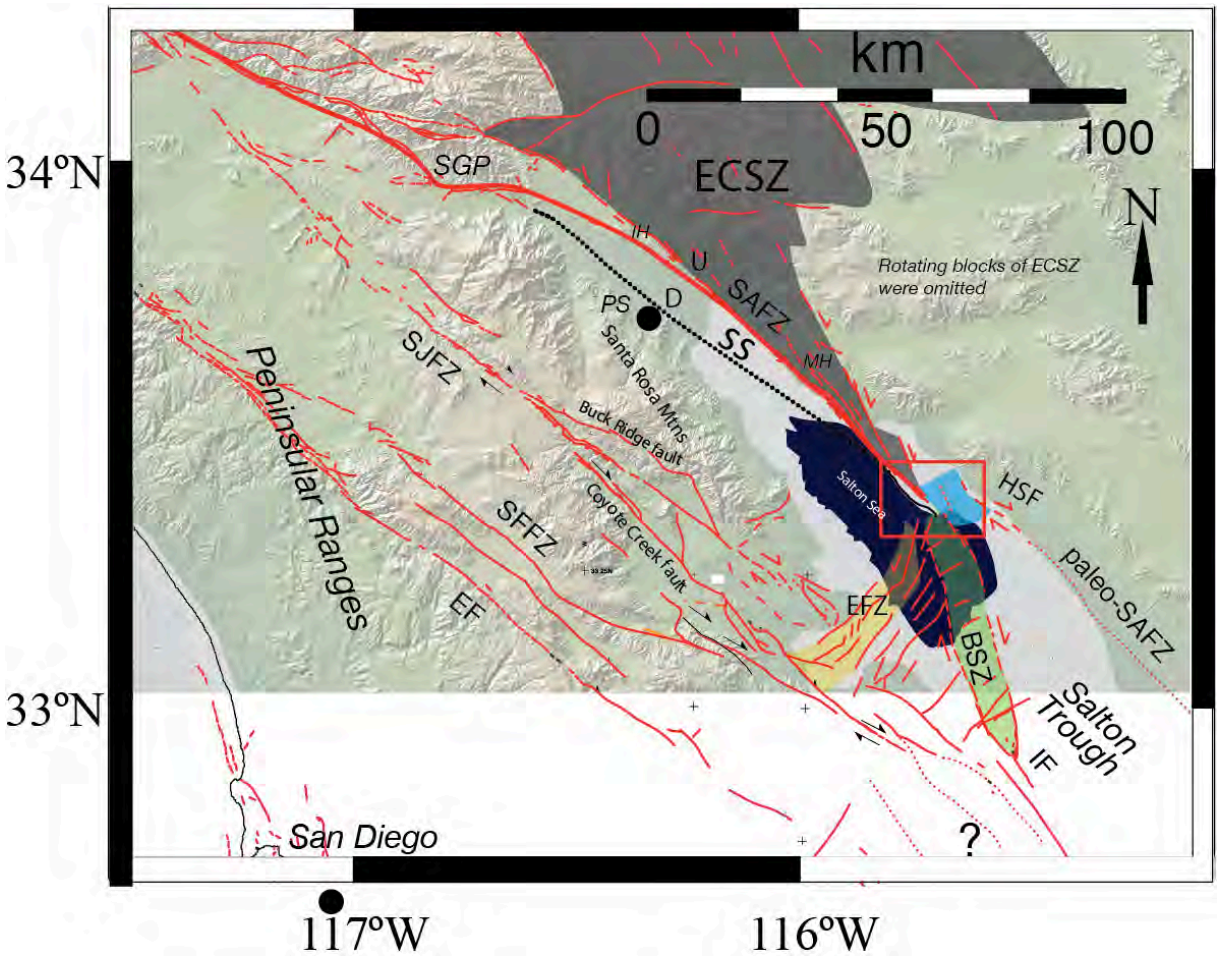

Figure 1. Structure map showing the 6 major fault zones or fault arrays that intersect on the northeast shore of the Salton Sea at Durmid Hill. Clockwise these are: 1) the southern San Andreas fault zone (red), 2) the Eastern California Shear zone (grey), 3) an extensional stepover to the Hot Springs fault (light blue), 4) the Brawley seismic zone (BSZ), 5) the Extra fault array (yellow), and (6) the Shoreline strand of the San Andreas fault zone (SS). All are active at different rates. We propose to 1) characterize this knot of active deformation and 2) produce the first detailed analysis of the damage zone of the southern San Andreas fault zone.

Technical description:

The only section of the San Andreas fault (SAF; Figs. 1 and 2) that has been locked for most of the historic period is the southern SAF in Coachella Valley (Sieh, 1986; Sieh et al., 1989; Philibosian et al., 2011). As a result, this section poses a higher than normal seismic hazard in California and it has been the model earthquake for recent ShakeOut Exercises (Jones et al., 2008; Porter, et al., 2011). The shaking resulting from propagating ruptures along this section is potentially catastrophic if a large earthquake nucleates near the Salton Sea (Olsen et al., 2006, 2008, 2009; Aagaard, 2008). Analyses of ground shaking as a function of rupture directivity (Olsen et al., 2006, 2008, 2009; Aagaard, 2008) contributed to the selection of a M 7.9 earthquake at Durmid Hill as the model earthquake for the ShakeOut Exercise in 2008 (Jones et al., 2008; Porter et al., 2011). The clear seismic hazard associated with and emanating from this section of the SAF necessitates integration of field mapping, structural data, and available geophysical and geo-imaging data to better understand of the interplay of the fault systems near the Salton Sea.

Building on a kinematic model of Hudnut et al. (1989)**,** Brothers et al. (2009 and 2011) interpreted high resolution reflection seismic evidence for cross faults under the Salton Sea and proposed that slip on these NNE-striking normal faults triggers slip on the southern SAF (Fig. 2). Their analysis implies an overdue condition along the southern SAF at Durmid Hill. It may also indicate that a northward propagating rupture along the SAF in Coachella Valley is more likely than a bilateral or southward propagating rupture.

Results:

Phase I of our integrated field and structural project tested the sawtooth (Bilham and Williams, 1985), cross-fault (Hudnut et al. 1989; Brothers et al., 2009, 2011), and contractional-stepover models of the southern tip of the SAF (Janecke, 2012 SCEC proposal). The stepover model is the only model that successfully explains the complex sigmoidal geometry of contractional strains in the Durmid Hill area and the Holocene faulting and folding along the northeast shore of the Salton Sea (Fig. 3). The focus of the next phase of our proposed research will shift to the SAF itself, in order to capitalize on exciting discoveries of phase one.

Mapping and structural analysis by Utah State University MS student Daniel Markowski and Janecke at Durmid Hill confirmed our working hypothesis of the presence of a contractional stepover between the main SAF and an active but previously unmapped dextral fault zone near the northeast shore of the Salton Sea (Janecke, 2012 SCEC proposal; Janecke and Markowski, 2013). We focused on the southwest side of the main strand of the SAF and the deformation near the shore of the Salton Sea (Fig. 3). We enumerate key results below:

Abundant evidence exists for a second active dextral strand of the San Andreas fault system ~3 km SW of the main trace of the SAF (Fig. 3). The central part of this newly identified Shoreline fault strand of the San Andreas fault system is probably offshore under the Salton Sea. It parallels the edge of the Salton Sea and likely produced a small step in the landscape along which the shoreline is localized.

Onshore deposits on the NE side of the Salton Sea provide field evidence for a wide and expansive damage zone of the Shoreline fault strand. Exposures include a 0.5-1.5 km wide band of highly deformed late Pleistocene Brawley and Ocotillo formations and unconformably overlying Holocene sediment striking NW, parallel to the fault zone. One major fault zone cuts Holocene sediment containing pumice clasts and is therefore likely to be a few thousand years old or younger (Schmitt et al. 2013a and b). Folded and faulted angular unconformities in the damage zone record active deformation during deposition of late Pleistocene to Holocene sediment.

Open to tight folds in the Brawley and Ocotillo Formations within the damage zone of the Shoreline and SAF zones have fold axes parallel to the fault zone and the shore (Babcock, 1974; Burgmann, 1991; Phase I of this research). These axes trend 30-50° clockwise of fold axes that lie between the two damage zones within the contractional stepover in the Durmid Hill area. Field tests detected few NE to NNE-striking sinistral faults in the Durmid Hill area (Fig. 3). Thus, the cross-fault models of Hudnut et al. (1989) and Brother et al. (2009, 2011) are unlikely to apply to the southern tip of the SAF. Contractional strains across the two strands of the SAF in the Durmid Hill area likely inhibit the nucleation of large ruptures there. Dan Markowski will explore the implications of the Shoreline strand of the SAF in his MS thesis and his defense is scheduled for the summer of 2014.

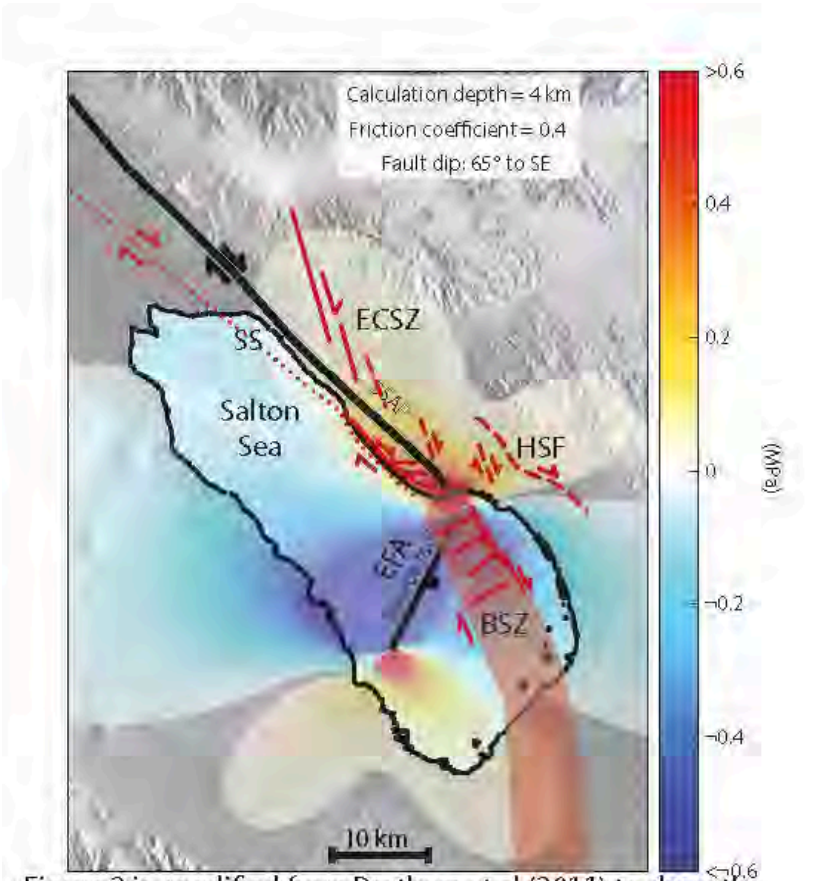

Figure 2 is modified from Brothers et al (2011) to show the many tectonic elements (red) in the Salton Sea area that must be considered to produce a meaningful understanding of the stresses acting on the southern tip of the San Andreas fault. Brothers et al. (2011) only considered the two faults (in black) in their analysis. EFA=Extra fault array and SSAF=Southern San Andreas fault. Phase one of our SCEC-funded research shows that 4 additional deforming zones, the Shoreline strand (SS) of the San Andreas fault, the Eastern California shear zone (ECSZ), the Brawley seismic zone (BSZ) and the Hot Springs strand of the paleo-SAF (HSF) all deform Holocene sediment and impact the stress on the southern SSAF at this "knot". The likelihood of the knot intiating or arresting a major rupture will be evaluated.

Some aspects of the "contractional-stepover model" of Janecke (SCEC proposal 2012) were incorrect or incomplete and will be investigated in Phase II of this work:

Instead of branching from the SAF north of Salt Creek, as predicted, the Shoreline fault diverges from the main SAF to the NW, and disappears northward beneath the Salton Sea. From that point, it may parallel the main trace of the SAF and lie a few kilometers SW of the main SAF in Coachella Valley. It is likely to correlate with fault strands detected geophysically by Fuis et al. (2013) and Langenheim et al. (2013) ~2.5 km SW of the SAF in the Mecca Hills. The fault might continue northward parallel to the SAF.

Our preferred interpretation, however, is that north of Mecca Hills, the ~10-15 km long Shoreline strand of the SAF strikes obliquely across the northern Coachella Valley with a N57°W strike and is the same structure as the 45 km long unnamed fault of Smeed and Brandt (2007), Tong et al., (2013), Wisely (2013), and Martin (2011) under Palm Desert, Rancho Mirage, Cathedral City, and Palm Springs along the front of the San Jacinto Mountains (Janecke and Markowski, 2013). InSAR subsidence patterns, barriers to groundwater flow, direct measurement of subsidence, and gravity data all document the unnamed fault under Palm Desert. The unnamed fault and the Shoreline fault strike toward each other across ~30 km of the valley floor in latest Holocene lakebeds, sand dunes, and fields.

Research Opportunity number one: Our prior work reveals that many structures with evidence for Holocene activity converge at the southern tip of the SAF (Fig. 2). We conclude that the contractional stepover model, like the cross-fault and sawtooth models that it replaces, are too simple to fully characterize stress and hazards in Coachella Valley. The southern San Andreas fault is not just a contractional stepover, but it is also the branch point between the SAF, the Extra fault array, the Brawley seismic zone, the southern tip of the dextral faults of the Eastern California shear zone (we exclude the rotating blocks for simplicity),

and an extensional, 6-9 km left-step between the main San Andreas fault and the Hot Springs fault (Figs 1-3).The Hot Springs fault is a low-slip-rate structure within the paleo-San Andreas system. Convergence of these **six major structural elements** is probably not a coincidence and suggests that this part of the plate boundary has been an important structural knot for millions of years. If our working concept is correct, the complexity may exceed that of the San Gorgonio Pass area. Figures 1 and 2 illustrate a greatly simplified possible plan-view interpretation of the complexity of this area. The level and nature of the new work that is required to resolve these new research questions is beyond the scope of Markowski's study.

Observations east of the study area

Reconnaissance field studies east of our main study area show that there is an unparalleled opportunity to characterize the damage zones of at least a dozen well-exposed faults in several different rock types, across a range of displacements. Every fault in the Durmid area has an obvious damage zone, from the smallest displacement to the largest displacements. Damage zone are extremely well displayed in map view across 5-10 square km. The inner damage zone of the SAF is generally >200 m wide and up to 500 m wide and consistently on the SW side of the principal slip surface. This asymmetry may record rupture directivity or some other process.

Gullies provide access to the cross sectional view on a regular basis. The SAF, Shoreline fault, and cross faults in the Durmid Hill area all have damage zones that are up to many hundreds of meters wide, exhibit a complex mixture of ductile and brittle deformation, "host" or "entrained" unusually large amounts of gypsum, and change along strike as the rheology of the host rock changes. Figure 3B shows our first reconnaissance map of the damage southwest of the SAF from imagery. Principal slip surfaces appear to be lacking in several fault zones and the deformation is distributed across some of the damage zones is a fairly even manner. Field studies have been limited because our funding was for a study of interacting fault zone, not for characterization of damage zones.

Janecke discovered that the 125-500 m wide damage zone of the main trace of the San Andreas fault is overlapped by the Brawley Formation about 3 km north of the Salton Sea (Janecke and Markowski, 2013). A newer cryptic strand must have formed somewhat farther east of its poorly mapped trace (Clark, 1972; Janecke and Markowski, 2013). We have narrowed down the new location of the San Andreas fault to lie within the green triangle in figure 3. The nearly flat geometry of the Quaternary sediment there makes locating structures more challenging BUT provides an opportunity to compare a mature damage zone with a nascent one along the same major fault zone, at the same structural level, in the same lithologies. Locating, mapping, and characterizing this brand new part of the San Andreas fault will be another core task of our second phase of research in the Durmid Hill area. This research will address goal 4c of the RFP: "***To provide*** Improvements to the CFM using better mapping, including LIDAR, and precise earthquake relocations."

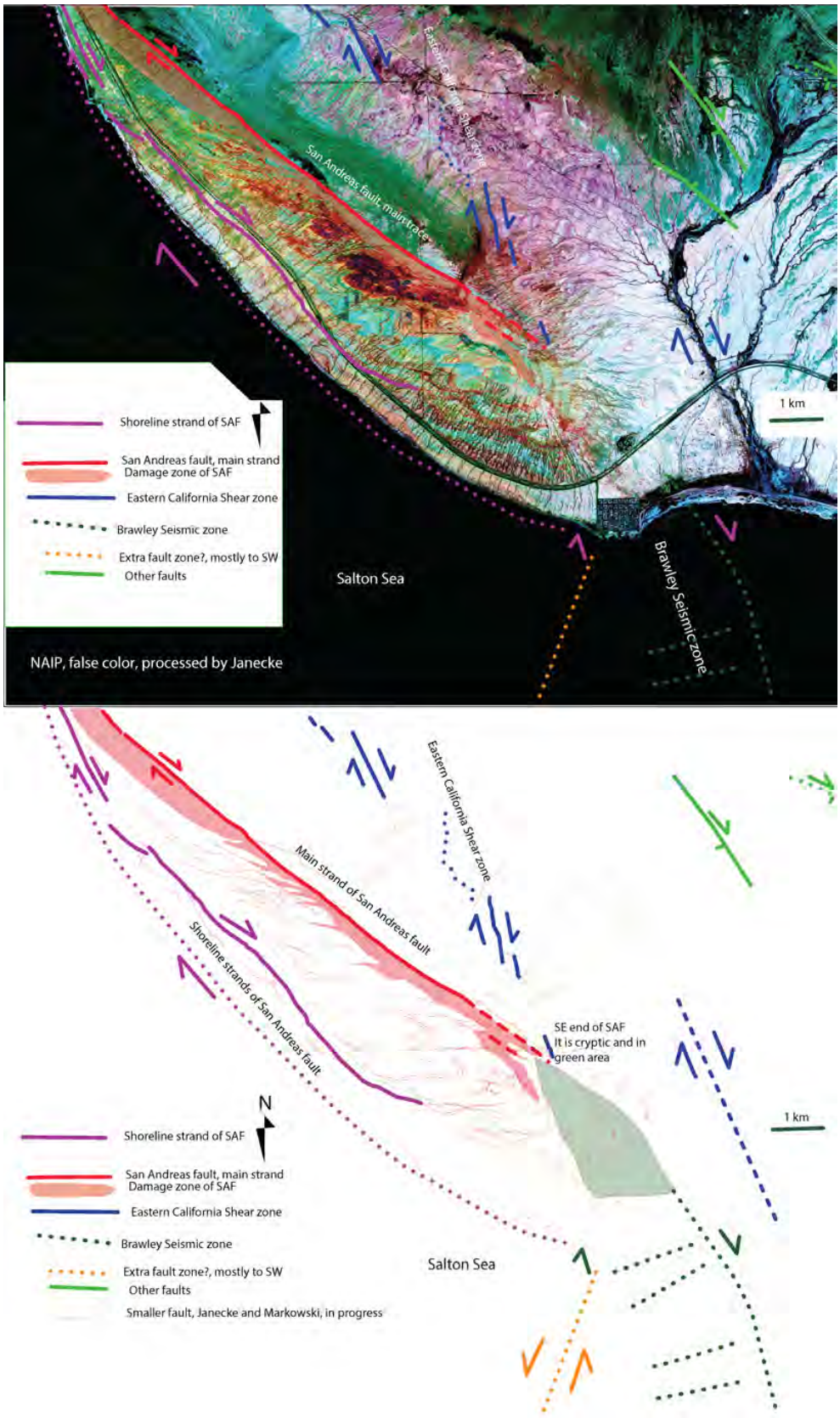

Figure 3 Geologic and structural map of Durmid Hill on a basemap of processed false-color NAIP aerial orthophotography. Related structures are coded with the same color. En echelon faults of the Eastern California Shear zone are blue. The Shoreline strand of the San Andreas fault is yellow, and the main strand of the San Andreas fault is red. Its strongly sheared damage zone is almost entirely on its southwest side (also red). Notice how the false color images allow marker units and fault zones to be identified. The Salton Sea is black in the west and south.

REFERENCES:

Aagaard, B., 2008. Southern California ShakeOut Scenario Ground Motion Animations, http://earthquake.usgs.gov/regional/nca/simulations/shakeout/, accessed 31 October 2011.

Babcock, E.A., 1974, Geology of the northeast margin of the Salton Trough, Salton Sea, California, Geol. Soc. Am. Bull., 85, 321-332, 1974.

Babcock, E. A., 1969, Structural geology and geophysics of the Durmid area, Imperial Valley, California, Ph.D. dissertation, 149 pp., Univ. of Calif., Riverside, 1969.

Bilham, R., and P. Williams, 1985, Sawtooth segmentation and deformation processes on the southern San Andreas Fault, California, Geophys. Res. Lett., 12(9), 557-560.

Brothers, D.S., N. W. Driscoll, G. M. Kent, A. J. Harding, J. M. Babcock & R. L. Baskin, 2009, Tectonic evolution of the Salton Sea inferred from seismic reflection data. Nature Geoscience, 2, 581-584.

Brothers, D., D. Kilb, K. Luttrell, N. Driscoll and G. Kent, Loading of the San Andreas fault by flood-induced ruptures beneath the Salton Sea, Nature Geosciences, pp. 1-7, NGEO1184, DOI:10.1038, 2011

Brown, N. N.; Fuller, M. D.; and Sibson, R. H. 1991, Paleomagnetism of the Ocotillo Badlands, southern California, and implications for slip transfer throughan antidilational fault jog. Earth Planet. Sci. Lett. 102:277–288.

Bürgmann, R., 1991,Transpression along the Southern San Andreas fault, Durmid Hill, California. Tectonics, 10, pp. 1152–1163.

Clark, M.M., 1984, Map showing recently active breaks along the San Andreas fault and associated faults between Salton Sea and Whitewater River - Mission Creek, California: U.S. Geological Survey Miscellaneous Investigations Series Map I-1483, 2 sheets, scale 1:24,000.

Dibblee, T. W., Jr., 1954, Geology of the Imperial Valley region, California, in Jahns, R. H., ed., Geology of southern California: California Division of Mines Bulletin 170, p. 21-28.

Fuis, G. , Bauer, K. , Robert W. Graves, Brad Aagaard, Rufus D. Catchings, and Mark R. Goldman, "Geometry Of The San Andreas Fault In The Salton Trough And Its Effect On Simulated Shaking For A Rupture Similar To That Of The Great California Shakeout Of 2008" (*2013 SCEC Annual Meeting poster*)

Hauksson E., W. Yang and P.M. Shearer, Waveform relocated earthquake catalog for southern California (1981 - 2011), manuscript in preparation, 2011.

Hudnut, K., Seeber, L., Rockwell, T., Goodmacher, J., Klinger, R., Lindvall, S., and McElwain, R., 1989, Surface ruptures on cross-faults in the 24 November 1987 Superstition Hills, California, earthquake sequence: Bulletin of the Seismological Society of America, v. 79, p. 282–296.

Janecke S.U., Dorsey, R.J., Forand, D., Steely, A.N., Kirby, S.M., Lutz, A.T., Housen B.A., Belgarde, B., Langenhim, V.E., Rittenour, T.M., 2010, High Geologic Slip Rates since Early Pleistocene Initiation of the San Jacinto and San Felipe Fault Zones in the San Andreas Fault System: Southern California, USA: Geological Society of America Special Paper 475, 48 p., doi:10.1130/2010.2475.

Janecke, S.U., 2011, Progress report: Digital mapping of active interpenetrating faults within the San Jacinto fault zone, southern California: SCEC annual report. http://sceccore.usc.edu/proposalfiles/2010reports/Janecke_10134_report.pdf

Janecke, S.U., and Markowski, D., 2013, New structures from the southern tip of the San Andreas fault zone near Durmid Hill: 2013 SCEC Annual Meeting poster.

Janecke, S.U., and Thornock, S.J., 2011, Interactions between the Clark strand of the San Jacinto fault zone and the Extra-Elmore fault arrays: 2011 SCEC Annual Meeting poster A-149.

Jones, L. M., Bernknopf, R., Cox, D., Goltz, J., Hudnut, K., Mileti, D., Perry, S., Ponti, D., Porter, K., Reichle, M., Seligson, H., Shoaf, K., Treiman, J., and Wein, A., 2008. The ShakeOut Scenario:

USGS Open File Report 2008-1150 and California Geological Survey Preliminary Report 25, http://pubs.usgs.gov/of2008/1150 and http://conservation.ca.gov/cgs, Sacramento, CA.

Kirby, S.M., Janecke, S.U., Dorsey, R.J., Housen, B.A., McDougall, K., Langenheim, V., and Steely, A., 2007, Pleistocene Brawley and Ocotillo formations: Evidence for initial strike-slip deformation along the San Felipe and San Jacinto fault zones, California: The Journal of Geology, v. 115, p. 43–62, doi: 10.1086/509248.

Langenheim, V.E., Scheirer, D.S., Gary Fuis, Mark Goldman, Rufus Catchings, Trond Ryberg, and Michael J. Rymer , "Comparison of potential-field and seismic-velocity structure along the Salton Sea Seismic Imaging Project transects, northern Salton Trough, southern California" (2013 SCEC Annual Meeting poster).

Lin, G.. 2013. Three-Dimensional Seismic Velocity Structure and Precise Earthquake Relocations in the Salton Trough, Southern California. Bulletin of the Seismological Society of America, 103(5), 2694-2708.

Lin, G., Shearer, P.M., and Hauksson, E., 2007, Applying a three-dimensional velocity model, waveform cross correlation, and cluster analysis to locate southern California seismicity from 1981 to 2005: Journal of Geophysical Research, v. 112, B12309, doi: 10.1029/2007JB004986.

Lyons, S. and D. Sandwell, 2003, Fault creep along the southern San Andreas from InSAR, permanent scatterers, and stacking, J. Geophys. Res . ,108 (B1), 2047, doi:10.1029/ 2002JB001831, 2003.

Martin, Peter, ed., with contributions by Brandt, Justin, Catchings, R.D., Christensen, A.H., Flint, A.L., Gandhok, Gini, Goldman, M.R., Halford, K.J., Langenheim, V.E., Martin, Peter, Rymer, M.J., Schroeder, R.A., Smith, G.A., and Sneed, Michelle, 2011, The source, discharge, and chemical characteristics of water from Agua Caliente Spring, Palm Springs, California: U.S. Geological Survey Scientific Investigations Report 2011–5156, 106 p.Olsen, K. B., Day, S. M., Dalguer, L., Mayhew, J., Cui, Y., Zhu, H., Cruz-Atienza, V. M., Roten, D., Maechling, P., Jordan, T. H., and Chourasia, A., 2009. ShakeOut-D: Ground motion estimates using an ensemble of large earthquakes on the southern San Andreas fault with spontaneous rupture propagation, Geophys. Res. Lett. 36, L04303

Olsen, K. B., Day, S. M., Minster, J. B., Cui, Y., Chourasia, A., Faerman, N., Moore, R., Maechling, P., and Jordan, T., 2006. Strong shaking in Los Angeles expected from southern San Andreas earthquake, Geophys. Res. Lett. 33, L07305.

Olsen, K. B., Day, S. M., Minster, J. B., Cui, Y., Chourasia, A., Okaya, D., Maechling, P., and Jordan T, 2008. TeraShake2: Spontaneous rupture simulations of Mw7.7 earthquakes on the southern San Andreas fault, Bull. Seism. Soc. Am. 98, 1162–1185.

Philibosian, B., T. E. Fumal, R. J. Weldon, K. J. Kendrick, K. M. Scharer, S. P. Bemis, R. J. Burgette, and B. A. Wisely (2009). Photomosaics and logs of trenches on the San Andreas Fault near Coachella, California, in U.S. Geol. Surv. Open-File Rept. 2009-1039.

Porter, K., Jones, L., Cox, D., Goltz, J., Hudnut, K., Perry, S., Ponti, D., Reichle, M., Rose, A.,Scawthorn, C., Seligson, H., Shoaf, K., Treiman, J., and Wein, A., 2011. The ShakeOut Scenario: A hypothetical Mw 7.8 earthquake on the southern San Andreas Fault, Earthquake Spectra 27, 239–261.

Rymer, M. J., and Lindvall, S. C., 2005. A Broad Holocene-Active San Andreas Fault on Durmid Hill, Southern California-A Zone of Interaction with the Brawley Seismic Zone?. In AGU Fall Meeting Abstracts (Vol. 1, p. 1385).

Sieh, K., 1986. Slip rate across the San Andreas fault and prehistoric earthquakes at Indio, California, Eos, Transactions, American Geophysical Union 67, 1200.

Sieh, K., Stuiver M., and Brillinger, D., 1989. A more precise chronology of earthquakes produced by the San Andreas Fault in southern California. Journal of Geophysical Research -Solid Earth 94, 603–623.

Sharp, R. V., and Clark, M.M., 1972, Geologic evidence of previous faulting neat the 1968 rupture of the coyote Creek fault: U. S. Geological Survey Professional Paper 787, pp. 131-140.

Schmitt, A. K., Martín, A., Stockli, D. F., Farley, K. A., & Lovera, O. M. , 2013, (U-Th)/He zircon and archaeological ages for a late prehistoric eruption in the Salton Trough (California, USA). Geology, 41(1), 7-10.

Schmitt, A. K., Martín, A., Weber, B., Stockli, D. F., Zou, H., & Shen, C. C., 2013, Oceanic magmatism in sedimentary basins of the northern Gulf of California rift. Geological Society of America Bulletin, 125(11-12), 1833-1850.

Sneed, M., and Brandt, J. T. 2007. Detection and Measurement of Land Subsidence Using Global Positioning System Surveying and Interferometric Synthetic Aperture Radar, Coachella Valley, California, 1996-2005. US Department of the Interior, US Geological Survey.

Steely, A.N., 2006, The evolution from late Miocene West Salton detachment faulting to cross-cutting oblique strike-slip faults in the southwest Salton Trough, California [M.S thesis]: Utah State University, 253 p., 3 plates, scale 1:24,000.

Steely, A. N., Janecke, S. U., Axen, G. J., Dorsey, R. J., 2009, Pleistocene reorganization of the southern San Andreas fault system: Initiation and structures of the San Felipe fault zone: Geological Society of America Bulletin, v. 121, no. 5/6; p. 663–687; doi: 10.1130/B26239.1; 15 figures; 1 table.

Sylvester, A. G., 1988, Strike-slip faults: Geological Society of America Bulletin, v. 100, p. 1666–1703.

Sylvester, A., R. Bilham, M. Jackson, and S. Barrientos (1993), Aseismic Growth of Durmid Hill, Southeasternmost San Andreas Fault, California, J. Geophys. Res., 98(B8), 14233-14243.

Tong, X., D. Sandwell and B. Smith-Konter, High resolution interseismic velocity data along the San Andreas fault from GPS and InSAR, Journal of Geophysical Research, 118, doi:10.1029/2012JB009442, 2013.

Wisely, Beth, 2012, Geophysical and Hydrogeologic Investigations of Two Primary Alluvial Aquifers Embedded in the Southern San Andreas Fault System: San Bernardino and Upper Coachella Valley [Ph.D dissertation]: University of Oregon. https://scholarsbank.uoregon.edu/xmlui/handle/1794/12427

Wojtal, S.F., 2007, Assessing the long-term displacement field associated with deformation of the borderlands of the San Andreas fault, Durmid Hill, CA: GSA Annual Meeting Abstracts with program, Paper No. 138-11.

PUBLICATIONS:

Janecke, S.U., and *Markowski*, D., 2013, New structures from the southern tip of the San Andreas fault zone near Durmid Hill: 2013 SCEC Annual Meeting poster, p. 199. http://www.scec.org/meetings/2013am/SCEC2013Proceedings.pdf

Pending:

Markowski, Daniel, 2014, Testing a new geometric and kinematic model of the San Andreas fault at its southern tip, Durmid Hill, southern California [MS thesis]: Utah State University.

NOTE: Janecke suffered the death of her 15 year old daughter in 2013 and appreciates being given extra time to submit this final report.

2016

Confirmation of a New Geometric and Kinematic Model of the San Andreas Fault at Its Southern Tip, Durmid Hill, Southern California

Daniel K. Markowski
Utah State University

Geologic map and some chapters were coauthored with Susanne Janecke

CONFIRMATION OF A NEW GEOMETRIC AND KINEMATIC MODEL OF THE SAN ANDREAS FAULT AT ITS SOUTHERN TIP, DURMID HILL, SOUTHERN CALIFORNIA

by

Daniel K. Markowski

A thesis submitted in partial fulfillment
of the requirements for the degree

of

MASTER OF SCIENCE

in

Geology

Approved:

Susanne U. Janecke Major Professor	James Evans Committee Member
Tammy Rittenour Committee Member	Mark McLellan Vice President for Research and Dean of the School of GraduateStudies

UTAH STATE UNIVERSITY
Logan, Utah

2016

ABSTRACT

Confirmation of a New Geometric and Kinematic Model of the San Andreas Fault at Its Southern Tip, Durmid Hill, Southern California

by

Daniel K. Markowski, Master of Science

Utah State University, 2016

Major Professor: Dr. Susanne U. Janecke
Department: Geology

The southern ~100 km long Coachella section of the San Andreas fault is the only section of the fault in southern California that has not experienced a historical earthquake, and it may be the most overdue section of the fault. Numerical models of rupture propagation shows that a large earthquake with a nucleation zone in the Durmid Hill field area would produce particularly destructive and deadly ground shaking in southern California. This is used as the model earthquake for the ShakeOut exercises in southern California because it is may represent the worst-case scenario for southern California but does not appear to be a very likely scenario following this research.

Building on existing geologic mapping that shows major Pleistocene to Holocene contraction near the hypothesized nucleation, we use geologic mapping to develop and validate a competing geometric and kinematic model for the southern tip of the San Andreas Fault. A ladder-like-fault model explains the widespread contraction in the Durmid Hill study area as the result of contraction between the main strand of the San

Andreas fault and East Shoreline strand. The East Shoreline strand of the San Andreas fault is the newly discovered fault and is dispersed across a zone between 0.5 to 1 km wide, and encompasses an area on the northeast shore of the Salton Sea. There is persistent and strong contraction across the entire ~1.5 to 3.5 km wide San Andreas fault zone because both dextral "side-rail" faults are counterclockwise, and in a contractional bend, relative to current plate motions. This contractional bend was previously documented for the main strand of San Andreas fault.

A new digital geologic map and field studies document the stratigraphy and structures at a range of scales between Bombay Beach and Salt Creek. Numerous folds, narrow strike-slip and oblique-slip faults, and sheared damaged rocks in latest Miocene (?) to Holocene sediment lie within the wide and very complex damage zone of the main strand of the San Andreas fault zone. The East Shoreline strand of the San Andreas fault system buffers the main strand from major stress changes produced by deformation along the sinistral to sinistral-normal Extra fault array under the Salton Sea.

(150 pages)

PUBLIC ABSTRACT

Confirmation of a New Geometric and Kinematic Model of the San Andreas Fault at Its Southern Tip, Durmid Hill, Southern California

Daniel K. Markowski

This study explains the origin of the deforming structures between the San Andreas fault and the Salton Sea within the Salton Trough in Southern California. ShakeOut simulations and other studies model shaking resulting from a large rupture on the San Andreas fault. These models simulate a start at the southern fault tip of the San Andreas fault that propagates to the northwest. A secondary strand of the San Andreas fault called the East Shoreline fault is located at the southern tip of the San Andreas fault near the shoreline of the Salton Sea. Between the East Shoreline fault zone and San Andreas fault is dominantly contractional and strike-slip faults leading to the uplift of Durmid Hill.

The main purpose of this study is to map and analyze the San Andreas fault zone, East Shoreline fault zone, and the structural geology between these two faults. The San Andreas fault zone is characterized by a wide strongly developed damage zone that is up to about 0.5 km wide. The discovery and characterization of the East Shoreline fault is especially important because this strand of the San Andreas fault system could buffer the main strand from large triggered slip events.

ACKNOWLEDGMENTS

First and foremost, I would like to thank the Southern California Earthquake Center (SCEC) for funding this research. Next, I would like to thank Susanne Janecke for the opportunity to live in northern Utah and work in the Salton Trough, this very unforgiving yet geologically beautiful place. Thank you for taking the time to meet with me at least once a week. Without her countless hours of advice, support, and motivation, none of my work would be of the quality it is. I'd like to thank the other members of my committee, Jim Evans and Tammy Rittenour for their input and helpful suggestions. Other personal shout outs go to Mitch Prante and Santiago Flores for your willingness to drop whatever you were doing to help me with a variety of things. Thank you Dr. Barbara Nash for your chemical correlation on my samples allowing us to confirm the existence of the Thermal Canyon Ash at Durmid Hill. Thank you all faculty, staff, and fellow students. It was a pleasure to meet you, learn from you, and grow with you. Thank you Rob Quinn for giving me a place to stay in my last field season. You were an awesome host and a blast to talk to. Not only that but you let me use your dirt bike to better access the field. That was pretty cool. I'd also like to thank my family for their support. Thanks Mom and Dad for always encouraging me. Mom thanks especially for helping me push through the tough times. Finally, thanks to my girlfriend Meagan who also did nothing but encourage me and all of my endeavors during graduate school.

Daniel K. Markowski

CONTENTS

Page

LIST OF TABLES

LIST OF FIGURES

LIST OF PLATES

INTRODUCTION

Structural Setting of Southern California

The San Andreas fault system is the main strand of the plate boundary between the North American and Pacific plates and is the most intensely studied fault in the world (Fig. 1) (Chester and Evans, 1993). In southern California the San Andreas fault system has multiple strands, ends southward, and changes its strike within the big bend region (Figs. 1 and 2). At the "big bend" about 75 km southwest of Bakersfield, California, the fault changes strike by 20° from about N40°W to about N60°W (Fig 1).

Displacements in the San Andreas fault zone is primarily dextral-slip motion that is split fairly evenly between the San Andreas fault and the San Jacinto fault zone with smaller contributions on the Elsinore and San Felipe faults in southern California (Sanders, 1989; Matti and Morton, 1993; Fialko, 2006; Janecke et al., 2010). These dextral fault zones and the Eastern California shear zone to the east take up most of the plate motion between the North American plate and Pacific Plate.

The Salton Trough, the depression that encompasses an area bounded by the West Salton detachment fault in the west and the San Andreas fault to the east lies in southern California and northwest Mexico (Fig. 1 and 2). This depression is the result of thinning and intrusion of new dense mafic crust below, sedimentation from above, and interactions between the several transform faults in Southern California (Biehler et al., 1964; Babcock, 1974; Fuis and Kohler, 1984; Hertzig and Jacobs, 1994; Parsons and McCarthy,

1996; Lewis et al., 2000; Hauksson, 2000; Schmitt and Hulen; 2008; Dorsey, 2010; Dorsey and Lazear, 2013; Lin, 2013). It is the landward continuation of the Gulf of California oblique rift system and opens southeastward toward the Gulf of California (Fig. 1)(Dibblee, 1954; Elders et al., 1972; Babcock, 1974; Axen and Fletcher, 1998; Schmitt and Hulen, 2008). Fault-bounded mountains composed of Proterozoic to Mesozoic igneous and metamorphic rocks surround the Trough (Muffler and White, 1969; Jennings and Bryant, 2010).

A belt of latest Miocene-Pleistocene age low-angle normal faults about 250-km long, extends from the northern end of the Salton Trough to Baja California and forms the western boundary of the Salton Trough (Fig.1)(Axen and Fletcher, 1998). Slip on the West Salton detachment system and Laguna Salada detachment system was dominant in the latest Miocene to Pleistocene and was largely synchronous with slip on the San Andreas fault system (Shirvell, 2006; Steely, 2006).

The formation of the Salton trough was controlled by the combined slip on the San Andreas fault in the northeast and the West Salton detachment fault in the west (Axen and Fletcher, 1998; Dorsey et al., 2011). The Salton Sea occupies the lowest elevation of the basin and has a fluctuating altitude of about 73 meters below sea level (Fig.1 and 2). The Salton Trough was cut off from the Gulf of California by construction of the Colorado River delta (Dibblee, 1954; 1984; 1996).

The San Andreas fault forms the northeast margin of the Salton Trough and is typically interpreted to terminate southward in the field area of Durmid Hill along the east edge of the Salton Sea (Fig. 1, 2, and 3) at Bombay Beach (Dibblee, 1954; Babcock,

1974; Bilham and Williams, 1985; Dibblee, 1986; Bürgmann, 1991; Dibblee, 1997; Dibblee and Minch, 2008; Brothers et al., 2009; Brothers et al., 2011). It is thought to transfer its strain to a north-northwest-trending zone called the Brawley seismic zone near Bombay Beach (Fig. 2)(Fuis and Kohler, 1984; Nicholson et al., 1986; Hudnut et al., 1989; Bilham and King, 1989; Shearer, et al. 2005; Janecke et al., 2010). The Brawley seismic zone is buried underneath the Salton Sea and a series of agricultural land, except at its southern end.

The small earthquakes within the Brawley seismic zone define an elongate lozenge, in map view of northeast, east-northeast, north and north-northwest-striking left- and right-lateral strike-slip faults (Shearer et al., 2005; Thornock, 2011). Some normal faults occur but strike-slip dominates within this shear-ladder structure (Magistrale, 2002 and Shearer et al., 2005). Some strain is also thought to transfer to the southwest by way of the Extra and Elmore Ranch fault arrays (Hudnut et al., 1989; Brothers et al., 2009, 2011; Janecke and Thornock, 2011; Thornock, 2011). The southern tip of the San Andreas fault in our field area is thought to separate a transpressional part of the North American plate boundary in the north from a transtensional part in the south (Atwater, 1970; Bürgmann, 1991; Axen and Fletcher, 1998).

The Durmid Hill Study Area

The region of interest in this study is an area of highly faulted and folded rocks from Pliocene to Holocene in age underlying Durmid Hill. It is near the southern-most

extent of the San Andreas fault, along the east shore of the Salton Sea (Figs 1 and 2)(Dibblee, 1954, 1986, 1996; Babcock, 1974; Sylvester, 1988; Bilham and Williams, 1989; Bürgmann, 1991) This area is within the Salton Trough and south of the Big Bend in the San Andreas fault in southern California (Figs 1 and 2). The most intense deformation and uplift are concentrated between the San Andreas fault and the Salton Sea but mildly deformed rocks are also present northeast of the San Andreas fault (Babcock, 1974; Dibblee and Minch, 2008).

The limited microseismicity near Durmid Hill indicate that the San Andreas fault is locked, may be late in the earthquake cycle, and has a steep northeast dip (Fig. 3)(Hauksson, 2000; Shearer et al. 2005; Fialko, 2006; Lin et al., 2007; Hauksson et al., 2012; Lin, 2013; Lindsey and Fialko, 2014; Fuis et al., 2014). Previous geologic mapping in this region predate the wide availability of high-resolution aerial photography, LIDAR imagery, and multispectral imagery, and, therefore, we are able to assess several unknown geological relationships in the area. The availability of numerous new and upgraded geophysical data sets (GPS, seismicity, InSAR, gravity, LIDAR, and magnetic data) informed my research allowing me to collect unique data that cannot be observed from site visits on the ground.

The map area encompasses about ~75 km^2 from Bombay Beach to Salt Creek and is about 5 km wide (Fig. 2). California Highway 111 is the access road that nearly cuts the field area in half. In addition, Range Road and a series of off-road trails provide access to many of the places of interest (Plates 1 and 2).

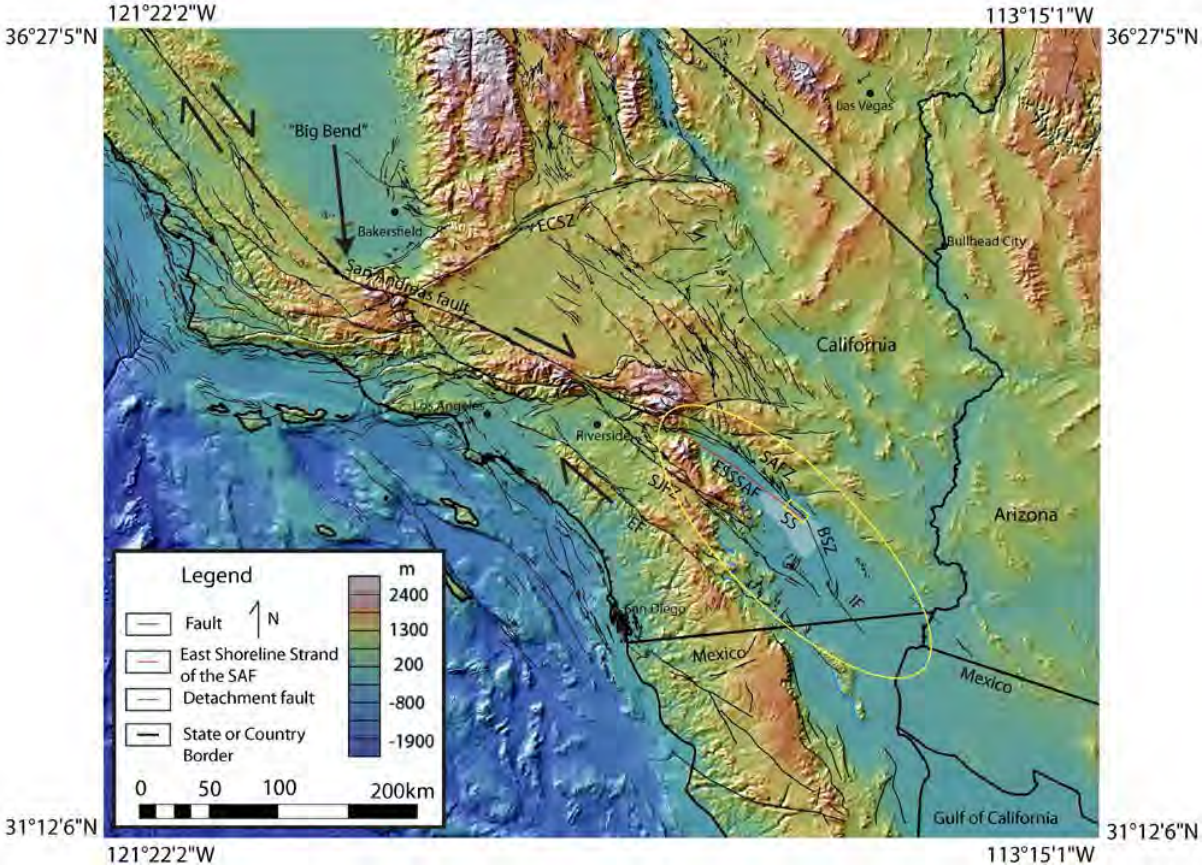

Figure 1. Regional map of the major fault zones of southern California and the northern Baja Peninsula, Mexico. DEM overlay highlights relief (meters). The yellow ellipse outlines the Salton Trough. The yellow rectangle outlines the study area. SAFZ- San Andreas fault zone, ESSSAF-East Shoreline Strand of the San Andrea fault, SJFZ- San Jacinto fault zone, WSD- West Salton detachment fault, EF- Elsinore fault, BSZ- Brawley seismic zone, IF- Imperial fault, AF- Algodones fault, GLFZ- Garlock fault zone, ECSZ- Eastern California shear zone, SGP- San Gorgonio Pass; SS-Salton Sea.

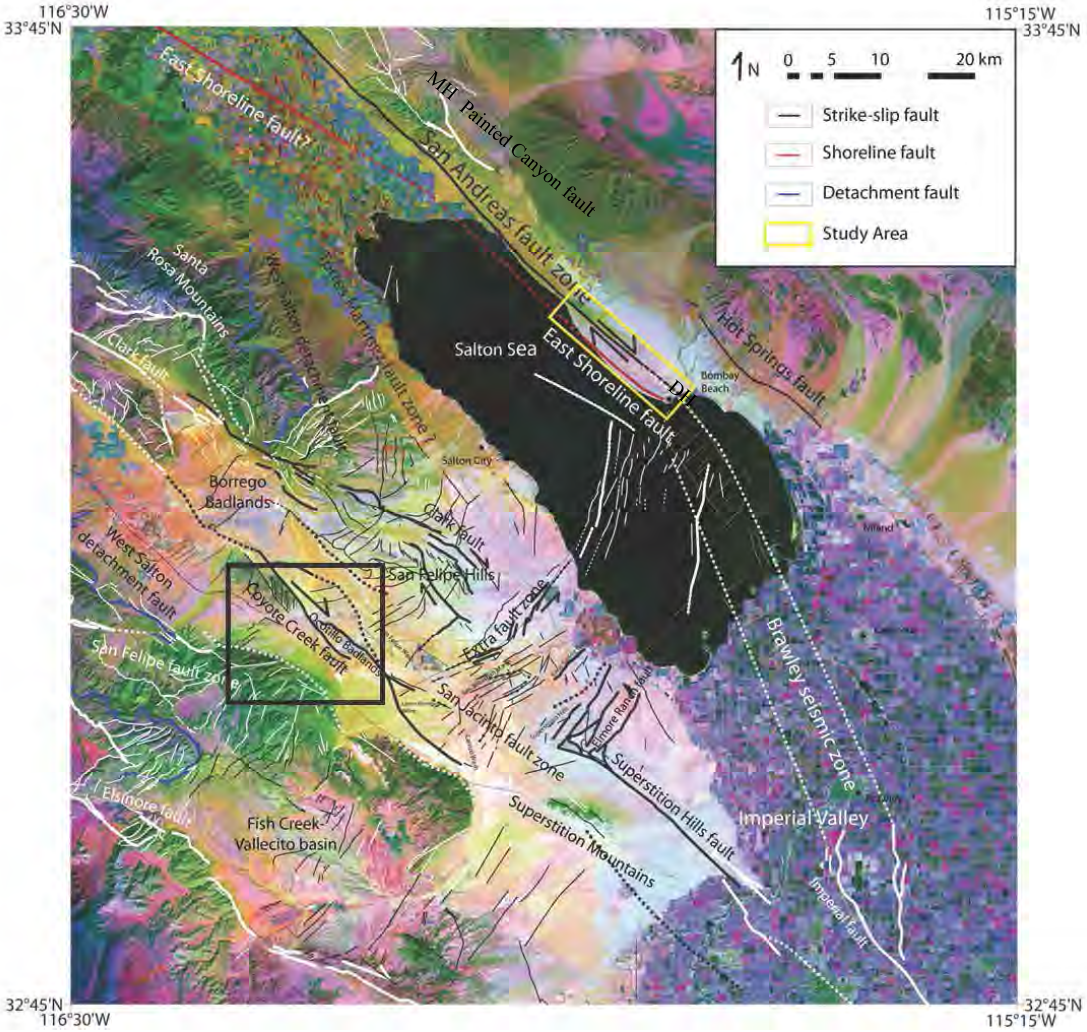

Figure 2. Regional map of the major fault zones of southern California in the Salton Trough. San Andreas fault zone, East Shoreline Strand of the San Andrea fault (red), San Jacinto fault zone, San Felipe fault zone, West Salton detachment fault (blue), Elsinore fault (white), Brawley seismic zone (white), Imperial fault, DH- Durmid Hill, Mecca Hills. The Landsat base map highlights different rock types. Yellow rectangle is the study area. The black box is the location of the Ocotillo Badlands step-over on the Coyote Creek Fault (Modified from Janecke and Thornock, 2011).

Seismic Hazard of the Southern San Andreas Fault

Previous studies have not been able to produce a geometric and kinematic model that successfully explains the origin of the Durmid Hill and the many contractional structures there. The disparate interpretations of the Durmid Hill area that emerged from geologic and geophysical studies also demonstrate the need for further investigation and a better understanding.

Relocated earthquake data from A.D. 1981 to 2011 show a lack of microseismicity near the southern tip of the San Andreas fault (Fig. 3)(Hauksson, 2000; Shearer et al. 2005; Lin et al., 2007; Hauksson et al., 2012; Lin, 2013). North of Salt Creek there is a low rate of seismicity and there are significantly higher rates of seismic activity to the south along the Brawley seismic zone and Imperial faults (Fig. 3)(Parsons and McCarthy, 1996; Hauksson, 2000; Lin et al., 2007 Weldon et al., 2005; Hauksson et al., 2012; Tong et al., 2012; Lin, 2013).

The Coachella segment of the San Andreas fault in this has been locked for about 336 years and it is thought that the risk for a large magnitude rupture on the southern San Andreas fault is high (Weldon et al., 2004). This segment of the San Andreas fault, between Cajon Creek and Bombay Beach has not experienced a major earthquake since A.D. 1680, and has accumulated a slip deficit of 5-10 meters (Weldon et al., 2004; Fialko, 2006; Olsen et al., 2009). Observations of stain rates from GPS and InSAR confirm that the San Andreas fault is approaching the end of its interseismic cycle (Weldon et al., 2004; Fialko, 2006; Olsen et al., 2009).

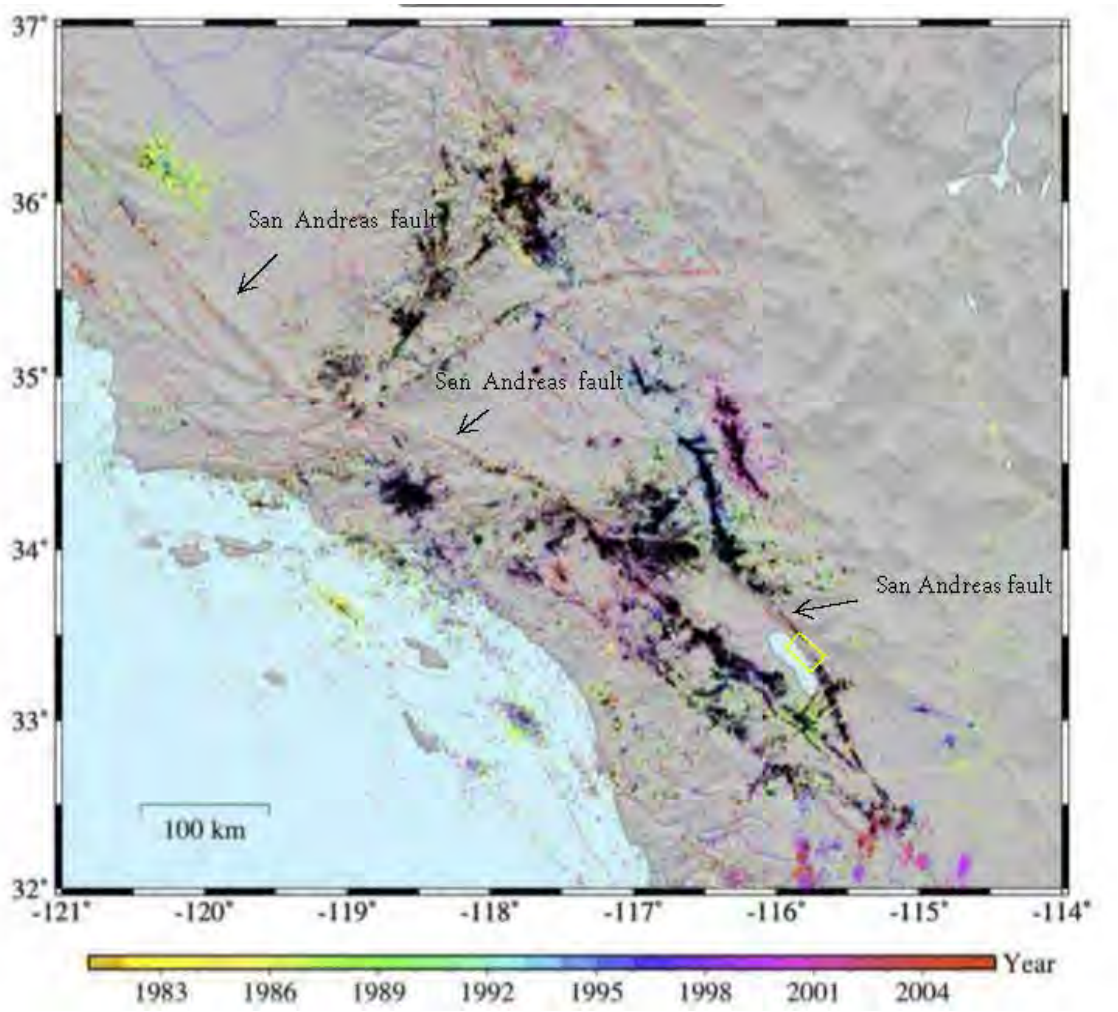

Figure 3. Relocated earthquake data of southern California from 1981 to 2005. Black dots show similar event clusters. About 25% of the events do not correlate and are plotted in color by year. Notice the lack of seismicity on the southern San Andreas fault and specifically the strand northeast of the Salton Sea. (Modified from Lin et al., 2007). The yellow rectangle is the study area.

ShakeOut Exercise

The ShakeOut Exercise involves a large multidisciplinary team that includes the

California Geological Survey, the United States Geological Survey, and almost 200 other partners in government whose goal is to understand the impacts of a large earthquake on the heavily populated southern California region. The Mw 7.8 earthquake scenario earthquake used in this readiness exercise was developed in 2008, initiated on the southern tip of the San Andreas fault, and propagated northwest for 300 km (Fig. 4)(Jones and Benthien, 2011). Based on the 180-year average recurrence for paleoearthquakes on the southern San Andreas fault and the 300 year elapsed time since its last major rupture, the southern San Andreas fault is over 100 years overdue for a large earthquake (Field et al., 2004; Brothers et al., 2011). Models predict that were such an event to occur and propagate northward, it would likely produce strong shaking and significant damage to the Los Angeles metropolitan area (Fig. 4)(Olsen et al., 2009; Brothers et al., 2011; Jones and Benthien, 2011). This damage is great than expected for the fairly large distance between the Los Angeles metropolitan area and the San Andreas fault zone (Fig. 4).

Motivations for This Study

We seek to test the likelihood of the ShakeOut scenario earthquake- a northwest propagating rupture that nucleates from the southern tip of the southern San Andreas fault (Fig. 4) We test, revise, and document a new contractional geometric interpretation of the southern San Andreas fault. A contractional regime would inhibit future ruptures there and not promote it. Therefore, the southern San Andreas fault may not be at risk of

triggered slip as suggested by previous studies and rupture directivity cannot be predicted. We test studies by Brothers et al., (2009), Brothers et al., (2011), and Hudnut et al (1989) that suggested that the southern San Andreas fault is at times, part of a transtensional regime. This was the basis for the ShakeOut scenario earthquake with northwest unilateral rupture nucleating at the southern tip of the San Andreas fault (Figs. 5 and 6).

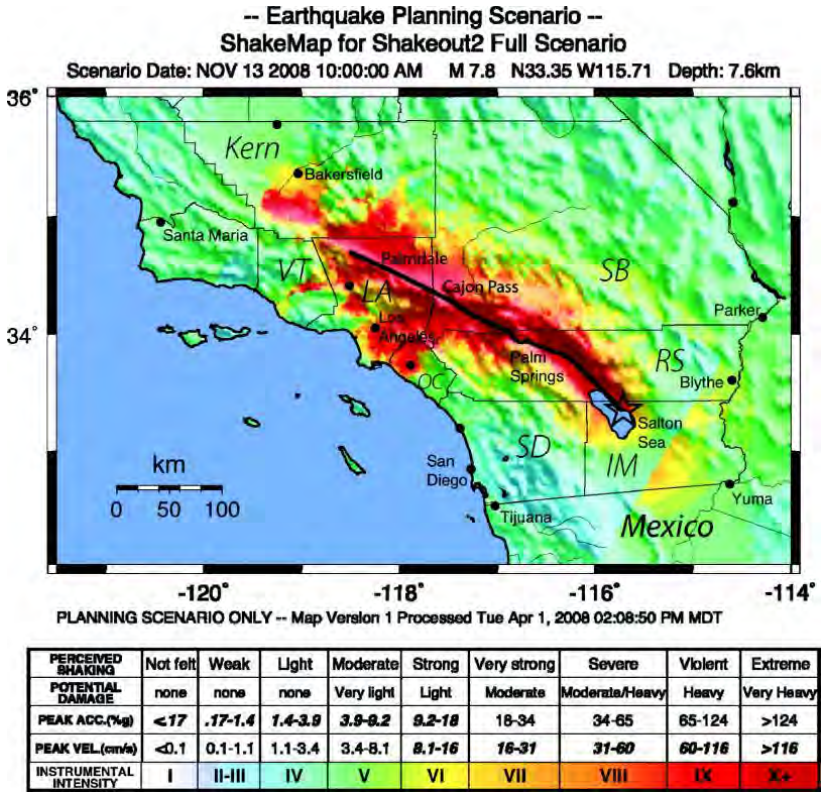

PERCEIVED SHAKING	Not felt	Weak	Light	Moderate	Strong	Very strong	Severe	Violent	Extreme
POTENTIAL DAMAGE	none	none	none	Very light	Light	Moderate	Moderate/Heavy	Heavy	Very Heavy
PEAK ACC.(%g)	<.17	.17-1.4	1.4-3.9	3.9-9.2	9.2-18	18-34	34-65	65-124	>124
PEAK VEL.(cm/s)	<0.1	0.1-1.1	1.1-3.4	3.4-8.1	8.1-16	16-31	31-60	60-116	>116
INSTRUMENTAL INTENSITY	I	II-III	IV	V	VI	VII	VIII	IX	X+

Figure 4. Predicted ground shaking in southern California produced by a large moment magnitude 7.8 earthquake along the southern San Andreas fault. The scenario earthquake nucleates from the southern terminus at Bombay Beach adjacent to the Salton Sea and propagates to the northwest. Shaking from the Salton trough is funneled through San Gorgonio pass and channeled along strike and transferred to the Los Angeles basin (Olsen et al., 2009).

Previous Structural Analysis

Prior studies have investigated the Durmid Hill area but many remote sensing datasets were not available and the scale of mapping was not sufficient to depict all of the faults in the area or to reveal the intense shortening and shear there (Dibblee, 1954, 1986, 1996; Babcock, 1974; Sylvester, 1988; Bilham and Williams, 1989; Bilham and King, 1989; Bürgmann, 1991; Jamison 1991; Krantz, 1995; Dibblee and Minch, 2008; Jennings and Bryant, 2010; Janecke, unpublished data). These studies documented the location of the main strand of the San Andreas fault and the numerous folds in the area but only a tiny fraction of the strike-slip faults mapped during this study were identified by previous workers. The most recent research near the Durmid Hill area (Brothers et al., 2009, 2011) suggest that cross faults with sinistral deformation and a moderate to large extensional component should be present. This is counter to previous research which showed only contractional and transpressional strain in the region (Dibblee, 1954; Babcock, 1974; Bürgmann, 1991; Dibblee and Minch, 2008). If correct, this cross-fault configuration could trigger a large earthquake on the southern San Andreas fault and is discussed below.

Cross-fault Configuration and Triggering Mechanism

On November of AD 1987, the ($M_{s,}$ surface wave magnitude scale) 6.2 Elmore Ranch earthquake occurred on a fault along the Elmore Ranch fault zone west of the Salton Sea (Fig. 2)(Hudnut et al., 1989). This was followed less than twelve hours later

by the M_s 6.6 Superstition Hills earthquake a few kilometers to the southwest (Hudnut et al., 1989; Sharp et al., 1989)(Fig. 2). Hudnut et al. (1989) and Magistrale et al. (1989) suggested that slip on faults in the Elmore Ranch fault zone can relieve normal stresses on the Superstition Hills Fault and initiate triggered slip (Fig. 5A). The Superstition Hills Fault is a northwest-striking dextral fault and the Elmore Ranch fault zone is northeast striking fault dominated by sinistral slip. Both faults are located southwest of the Salton Sea (Fig 2).

If the San Andreas fault has the geometry hypothesized by Hudnut et al. (1989) then the same scenario may be possible in Durmid Hill, with another fault called the Extra Fault zone. This assumes that the Extra Fault zone that extends to the eastern shoreline of the Salton Sea, is obscured under the young stratigraphy, and is laterally continuous to San Andreas fault to the east (Fig. 5 B). The Extra Fault zone is an area of northeast trending left-lateral to normal oblique-slip faults (Fig. 2). This zone is about 15 km wide and its known length is about 20 km from the Superstition Hills fault to the northeast across the Salton Sea (Fig. 2). No known published map extends the Extra fault northeast of the Salton Sea onshore to Durmid Hill.

In a variant of the Hudnut model of cross-fault triggered earthquakes, Brothers et al. (2009) interpreted various seismic reflection profiles over the Salton Sea. Their initial work identified faults of the Extra Fault zone and suggested that slip is partitioned spatially and temporally into vertical and horizontal domains (Brothers et al., 2009). Building on this model they investigated stress changes under the Salton Sea (due to the presence of hypothesized left-normal to normal faults) and how that might affect the state

of stress on the San Andreas fault. They argue that an earthquake with 1.0 meter normal displacement along an extensional fault in the Salton Sea results in a change of the Coulomb stress field and a positive northwest oriented lobe along the trend of the San Andreas fault (Fig. 6).

This analysis predicts that the Durmid Hill area should preserve many active north-northeast to northeast-striking left-normal to normal faults. If so, the Coulomb stress field could be much higher than predicted in their model (Fig. 6). If the two fault systems are not directly connected, other faults may buffer the San Andreas fault from stress perturbations, that would allow it to resist triggered slip.

Bends in San Andreas Fault

The southern San Andreas fault (Coachella segment) contains 6 individual segments named the Indio, Canal, Mecca, North Shore, Durmid, and Bombay Beach segments (Bilham and Williams, 1985)(Fig. 7). The more westerly striking pieces of the fault were thought to produce contraction because they are misaligned relative to the motion of North America and the Pacific plate. A 7.5° bend is thought to exist between the Bombay Beach segment and the Durmid segment (Fig. 7)(Bilham and Williams, 1985). This geometric configuration produces contraction, uplift and young deformation at Durmid Hill, the Mecca Hills, and the Indio Hills according to these authors due to the impedance between the plate slip vector and strike of the fault (Fig. 7)(Bilham and Williams, 1985; Sylvester, 1988). This hypothesis is widely accepted the origin of uplift and deformation at Durmid Hill. However, the spatial pattern of uplift and bends are not

entirely consistent with the Bilham and William's model (Fig. 7).

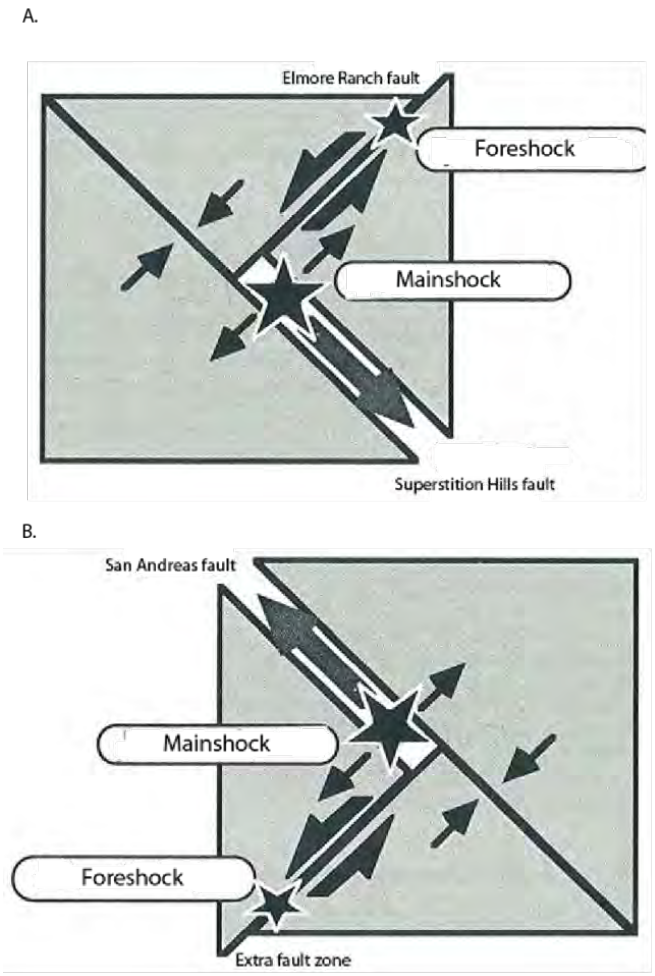

Figure 5. Illustrations of the geometry of the Elmore Ranch fault and Superstition Hills fault and the possible geometry of the San Andreas fault and the Extra fault zone. A) Illustrates the geometry of the Elmore Ranch fault and Superstition Hills fault as described by Hudnut (1989).This model simulates a foreshock that releases normal stresses from slip on the sinistral fault (Elmore Ranch fault) triggering a mainshock on the Superstition Hills fault. Modified from (Hudnut, 1989). B) Figure A inverted and redrafted to illustrates the possible geometry of the San Andreas fault and Extra fault Array; similar to that of the Elmore Ranch fault and Superstition Hills fault. This model simulates the release of normal stresses from slip on the sinistral fault (Extra Fault array) triggering slip on the main fault (San Andreas fault). Notice the northwest propagating rupture in the opposite direction of increased normal stress. Modified from Hudnut (1989).

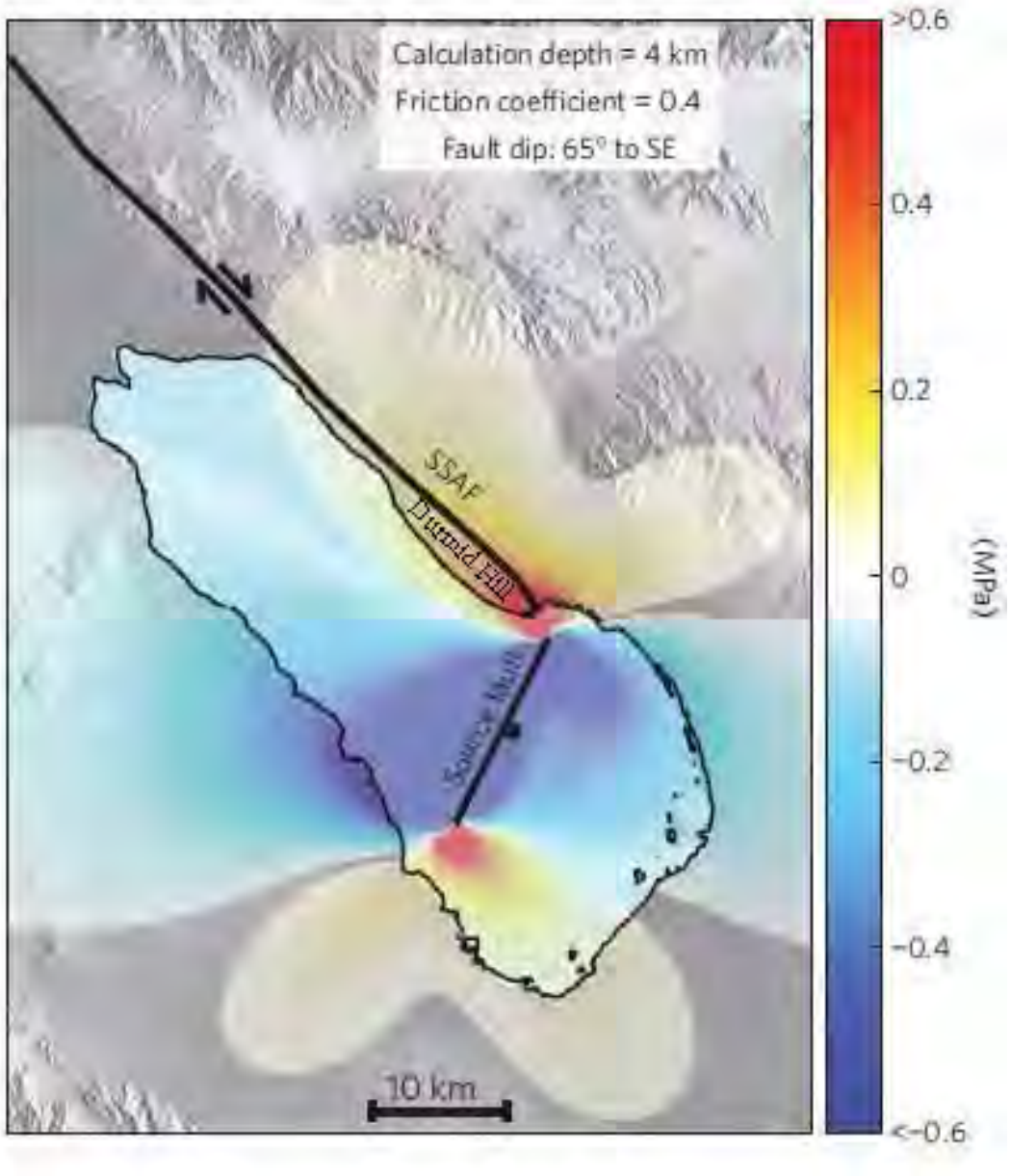

Figure 6. Coulomb stress generated by rupture of a normal fault beneath the Salton Sea. This simulation applies 1.0 m of down to the southeast normal displacement to the source fault. Resulting stresses are derived on fault planes that are oriented parallel to the southern San Andreas fault (Strike =325°; Dip =90°; Rake = 180°). Warm colors indicate areas where failure is promoted and cool colors where failure is inhibited. Stress lobes are saturated at ±0.6 MPa. Modified from Brothers et al., (2011).

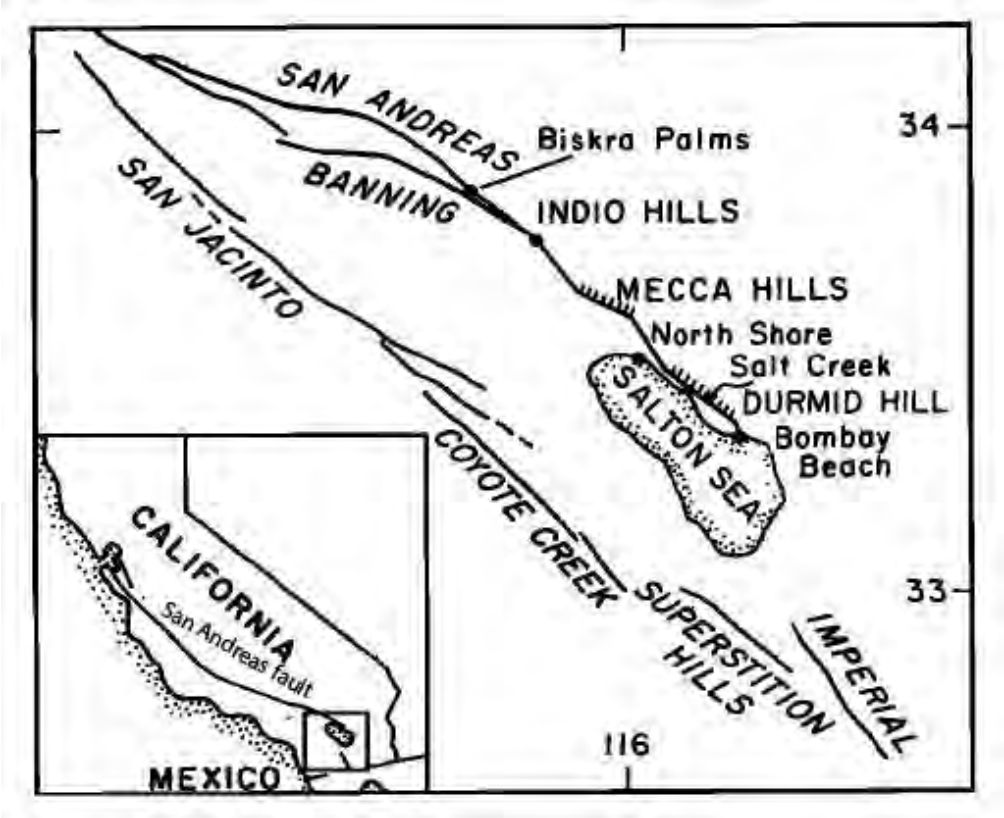

Figure 7. Sawtooth geometry of the six segments of the southern San Andreas fault system. Some segments, marked with a tick pattern, strike more westerly than the intervening parts of the San Andreas fault. The north-northwest-striking parts align with relative plate motions whereas the more westerly striking parts create come contraction across them. (Modified from Bilham and Williams 1985).

From Bombay Beach to San Gorgonio Pass there are eight bends and up to four branch points on the San Andreas fault that are thought to explain topographically high or topographically low areas and areas of intense deformation (Fig. 1 and 8). The Indio, Mecca, and Durmid Hills historically have been thought to be the result of the contractional bends of the San Andreas fault (Fig. 7)(Bilham and Williams, 1985; Sylvester, 1988). Janecke mapped the locations of the bends more precisely and

compared this spatially to contractional deformation, topographic uplifts, and depressions and found that bends on the San Andreas fault do not always correspond with topographic uplifts or depressions (Fig. 8).

At the Indio, Mecca, and Durmid Hills uplift is expected on both sides of west-striking sections of the San Andreas fault and not adjacent to more northerly striking parts. These west-striking or "contractional segments" should be the only areas where contractional deformation and uplift is observed if the saw-tooth configuration is correct (Fig. 8).

Folds at Durmid Hill

Babcock (1979) conducted in-depth mapping, structural analysis, stratigraphic analyses, and geophysics at Durmid Hill. He produced a detailed geologic map that documents significant transpression on the southwest side of the San Andreas fault zone (Fig. 9). Existing geometric models of strain adjacent to major strike-slip faults predict that the intensity of folding and rotation of fold axes should decrease away from the San Andreas fault (Bürgmann, 1991), but instead Babcock's and Bürgmann's maps show numerous intense close and tight folds up to 5 kilometers southwest of the San Andreas fault (Fig. 9). Fold axes become more sub-parallel to the San Andreas fault with distance away than the folds adjacent to it (Fig. 9). The map also shows the presence of tightly spaced folds in younger rocks near Bombay Beach. The Bishop Tuff (a prominent marker bed) splits this domain of tightly spaced folds with longer wavelength folds to the north (Fig. 9)(Babcock, 1974).

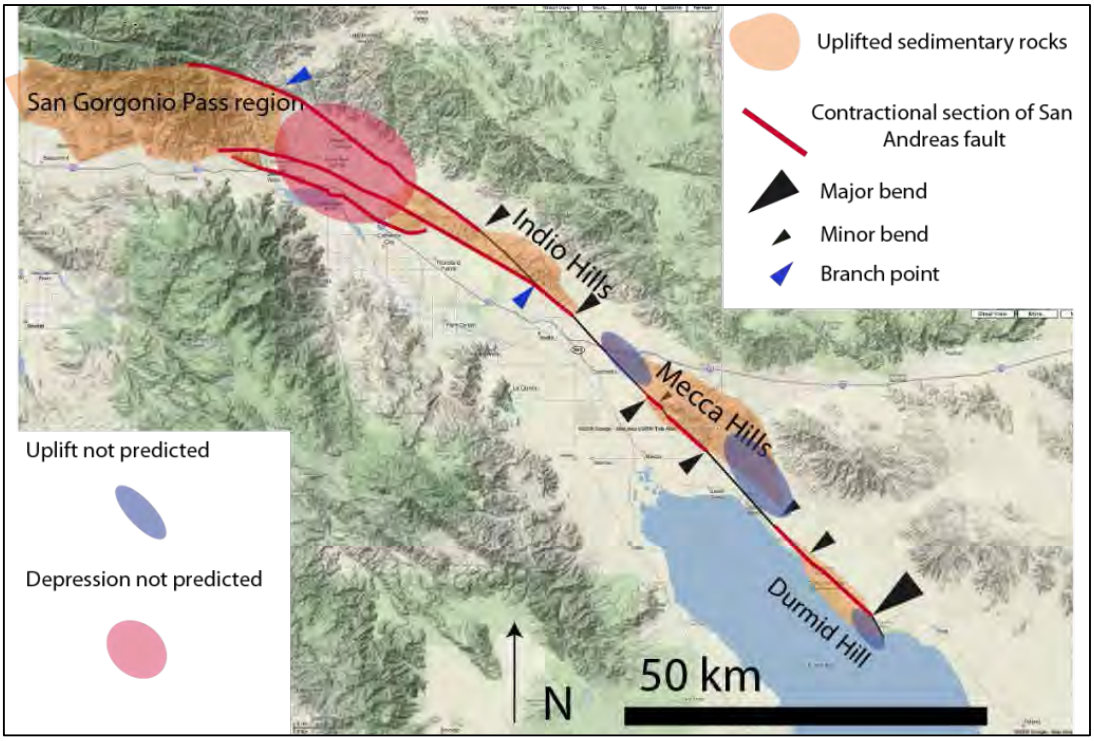

Figure 8. Map comparing actual uplifts and contractional bends along the San Andreas fault with ones predicted by the sawtooth model. Notice several uplifts occur where they are not predicted (purple), and inversely, some areas are subdued and low lying where uplift is predicted by the sawtooth model (red). Orange reflects uplifted rock masses that are both observed and predicted by the sawtooth model. Modified from Janecke (2008) with her permission.

Bürgmann (1991) built on the work of Babcock (1979) and analyzed the orientation and character of the folds, shortening, and extension at Durmid Hill in order to develop a transpressional model there (Fig 10). He mapped the traces of fold axes between the San Andreas fault and Salton Sea and also found that the fold axes exhibit a sigmoidal pattern. The hingelines of the folds trend towards parallelism with the main strand of the San Andreas fault, trend close to east west farther west and return to NW-trends near the shore of the Salton Sea on the west side of Highway 111 (Fig. 9 and

10)(Bürgmann, 1991). This evidence may suggest the presence of another shear-zone boundary (East Shoreline strand of the San Andreas fault) at, under, or near the Salton Sea (Bürgmann, 1991; Jameson, 1991).

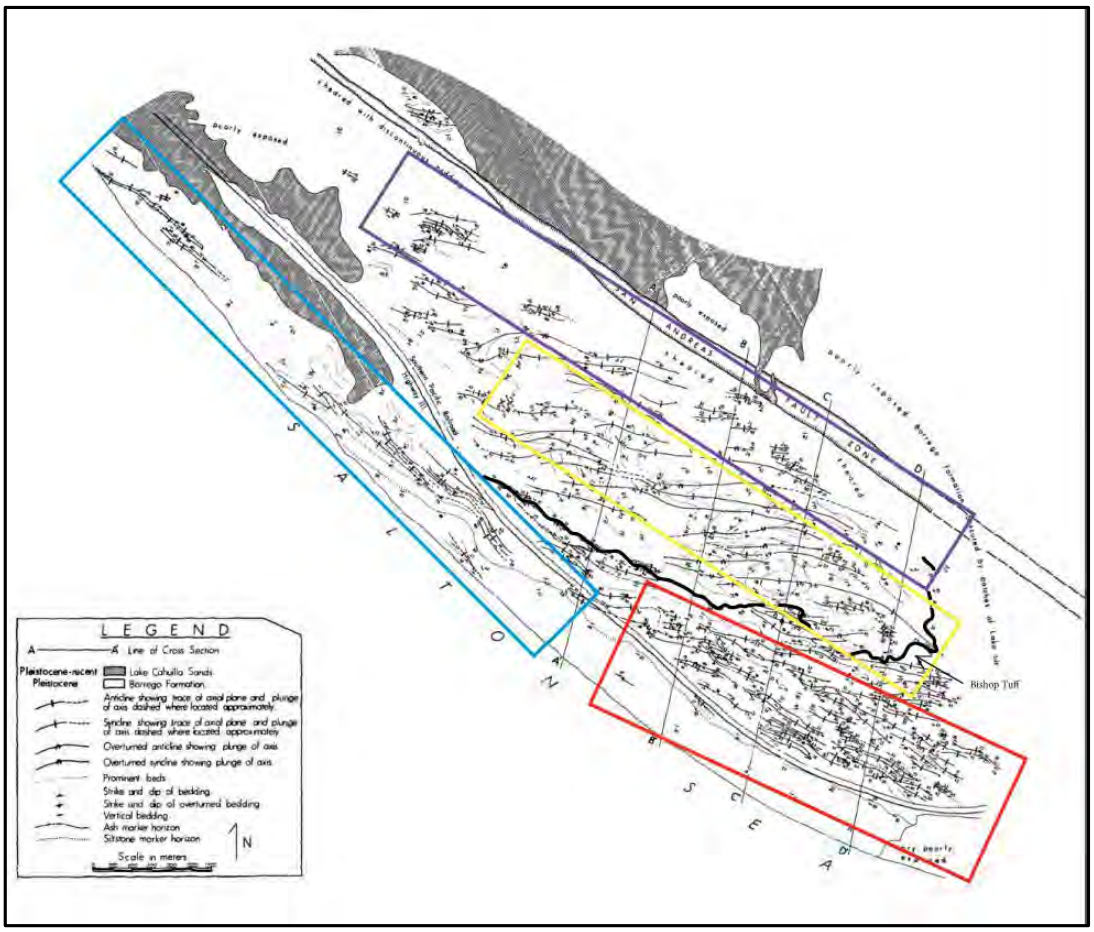

Figure 9. Geologic map of Durmid Hill modified from Babcock (1974).This map highlights the folds in the mapping area. Notice the fold axes that are nearly parallel to the strike of the San Andreas shear zone near the Salton Sea (blue box) and the sub-parallel folds adjacent to the main strand of the San Andreas fault (purple box). In the southwest corner of the yellow box folds trend east-west. This sigmoidal folding pattern is suggestive of another strand of the San Andreas fault. Furthermore, notice the shorter wavelength folds in the south (red box) and larger wavelengths northwest of there (yellow box). The dark black line is the Bishop Ash marker unit.

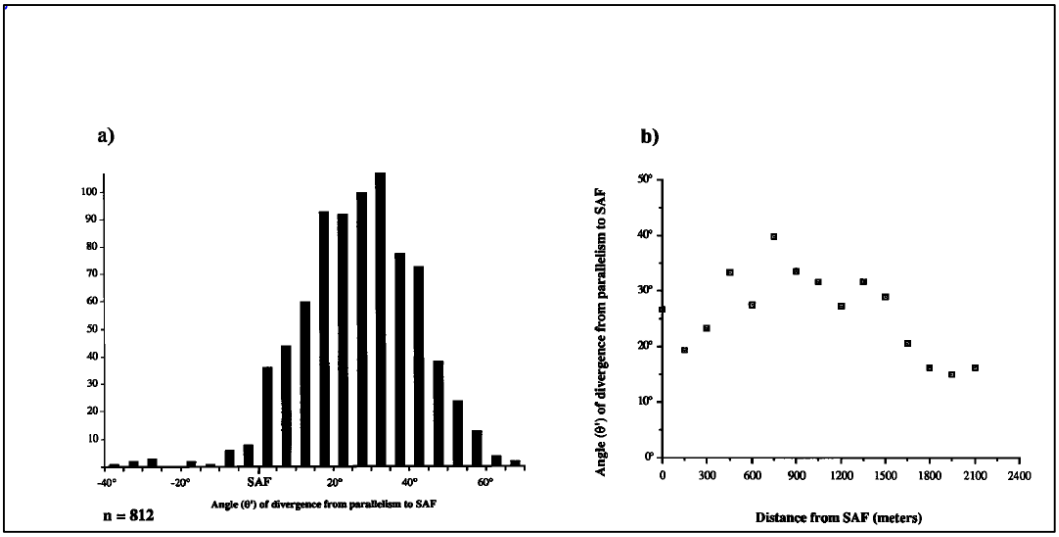

Figure 10. Bürgmann's (1991) analysis of fold orientations at Durmid Hill. A) Histogram of the orientation of 812 segments of fold-axial traces (length = 60m) mapped at Durmid Hill. Theta is the angle between the average strike of the San Andreas fault at Durmid Hill (N47.5° W) and the orientation of the fold-axial traces. B) Variation of theta with distance from the San Andreas fault. Modified from (Bürgmann, 1991). Notice that folds 1800 to 2100 m southwest of the San Andreas fault more closely parallel the main strand of the San Andreas fault than folds immediately adjacent to it, at 0-300 m.

Hypothesis

Prior works has well documented contractional strains at Durmid Hill but it does not fully explain all of the structural geology and the actively deforming rocks up to 5 kilometers southwest of the southern San Andreas fault at Durmid Hill. A better geometric model is needed that accounts for all of the observed structures there. The origin of the sigmoidal folds, left-lateral cross faults, and cause of spatial variability of tightly and wide spaced folds has not been fully explained. Moreover, it is not clear

whether brittle deformation is observed rather than ductile extension parallel to fold axes (Bürgmann, 1991).

In order to better explain the origin of deformation both near and far from the San Andreas fault, it is hypothesized that another strand of the San Andreas fault that we named the East Shoreline fault, lies southwest of the main strand of the San Andreas fault and exists roughly between the Salton Sea and Highway 111. We first hypothesized that the contraction at Durmid Hill evolved from a left-stepping pair of dextral faults. This creates a transpressional regime bounded to the west by a nascent cryptic fault (East Shoreline strand of the San Andreas fault) and to the east by the main strand of the San Andreas fault. In a very simplified analogy, for right lateral faults, a left step between fault strands creates contraction or transpression (Fig. 11 A). Dextral right-stepping faults create extension or transtension (Fig 11 B). These significant local strains can result in surface topographic expression in response to continued slip (Fig 11 C) (Sharp and Clark, 1972). The left-stepping strands of the Coyote Creek fault at the Ocotillo Badlands and the contraction in the step-over was the analog for our working model (Fig. 12).

Later in this study, it became clear that contraction was much more widespread than previously reported, and that neither the East Shoreline nor main strand of the San Andreas fault terminate--as required for a step over interpretation to be accurate. The along strike overlap of the two strands of the San Andreas fault instead defines a contractional ladder-like geometry that is at least 15 km long, rather than a more aerially restricted left-stepping geometry. Although there are many structural similarities between contractional step-overs and contractional ladder-like fault zones, ladder faults have a

greater aerial extent of potentially deforming land. Ladder-like faults are a particular type of trans-rotational fault zones that have side-rail faults that are much longer than their internal cross faults (Dickinson 1996).

Our current interpretation of the two strands of the San Andreas fault (East Shoreline fault and the main strand of the San Andreas fault) posits that they are the master faults, or side-rails of a major ladder-like fault zone and that the connecting left-lateral and right lateral faults in between are the rungs (Plate 1 b). Ladder-like fault zones occur immediately south of this field area within the Brawley seismic zone and they may be neutral, contractional or extensional depending on details of their overall and internal geometry (Fuis and Kohler, 1984; Nicholson et al., 1986; Hudnut et al., 1989; Bilham and King, 1989;; Janecke et al., 2010). The Durmid ladder structure is strongly contractional at every scale of observation. The ladder fault in the Brawley seismic zone is dominantly extensional to trans-rotational (Shearer et al., 2005; Lin, 2013).

Tests and Predictions for the Four Geometric Configurations

Four different configurations of fault geometry have been proposed. The saw-tooth configuration of (Bilham and Williams, 1985; Sylvester, 1988), cross-fault trigger configuration (Hudnut,1989; Brothers et al., 2009; Brothers et al., 2011), step-over configuration (Janecke, 2012) and a later developed hypothesis the two-fault ladder-like geometry (Fig. 5, 7, and 11). Each one implies a different earthquake hazard and nucleation point (Table 1).

The saw-tooth configuration creates contraction at restraining bends in which triggered slip is inhibited and extension at releasing bends. In this configuration, restraining bends clamp the fault together and extensional bends release stresses. A higher probability of an earthquake nucleating at an extensional bend or extensional step is predicted with this configuration.

The cross-fault model (Fig. 5) predicts the presence of important northeast striking faults in the Durmid Hill area. These faults are predicted to be a continuation of the left-lateral strike-slip to oblique normal faults of the Extra fault array (Fig. 2). This configuration predicts no contractional strain except for very little near the cross-faults intersection with the San Andreas fault and promotes triggered slip (Fig. 5). This configuration predicts that ongoing loading of transtensional faults under the Salton Sea adjacent to the San Andreas fault is reducing the time to expected rupture (Fig. 6)(Brothers et al., 2009; Crowell et al., 2010; Brothers et al., 2011). If this model is correct then it predicts a northwest propagating rupture with a higher earthquake hazard by release of normal stress that previously clamped the fault together.

In the step-over model, the East Shoreline fault buffers the main strand of the San Andreas fault from the cross-over connecting faults (Extra Fault Zone) and predict lower earthquake hazard from triggered-slip at least along that strand. The main strand of the San Andreas fault must terminate and the step-over fault would continue.

The analog model is the Coyote Creek fault at the Ocotillo Badlands and are a result of a left step in the Coyote Creek fault within the San Jacinto fault system (Sharp and Clark, 1972); (Fig. 12). This left-step creates a contractional regime in which

Borrego Formation and the Ocotillo Formation are exposed. Similar structural characteristics are found at the Ocotillio Badlands as Durmid Hills. The folds at the Ocotillo Badlands exhibit a sigmoidal pattern and the deformation appears to be confined between the step-over zone (between the two master faults)(Fig. 12).

The ladder-like fault geometry is similar to the step-over configuration and similar structures and style of deformation should exist. This would also buffer the main strand of the San Andreas fault from cross-over connecting faults and predict a lower earthquake hazard in the Durmid Hill area. This configuration does not require the termination of either of the main ladder faults.

The only known possible geometric configurations that favor a triggered slip earthquake on the San Andreas fault are the cross-fault configuration and releasing bends along the main strand of the San Andreas fault.

For the four different models of fault geometry at the southern San Andreas fault, some important questions need to be answered. The questions I pose here include: Does the shortening and faulting at Durmid Hill match any of the predictions of any of the models? Does the intensity and distribution of folding match any of the four models? Predictions can be made to which type of structural regimes should exist spatially with each model (Table 1), and we use these predictions to test which, if any of the models adequately explain the structures that are discovered at Durmid Hill. Bends in the San Andreas fault are inconsistent with the geology of the area and do not agree with my hypothesis dominantly because of spatial folding and faulting patterns and relationships (Table 1). If the hypothesis is correct that the geometric configuration of the southern

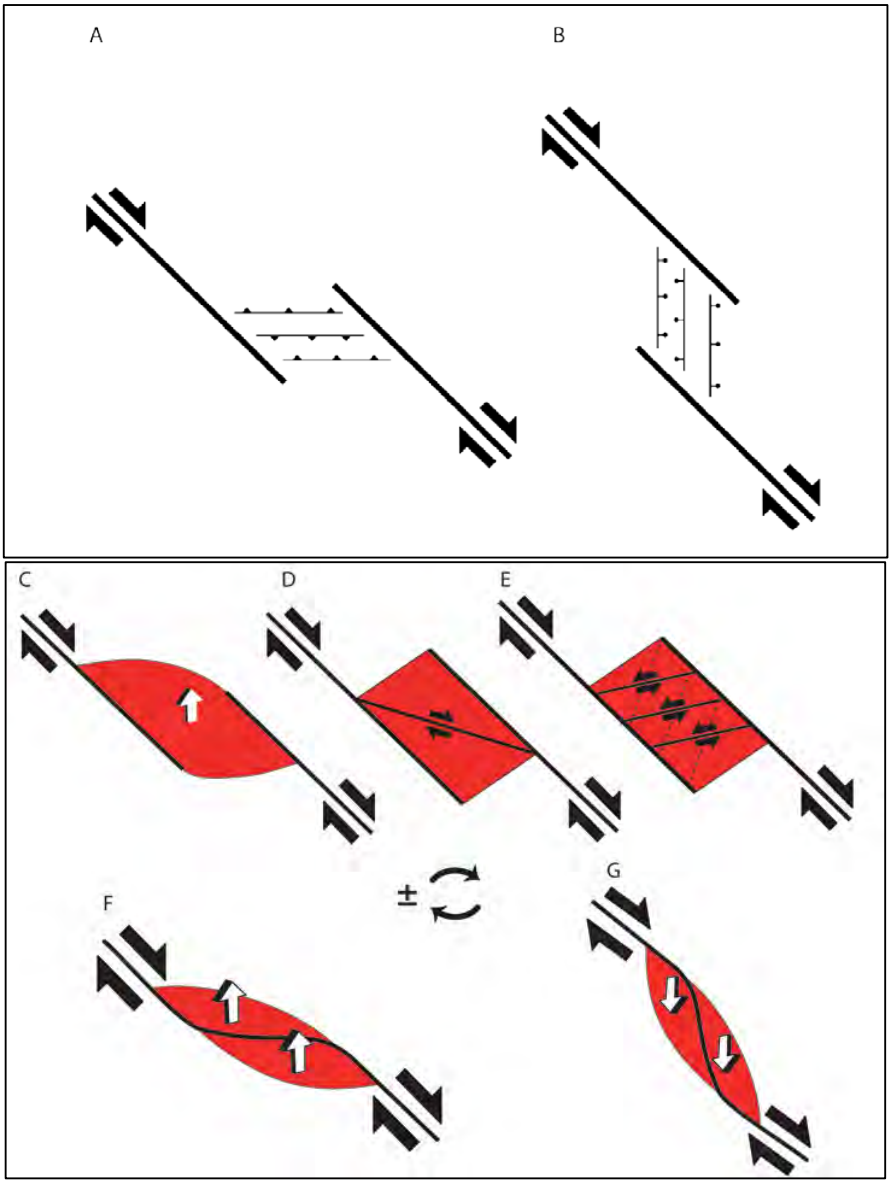

Figure 11. Schematic diagrams of structures associated with strike slip step-overs. A. Simplified schematic diagram of a left-step in a dextral strike-slip fault (Durmid Hill). B. Simplified schematic diagram of a right-step in a dextral strike-slip fault. C. Uplift as a result of a left-step in a right-lateral strike slip fault. D. Connecting faults as a result of a left-step in a dextral strike-slip fault. E. Antithetic connecting faults as a result of a left-step in a dextral strike-slip fault. F. Uplift as a result of a bend along a right-lateral strike-slip fault. G. Extension as a result of a bend along a right-lateral strike slip fault. Diagrams C-E may or may not experience rotation and each type of structure is found at Durmid Hill.

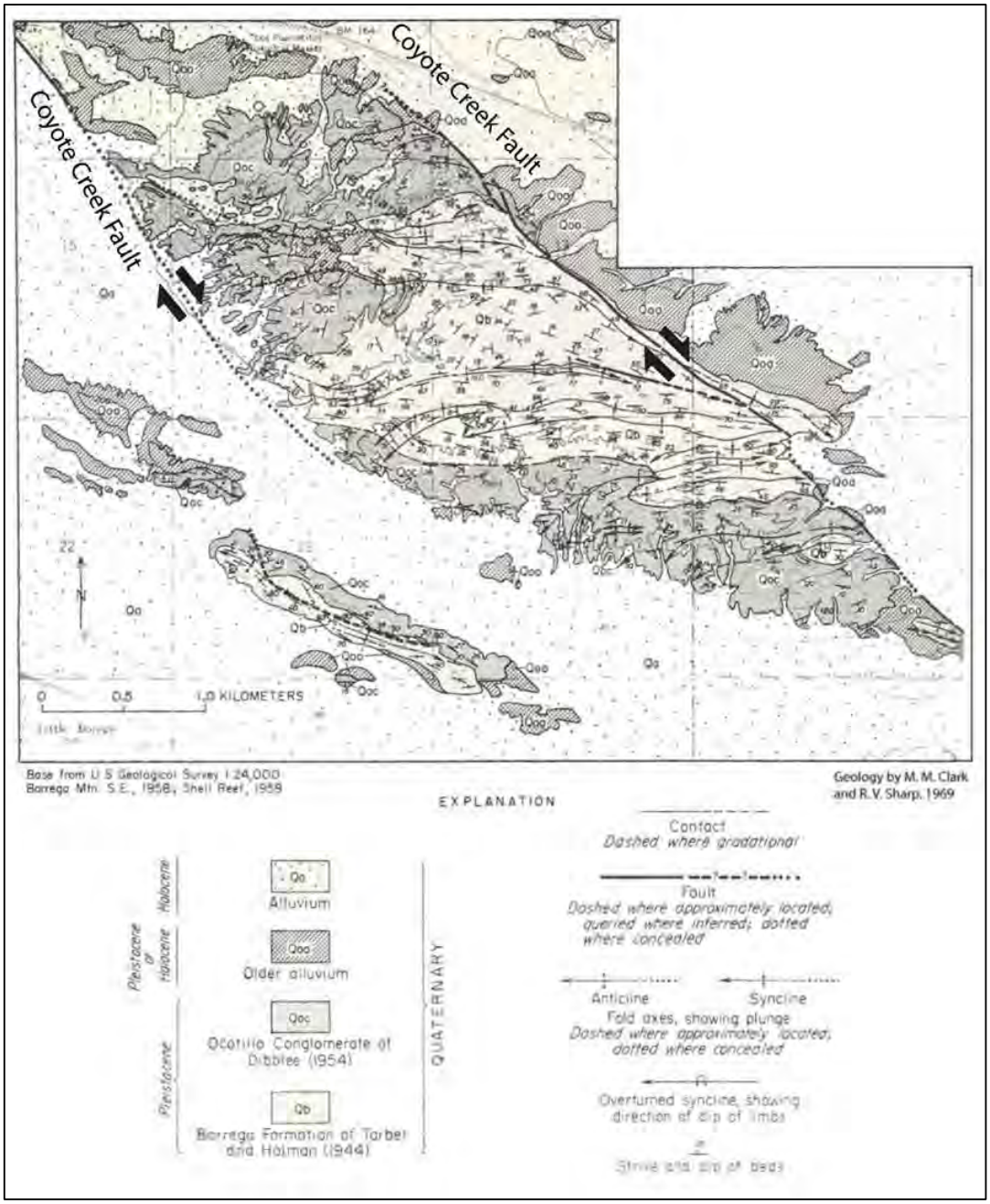

Figure 12. Geologic map of the left step in the Coyote Creek fault at the Ocotillo Badlands. Notice the sigmoidal pattern of folds in between the step. Near the two main strands, folds verge towards parallelism with the strike of the fault. Modified from Sharp and Clark (1972).

Table 1. Predictions of each of the competing geometric models at Durmid Hill

Observed features of Durmid Hill area: below / COMPETING MODELS: TO RIGHT	SAWTOOTH MODEL OF BILHAM AND WILLIAMS, 1989	CROSS-FAULT MODELS OF HUDNUT ET AL., 1989 AND BROTHERS ET AL., 2009	LEFT-STEPOVER MODEL OF JANECKE IN SCEC PROPOSAL 2012	LADDER-LIKE-MODEL OF JANECKE AND MARKOWSKI, THIS STUDY
Strong contractional strain adjacent to the NW-striking parts of the main strand of the SAF	**YES**. The sawtooth model predicts contractional strains adjacent to the NW-striking parts of the main SAF.	No, neither cross-fault model predicts contractional strains in this area.	**YES**, the step-over model predicts contractional strain between two right-lateral left-stepping faults.	**YES**, the ladder-like model predicts contractional strain between two right-lateral faults.
Contraction strain adjacent to more northerly striking parts of the SAF south of the hooked spit (see fig. 17 for its location)	No, the sawtooth model predicts no contractional strain south of the more north-northwesterly striking parts of the SAF.	No, neither cross-fault model predicts contractional strains in this area.	**YES**, contractional strain can persist throughout a contractional step-over between its boundaries	**YES**, contractional strain can persist throughout the ladder and outside its rails.
Sigmoidal map pattern of folds in Durmid Hill area.	No, with the sawtooth model the orientation of the folds are predicted to be oriented sub-parallel to the SAF and diverge with distance away from the fault.	No, folds associated with contraction are not predicted, nor are changes in the trends of folds.	**YES**, folds that are oriented sub-parallel to each major fault strand and folds that diverge from them within the transfer zone are predicted.	**YES**, folds that are oriented sub-parallel to each major fault strand and folds that diverge from them within the two side-rails is predicted
One-sided contractional strains that are concentrated almost exclusively on the SW side of the main strand of the SAF	No, one-side strain is not predicted. Neither is it ruled out.	No contraction is predicted by either of these two models.	**YES**, this model predicts strong contraction between the two strand of the SAF and much less shortening outside the step-over structure.	**YES**, this model predicts strong contraction between the two strand of the SAF and much less shortening outside the sheared ladder-structure.
Presence of a major right-lateral shear zone near the Salton Sea shoreline.	No, this model does not predict a second dextral fault strand.	No, this model does not predict a second dextral fault strand.	**YES**, this model predicts a secondary strand of the SAF	**YES**, this model predicts a secondary strand of the SAF
Major east-striking left-lateral faults at Durmid Hill	No, the sawtooth model does not predict any major east-striking left-lateral faults.	No, the cross-fault trigger predicts major northeast to NNE-striking left-lateral and	**YES**, the step-over model predicts major left-lateral faults. Their orientation is not	**YES**, the ladder-like geometry predicts and must contain major left-lateral faults. Their

		left-normal faults, not the observed east-striking ones.	specified but could be E-W.	orientation is not specified but could be E-W.
Tight folds near the northeast shoreline of the Salton Sea	No, the sawtooth model predicts that shortening strain should decrease with increasing distance from the SAF and not increase again at the shoreline of the Salton Sea.	No, folds associated with contraction are not predicted anywhere.	**YES**, folds associated with a second strand of the SAF are predicted near the shoreline of the Salton Sea.	**YES**, folds associated with a second strand of the SAF are predicted near the shoreline of the Salton Sea.
Contraction between the two strands of the San Andreas fault persisting for at least 15 km along the strike of the fault	No, this model does not predict another strand of the SAF.	No	**NO.** Step-overs tend to be smaller in their dimension. There was no sign of either the main strand of the SAF or the East Shoreline strand terminating, as is required for a step-over geometry	**YES**

Does each model predict or explain the observed features of the Durmid Hill area, southern California?

San Andreas fault resembles that of a ladder structure, then the unrecognized strand of the San Andreas fault may buffer the main northeast strand of the San Andreas fault from cross faults (Extra Fault Array) and stress changes originating under the Salton Sea while also resisting the initiation of large ruptures there. There are also certain predictions that can be made about the structural geology of the field area within a contractional step. These predictions include: A. Contractional steps can develop block rotation, connecting faults, and isolated lenses of uplift (Fig. 7, 9, 10, 11, and 13)(Kim et al, 2002). Some of the faults in the steps between master faults show a sigmoidal shape, implying distributed simple shear within the step (Ramsay and Huber, 1983; Kim et all, 2002; Olsen and Pollard, 1991). B. There should also be typical contractional features localized between the San Andreas fault and the East Shoreline strand of the San Andreas fault such as

should be oriented relatively perpendicular to folds axes. The ladder-like model predicts overall contractional strains. C. Uplift further south than the saw-tooth configuration. D. Sigmoidal map pattern of folds (Fig 9 and 10). E. The secondary strand of the San Andreas fault (East Shoreline strand of the San Andreas fault) exists.

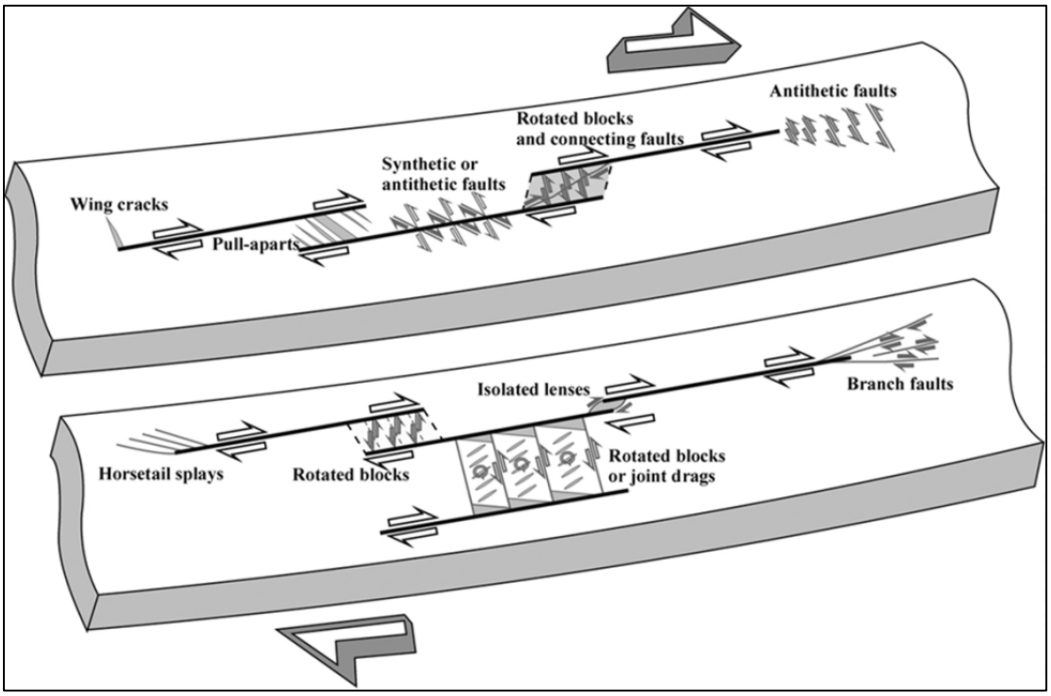

Figure 13. Structures associated with strike-slip fault step-overs. Left-steps in dextral faults produce contractional structures such as isolated lenses of uplift, reverse or thrust faults, positive flower structures, antithetic faults, synthetic faults. Right-steps in dextral faults produce pull aparts, normal faults, negative flower structures. Fault tips produce a variety of structures including branch faults, horsetail splays, and wing cracks. Figure from Kim et al. (2002).

OTHER TECTONIC ASPECTS OF THE SALTON TROUGH

Volcanism in the Salton Trough

Localized recent and late Pleistocene volcanic rocks in the Salton Trough along with data from high heat flow, exploration drill holes, and geophysical studies show that large volumes of young magmatic material are present in the subsurface beneath the central axis of the Salton Trough (Herzig and Elders, 1988; Elders and Sass, 1988; Schmitt and Hulen, 2008; Schmitt et al., 2013). A two-stage tectonic model has been proposed to explain rifting synchronous with major strike-slip faulting. Recent U-Pb zircon geochronology studies have documented pulses of rhyolite volcanism in the Salton Trough between 420 and 479 ka using U-Pb zircon geochronology (Schmitt and Hulen, 2008). Comparing these dates and depths to the Bishop Tuff (770 ka) from the State 2-14 Borehole, suggest rapid subsidence rates near the center of the Salton Trough (Herzig and Elders, 1988; Elders and Sass, 1988; Schmitt and Hulen, 2008).

Geothermal System of the Salton Sea

Geothermal activity and the latest Holocene volcanism in the southernmost Salton Sea are spatially associated within the Brawley seismic zone. There is a change in the geometry of the plate boundary from a more localized San Andreas fault, with an roughly N45°W strike, in the north, to the broad complex Brawley seismic zone with a N20°W strike (Kelly and Soske, 1936; McKibben et al., 1987; Schmitt and Vazquez, 2006;

Mazzini et al., 2011; Schmitt et al., 2013). This study explores the junction where these two major structural elements exhibit changes, but volcanism and geothermal activity are strictly restricted to within the Brawley seismic zone.

The Salton Sea geothermal system currently has 11 power plants that produce roughly 400 megawatts per year (U.S. Energy Information Administration, 2014). The active geothermal field, southeast of the Salton Sea, is associated with a northeast-trending zone of localized episodic rhyolite volcanism and coupled with high heat flow, metamorphism, and basaltic intrusive activity (Schmitt and Hulen, 2008). These include the presence of surficial features such as gryphons or mud volcanoes (Schmitt and Hulen, 2008).

The geothermal field is also responsible for the active metamorphism and transformation of Cenozoic rocks into low-grade green-schist facies at about 3,000 feet (914.4 m) (Muffler and White, 1969). Aeromagnetic maps also agree with Bouygues gravity maps in the Salton Sea Geothermal Field. They show where intrusive rocks penetrate the shallow crust and where mineralized faults are located (Biehler, 1971; Griscom and Muffler, 1971; Younker et al., 1982; Hulen et al., 2003). Hematite seems to precipitate along them and therefore we can see them on filtered aeromagnetic maps (Hulen et al., 2003).

Background About the Late Cenozoic Stratigraphy of the Salton Trough

Sedimentary rocks within the Salton Trough range from late Miocene to Holocene and are mostly deltaic and lacustrine sands, silts, and clays (Fig. 14)(Dibblee, 1954;

Babcock, 1974; Dibblee, 1984; Dibblee, 1996; Winker and Kidwell, 1996; Kirby, 2005; Kirby et al, 2007; Steely, 2006; Steely et al., 2009; Dorsey et al., 2009; Dorsey et al., 2011). The mud-rich Brawley and Borrego Formations are dominant in the central, lowest parts of the valley whereas sand, pebbly sandstone to conglomerate, and sedimentary boulder breccias dominate along the basin margins (Fig. 15)(Dibblee, 1954; Babcock, 1974; Dibblee, 1984; Herzig et al, 1988; Dibblee, 1996; Winker and Kidwell, 1996; Kirby, 2005; Kirby et al, 2007; Steely, 2006; Steely et al., 2009; Dorsey et al., 2009; Dorsey et al., 2011). The sediments near the depositional axis of the Trough are deltaic sand, silt, and clay deposited by the Colorado River and lacustrine processes. Sandstones were deposited in lakeshores, meandering channel fills, and lacustrine delta environments (Herzig and Elders, 1988). These Colorado River sediments are the Palm Springs Group of middle Pliocene and early Pleistocene age (Fig. 14)(Dorsey et al., 2011).). The Arroyo Diablo, Olla formations, and Canbrake Conglomerate are part of the previously defined Palm Springs Formation by Dibblee (1954). Winker and Kidwell (1996) raised the Palm Springs Formation to a group.

The Imperial Group consists of late Miocene to early Pliocene age of marine rocks that varies from sandy turbidites to large subaqueous rock avalanche deposits lain near the basin margins of the Salton Trough (Fig. 14)(Winker and Kidwell, 1996; Dorsey et al., 2011). Below this group of rocks is the Mecca Formation of the late Miocene that varies from maroon to light green colored poorly sorted cobble to small boulder conglomerate (Fig 14).

The Mecca Formation is exposed in the Mecca Hills location (Fig. 2). The main exposures are on the southwest side of the Painted Canyon fault from which it grades up section into Palm Spring formation (McNabb, 2013). It is a conglomerate composed of large angular clasts ranging from cobble to pebble in size. The Mecca Conglomerate alternates from a red maroon oxidized beds to green reduced beds, much like the Shavers Well Formation. In the reduced green sandy units, burrows were discovered (Janecke, unpublished, 2014), raising the possibility that these rocks are part of the much older marine Imperial Group. Resolving this correlation is beyond the scope of this project.

Existing Stratigraphic Correlations of Northeast Salton Trough

As an overall goal to better understand the structural geology of Durmid Hill, a good understanding of the stratigraphy and stratigraphic corrections are essential. On the contrary, understanding the structural geology can lead to more insight on the stratigraphy as well.

Seismic reflection profiles, borehole drilling, and other geophysical methods were used to show that meta-sedimentary and igneous intrusive rocks are at the base of the stratigraphic section in the study area and most of the Salton Trough (Muffler and White, 1969; Fuis et al., 1982; Fuis and Kohler, 1984; Elders and Sass, 1988). These basement rocks are at a depth of 2-3 km, and are shallower toward Salt Creek (Fig. 2)(Fuis and Kolher, 1984). The presence of basement highs determined by Fuis and Kohler (1984) are thought to be associated with the geothermal areas in the Salton Trough. But instead

of the granitic crystalline basement rocks that form the Chocolate Mountains it is underlain by dense mafic intrusive rocks (Bürgmann, 1991; Fuis and Kolher, 1984).

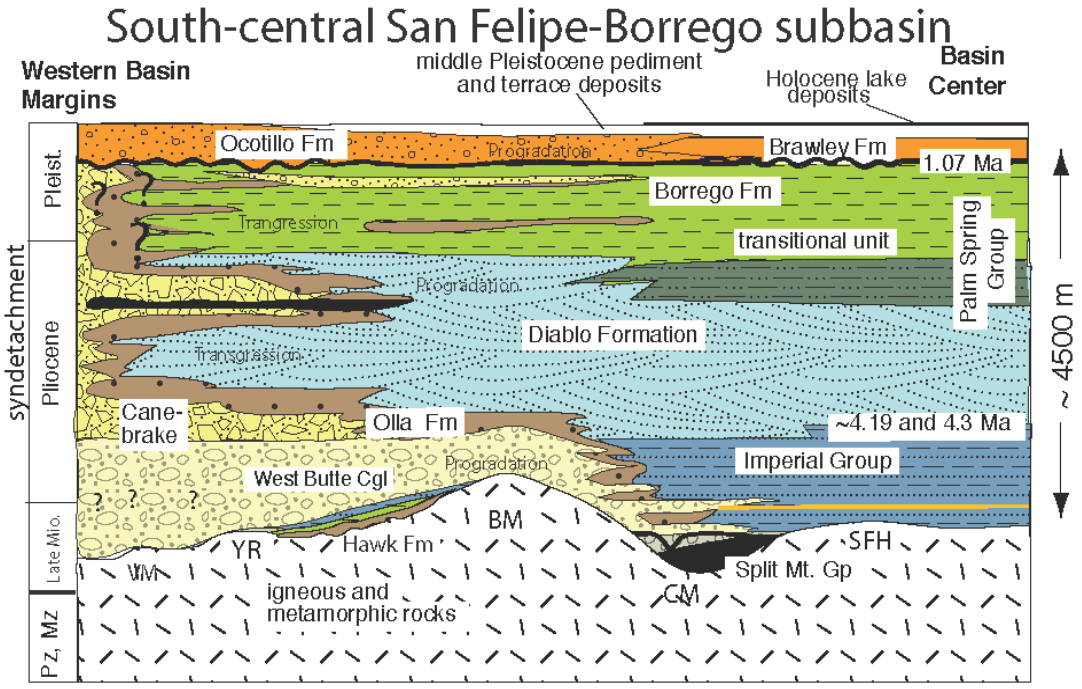

Figure 14. Stratigraphy of the South-central San Felipe–Borrego subbasins . Data were synthesized from many sources, including Dibblee (1954, 1984, 1996); Woodard (1963, 1974); Winker and Kidwell (1996); Dorsey (2002, 2006); Dorsey et al. (2007); Kairouz (2005); Kirby (2005); Lutz (2005); Steely (2006); Shirvell (2006); Belgarde (2007); this study. Work in this thesis shows that this stratigraphy applies to the Durmid Hill area as well. Units found at Durmid Hill include Canebrake Conglomerate, Palm Spring Formation, Borrego Formation, Brawley Formation, and Ocotillo Conglomerate. The Borrego Formation is unusually thin, and may not be present. Modified from Janecke et al. (2010).

The Pliocene (?) Shavers Well Formation at Durmid Hill is a pebble conglomerate and was previously correlated to the Canebrake Conglomerate in the Palm Spring Group (Fig. 16)(Dibblee, 1954; Babcock, 1974; Sylvester, 1988; Bilham and Williams, 1989;

Bürgmann, 1991, Jamison 1991; Dibblee and Minch, 2008; Jennings and Bryant, 2010). This formation is exposed east of the San Andreas fault about 3 kilometers north of Durmid Hill at Bat Caves Butte. In this locality, about 765 meters of the uppermost Palm Spring Formation is exposed and consists of hard, alluvial pinkish gray sandstones and conglomerates (Babcock, 1974). The colors vary from green to light gray and maroon (Fig 18) Units within this formation have both Colorado River derived (c suite) and locally derived (l suite) provenance. C suite provenance includes hematite coated stained quartz grains while l suite provenance includes micas including muscovite and biotie. The upper surface of the Shavers Well Formation is thought to be a depositional contact and the base is not exposed in this locality due to faulting. On the basis of lithological similarities, the lower 550 meters of the formation was assigned to the Sea View Member and the upper 215 meters was assigned to the Skeleton Creek Member (Fig. 16)(Hays, 1957; Babcock, 1968; 1974).

The mud-rich Borrego Formation was deposited in a brackish lake that occupied the Salton Trough and was repeatedly desiccated much like the modern environment (Bürgmann, 1991). It was divided into six informal units (Fig. 15)(Babcock, 1974). It is thought to crop out on the plain northeast of Durmid Hill (Babcock, 1974). The Durmid area itself is dominated by these Pleistocene lacustrine deposits that are upended and highly contorted (Dibblee, 1954). The section exposed at Durmid Hill is about 1,475 meters and consists largely of interbedded claystone, siltstone, and sandstones. Some units contain interbedded gypsum beds and even gypsum cemented sandstone (Babcock, 1974).

Lacustrine sediment is the main Holocene deposits in the Durmid Hill area. During the late Holocene, Lake Cahuilla occupied the Salton Trough, fed primarily by inflow from the Colorado River (Babcock, 1974; Winker and Kidwell, 1986). This left behind sandy sheet deposits, spits, bars, and recessional shoreline deposits after the lake a receded (Bürgmann, 1991). These mud, silt, and sand shoreline deposits once draped these surficial deposits have been removed by the recent uplift and subsequent erosion (Bürgmann, 1991). There are some young alluvium deposits inset along gullies eroding down through Durmid Hill, though most alluvial deposits lie further to the east out of the field area (Dibblee, 1954; Babcock, 1974).

Dibblee (1954) explored the stratigraphy at Durmid Hill and compared the stratigraphic correlations of the Durmid Hill area to strata seen elsewhere in the Salton Trough (Fig. 14). He described 1860 meters (6,100 ft) of lacustrine sediment, the lowest 365 meters (1,200 ft) of which consists of indurated, buff sandstones with interbedded claystones (Fig. 14)(Dibblee, 1954, 2003). The next 823 meters (2,700 feet) of sedimentary deposits are light gray, thin bedded claystones that contain interbeded sand, and layers of evaporites up to 1.5 meters (5 feet) thick as part of the Borrego Formation (Fig. 14)(Dibblee, 1954). The upper 670 meters (2,200 ft) of rock are light gray claystone with a small amount of sandstone similar to that of the Brawley lacustrine facies (Fig 14)(Dibblee, 1954). Dibblee (1954) noticed the similarity to the Brawley Formation but ended up assigning the units to the underlying Borrego Formation.. Although Dibblee (1954) mentioned the presence of more than two formations at Durmid Hill, the two Late Cenozoic deformed units identified in most prior geologic maps are the Plio-Pleistocene

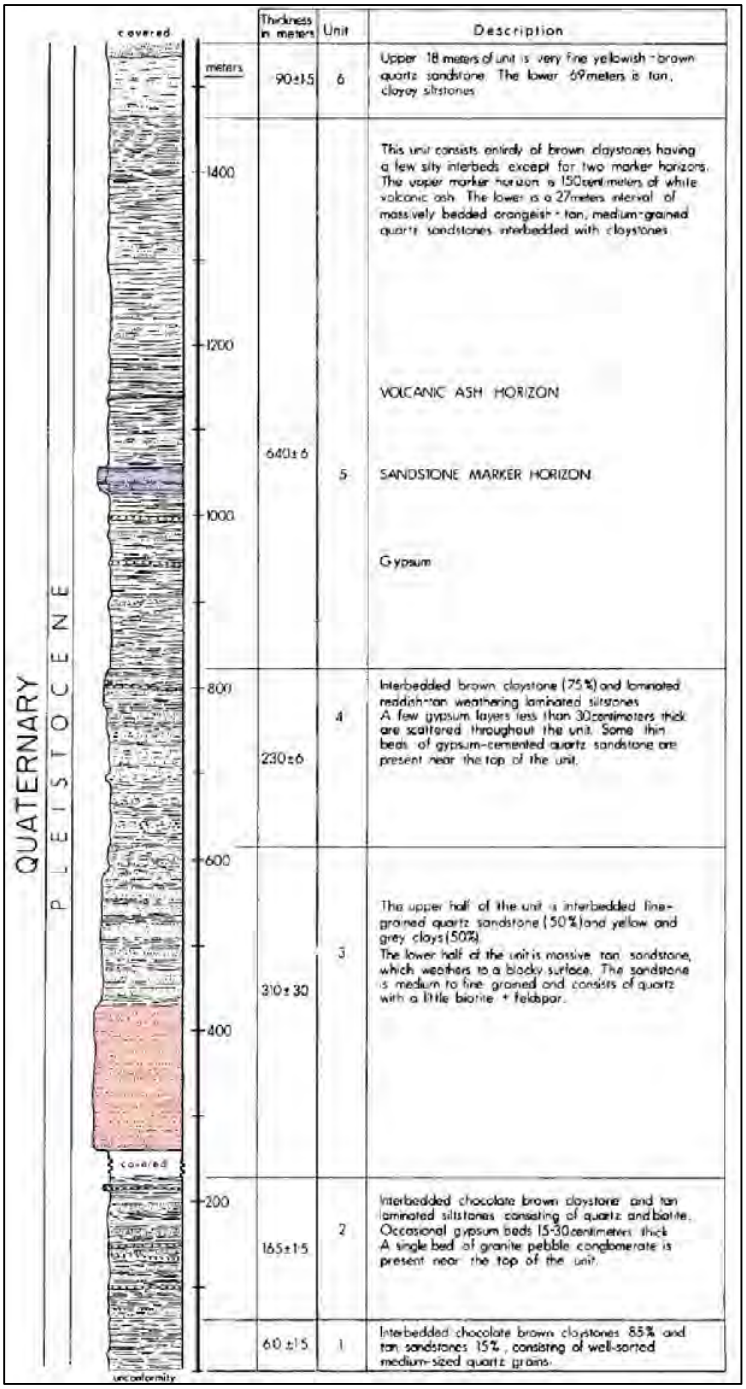

Figure 15. Composite columnar stratigraphic section of the sedimentary rocks in the Durmid Hill area east of the Salton Sea, California. This entire section was mapped as Borrego Formation by Babcock 1974. Modified from (Babcock, 1974).

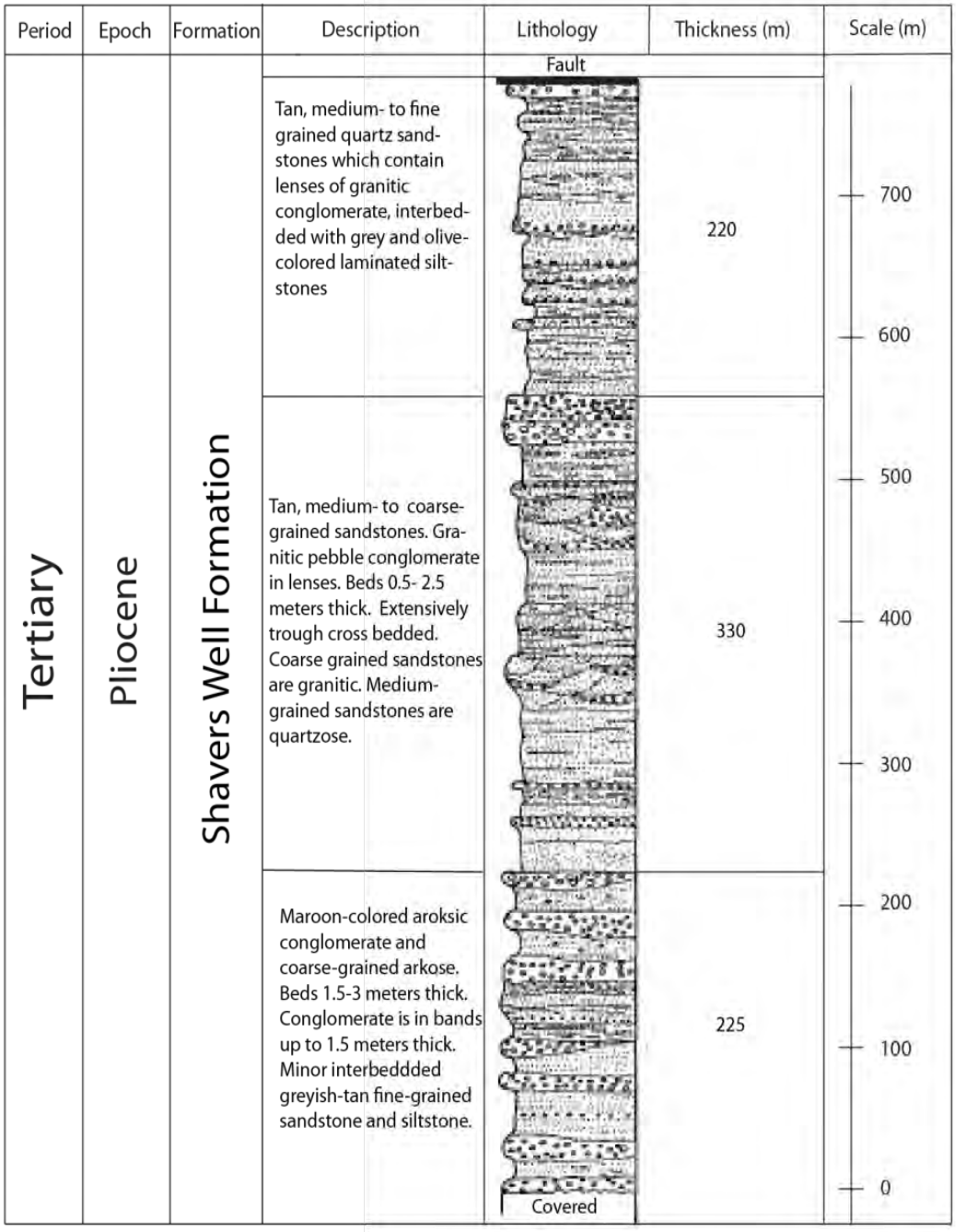

Figure 16. Columnar section of the Shavers Well Formation. Dibblee mapped these rocks as the Palm Springs Formation. Modified from (Babcock, 1974).

Borrego Formation (Fig. 15) and the older Shavers Well Formation (Fig. 16)(Dibblee, 1954; Babcock, 1974; Sylvester, 1988; Bilham and Williams, 1989; Bürgmann, 1991, Jamison 1991; Dibblee and Minch, 2008; Brothers et al., 2009; Brothers et al., 2011). Our fieldwork revise and expand the stratigraphic correlations in the Durmid Hill area.

Babcock (1974) produced a 2 km composite stratigraphic column for the Durmid Hill area and described sandy, silty and gravel-bearing units exposed there (Fig. 15 and 16). However, the composite nature of this stratigraphic column, the lack of a line of section, its mismatch with current nomenclature, new age control, and the likelihood of his having measured section across unmapped faults, somewhat limited its utility for this research.

METHODS AND DATA COLLECTION

In order to test if another strand of the San Andreas fault exists near the Salton Sea, I used a combination of field mapping, data collection, and analysis of remote sensing data. The field data for this study was collected on Jan-Feb 2013 and Dec 2013 and mapping was done in the field and in the office using remote sensing data. Using new technology and more mapping, I was able identify and characterize many small to moderate displacement faults, their associated damage zones, the block-in-matrix damage on the southwest side of the main strand of the San Andreas fault zone, and the major East Shoreline strand of the San Andreas fault near the Salton Sea.

In order to identify faults, fold axes, marker beds, and offset streams or drainages, I used Google Earth imagery (5/28/2005 to 5/27/2012), B4 LIDAR dataset in Open Topography, Salton Sea LIDAR dataset in Open Topography (http://www.opentopography.org/), NAIP (National Agricultural Imaging Program) data (http://atlas.ca.gov/casil/imageryBaseMapsLandCover/imagery/naip/naip_2012/doqqs_combined_color-nir/33115/), and 1 foot spatial resolution orthoimagery (http://viewer.nationalmap.gov/viewer/) were the imagery sources. Preliminary maps drafted in the lab were used to aid field mapping and to more efficiently gather data on the ground.

The most commonly used dataset for mapping was NAIP data and processing techniques were used to highlight the geology. The NAIP dataset includes four bands, that are red, green, blue, and infrared. The infrared band was put in the place of the red band and then saturation and contrast levels were boosted. The result enhanced the colors

of various lithologies and essentially made it possibly to call out different rock types from the imagery with quick field checks.

A Panasonic Toughbook computer was used in the field to locate, map, and compile structural and stratigraphic data. All of my data points are plotted in the NAD 83 datum, consistent with Google Earth's datum. A Garmin GPS capable of recording NAD 83 was used for backup. Data such as stop number, bedding and fault orientation, and other important information were recorded in Google Earth kmz files. In addition to Google Earth, the data recorded consists of a number of important stops recorded in a field notebook. More detailed observations and descriptions is written in the field book and each field date was noted and supplemented by a corresponding kmz file and GPS capable pictures (see appendicies and attached cd).

Different geophysical methods were used in order to map and make different interpretations within the field area. The methods used include GPS (Tong et al., 2012), InSAR (Lyons and Sanswell, 2003; Sneed and Brandt, 2011; Tong et al., 2012), seismicity (Hauksson, 2000; Lin et al., 2007; Hauksson et al., 2012; Lin et al., 2013), gravity (Babcock, 1969; Biehler, 1971; Fuis and Kohler, 1984; Langenheim et al., 2007; Langenheim and Christensen, 2011; Langenheim et al., 2012; Langenheim et al., 2014), and magnetic maps (Babcock, 1969; Griscom and Muffler, 1971; Langenheim et al., 2012), that allow for identification of structures that are not seen at the surface. GPS and InSAR measurements allow for the estimate of ground movement and rates. Relocated seismicity allows us to see faults in the subsurface. Gravity and magnetics help to determine depth the anomalous bodys or depth to basement rocks. Geophysical datasets

allow us to test our structural interpretation of the area and to project major structures outside of the field area.

The data collected in the field was used to help test the hypothesis that there is a strand of the San Andreas fault near the Salton Sea separate from the main strand of the San Andreas fault. This data includes the locations and traces of faults, damage zones, and contacts such as bedding traces, structural data such as strike and dips of fault planes, bedding planes, and trend and plunge of slickenlines. Slickenlines and offset bed markers were used to aid in determining the sense of slip along faults. Stratigraphic relations and locations of key marker units were used to identify deformation and sense of movement.

The first key task was to characterize the San Andreas fault zone, the east-west left-lateral fault zone, and the hypothesized East Shoreline strand of the San Andreas fault. Structural analysis, stereonets, cross-sections, slickenlines, and detailed descriptions are all factors that helped to characterize the area into separate domains. Domains are defined to have similar strikes of faults and similar trends of fold hingelines, and to have similar intensities and styles of deformation. After the first analysis of domainal boundaries and structures within them, the boundaries were repositioned slightly in order to better differentiate between domains with gradational boundaries. Average orientations of structural elements were calculated within each domain. Once structural domains were clearly laid out, structural analysis revealed the trend and plunge of the dominant fold axis, attitude of the axial surfaces, typical limb dips, and orientations of faults within each domain.

In the fold analysis, equal area lower hemisphere stereonets were used. Kamb

contours were calculated with intervals ranging from one sigma to two sigma. Then dominant limbs for each fold in each domain were picked. The error in the interlimb angles of fold was calculated by counting five sigma from the dominant limb contours along the plane to the pole of the fold axis. These four values were averaged to calculate the angle of error. In multimodal domains where the folds have more than one dominant limb, an average limb was picked favoring the limb with a higher cluster of data.

To determine the thickness of the Brawley Formation, cross-sections were used. This constrains how much stratigraphy is missing from the faulting of the East Shoreline fault zone. These cross-sections were strategically picked and done in piecewise fashion in order to miss the many important faults that would underestimate the total thickness. Distinct marker beds that were mapped prior using image analysis and field work was the primary focus of the cross-sections. Cross-sections were also used to determine and estimate the amount of stratigraphic section cut out by the East Shoreline fault zone.

RESULTS

Understanding the sedimentary sequences of the Salton Trough is crucial for understanding the Quaternary to late Tertiary structural geology of the region. The deposits, their ages, and thicknesses add important information about time-space patterns of deposition and deformation, and thus the tectonic evolution of the Salton Trough. In addition, these data can aid in developing a better understanding of the role of bends in the strike of the San Andreas fault in deformation, or more localized relationships between weak mud and gypsum and the characteristics of folding and faulting. Large sections of stratigraphy missing can be a clue to the presence of a large fault. Visual offset or deformation observed by various geophysical datasets can also aid in understanding the structural geology of the study area.

Stratigraphy

Based on field mapping, mapping using remote sensing, and the creation of a stratigraphic column, we revise the age, lithology, correlation, and formation names of several map scale units in the Durmid Hill area relative to the earlier work. We propose a revision of the sedimentary stratigraphic nomenclature in the Durmid Hill area. Results of this study have identified the Brawley Formation, Arroyo Diablo and Olla formations, Canebrake Conglomerate, and Shavers Well-Mecca? formation (Plate 1 and Plate 2).

Brawley Formation covers most of the field area at Durmid Hill (Plate 1 and Plate 2). From Bombay Beach to Durmid Anticline the Brawley Formation is exposed on the

surface and highly folded and faulted (Fig. 17). Towards the shoreline of the Salton Sea and in a few select locations to the east of Highway 111, the upper Brawley Formation is exposed (Fig. 17, Plate 1 and Plate 2). In this location, upper Brawley Formation and lower Brawley Formation are significantly deformed in the East Shoreline fault zone (Plate 1).

From Durmid Anticline to the west and northwest the Arroyo Diablo Formation is exposed (Fig. 17, Plate 1 and Plate 2). Also exposed in this area is Olla Formation and Canebrake Conglomerate (Plate 1 and Plate 2). In this locality the rocks are so heavily sheared that bedding traces cannot be resolved and nor can a clear contact between the interfingering Arroyo Diablo, Olla, and Canebrake geologic units (Plate 1 and Plate 2).

In the far northwest of the field area, at Salt Creek, Borrego Formation is juxtapose Shavers Well Formation and this is the only location in which the Borrego Formation is exposed.

The oldest rocks in the field area are the Shavers Well Formation and they are exposed at Bat Caves Butte on the Northeast side of the San Andreas fault (Fig. 17). Babcock (1974) estimated a thickness of about 765 m but the basal contact is not exposed. The rock types vary from green to light gray and maroon arkosic coarse sandstones to granitic pebble conglomerate (Fig. 18). Units within this formation have both c suite and l suite provenance and cross-bedding is a common sedimentary structure observed within the Shavers Well Formation. The rocks here are much more resistant to erosion than rocks on the southwest side of the San Andreas fault and form a topographic high.

Arroyo Diablo Formation and Lateral Equivalents

The oldest rocks in the study area on the southwest side of the San Andreas fault in Durmid Hill are medium to thick bedded sandstones that are exposed in two complex plunging anticlines and in fault blocks farther north (Plate 1). This is where the Arroyo Diablo crops out at Durmid Hill southwest of the San Andreas fault and west of Range Road at Durmid Anticline (Fig. 17). It is a resistant yellow-brown to tan, medium to coarse grained sandstone (Fig. 19). Sandstones are interbedded with mudstone but contain more sand-rich beds than mudstone within it. The unit fines up section from sections below that are as much as 70% sand. The quartz grains are within the sandstone are reddish and hematite coated typically associated with Colorado River derived sediments. It does not contain gypsum of any type or any ash intervals like the above Brawley Formation. Local residents have reported that petrified wood weathers out of this formation. Concretions are abundant and they range in size from gravel to boulder-sized and elliptical to round. Outcrops of Arroyo Diablo Formation form large anomalous exposures or blocks of rock in some areas. Durmid anticline is an example of where a coherent block of Arroyo Diablo crops out (Fig. 17 and 19).

The Olla Formation is defined as containing more locally-derived arkosic and mica-rich sand grains than pink, iron-coated quartz grains from the Colorado River (Winker and Kidwell, 1996; Kirby et al., 2007; Steely et al., 2009). It is a lateral equivalent of the Arroyo Diablo Formation that occurs along the margin of the Salton

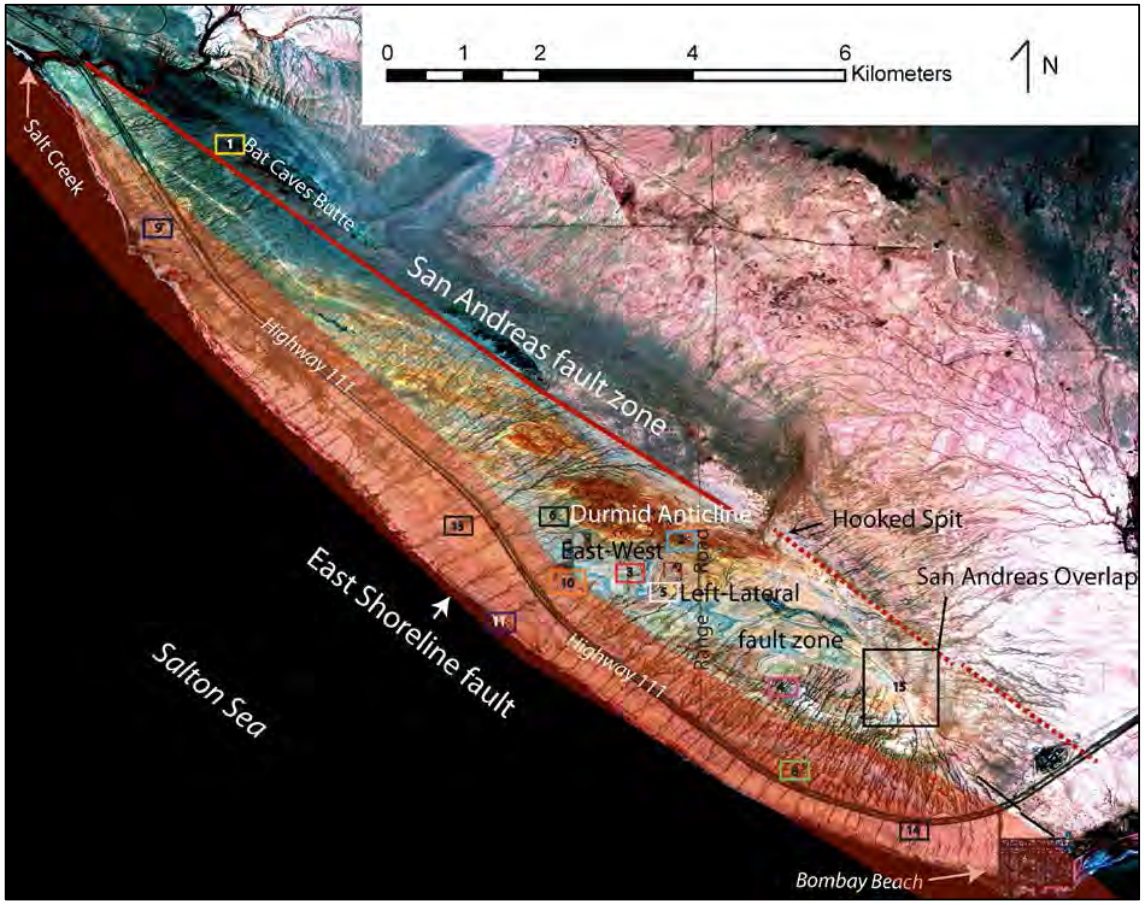

Figure 17. Map of relevant geographic locations in this study. The three major faults zones are highlighted, the major roadway access, Salt Creek, Bat Caves Butte, the hooked spit, San Andreas Overlap, and Bombay Beach. The different colored boxes are locations of field photographs described later in this thesis. The red transparency denotes the broad damage zone of the East Shoreline strand of the San Andreas fault. A similar broad damage zone is present along the main strand of the San Andreas fault southeast of the hooked spit, but it is not shown here.

Figure 18. Field Photographs of the Shavers Well Formation. Photograph locations can be found on Fig. 17 location number 1. All photographs are southeast looking except for the bottom right photograph.

basin and interfingers with the Arroyo Diablo Formation northwest of Durmid Anticline (Fig. 17). Northwest of this anticline Arroyo Diablo Formation becomes less continuous, and is severely sheared (Plate 1). Within these highly deformed damage zones is mostly Arroyo Diablo Formation and Olla Formation. Discrete boundaries are complex because they are all highly sheared within a matrix of Brawley Formation.

Further to the northwest near Salt Creek, a finer equivalent of Canebrake Conglomerate appears to be present (Fig. 17, Plate 1 and Plate 2). It is dominantly a

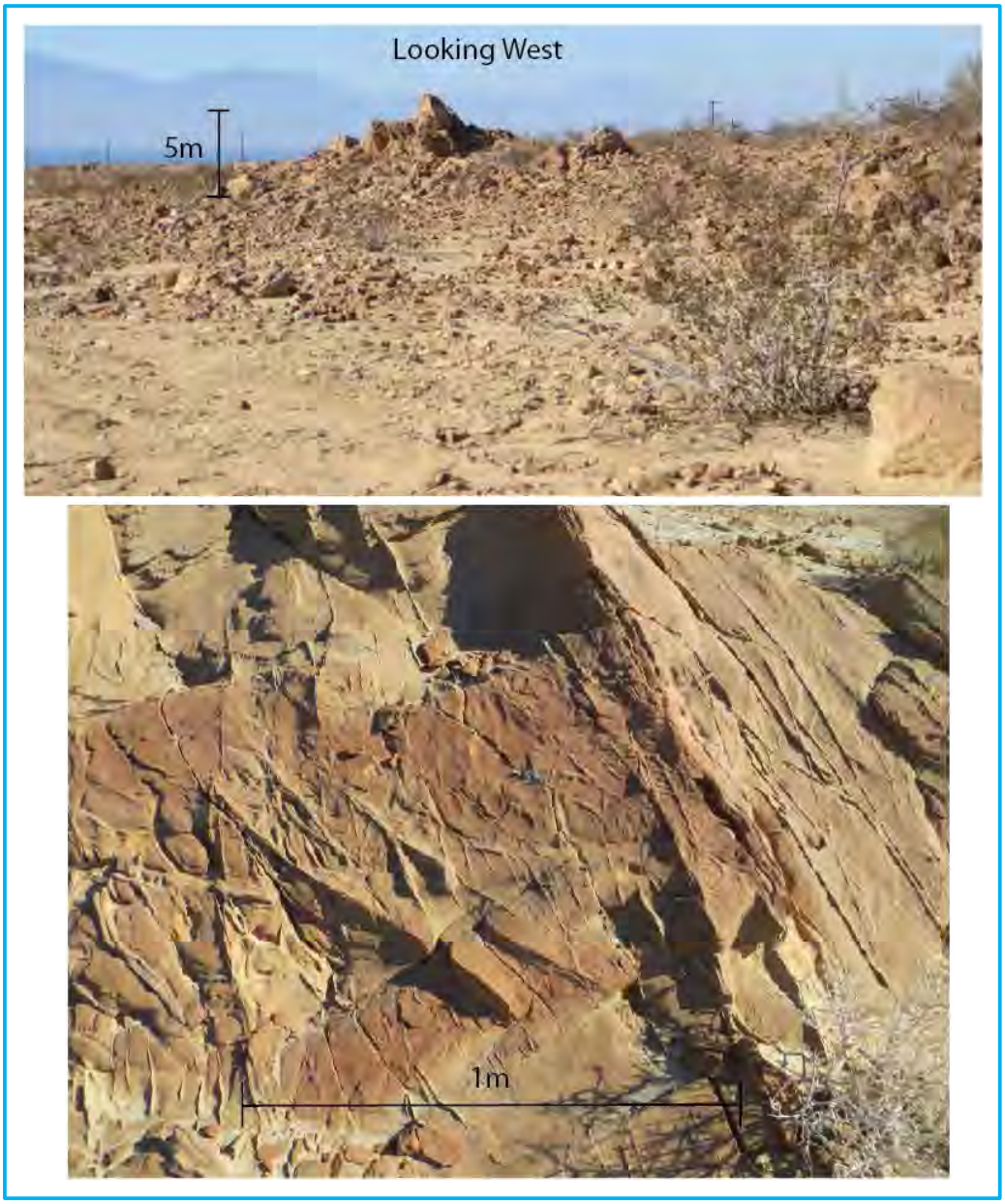

Figure 19. Field photographs of the Arroyo Diablo Sandstone exposed near Durmid Anticline. Photograph locations can be found on Fig. 17 location number 2.The Arroyo Diablo is a resistant sandstone, which underlies the majority of the crest of Durmid Hill. The creosote bush is about 1.5 m high. The lower photograph highlights deformation bands that are common throughout the Arroyo Diablo Sandstone in the field area. Note how the complex conjugate sets of deformation bands mirror the map patterns of structures in this area.

granitic pebble conglomerate but alike the Olla and Arroyo Formations at Durmid Hill, the Canebrake Conglomerate is sheared into a matrix of Brawley Formation. The nature of the upper and lower contact is unknown or not exposed and is most likely faulted. It is similar to Shavers Well Formation in that it is composed of granitic and schist clasts. Unlike the Shavers Well Formation at Durmid Hill, the Canebrake Conglomerate ranges from granitic pebble conglomerate to red interbedded mudstones.

Brawley Formation

The Brawley Formation and its coarser lateral equivalent, the Ocotillo Formation, are the youngest highly deformed units in the stratigraphy at Durmid Hill. The Brawley Formation is made up of mudstone, claystone, siltstone, sandstone, bedded gypsum, minor pebble conglomerate, and ash beds (Fig. 20). Sedimentary structures that are common in the Brawley Formation include channel fills, climbing ripples, and cross-bedded sands, and casts of mudcracks. The type section of this formation is west of U.S. highway 99 and west of the south end of the Salton Sea, where about 610 meters feet of light gray claystone and thin interbeds of buff sandstone is exposed (Dibblee, 1954). I assign the upper 150 meters of the section in Durmid Hill to the Upper Brawley Formation and the lower 1,350 meters to the lower Brawley Formation (Fig. 21). This contact between upper and lower Brawley Formation is an angular unconformity and is faulted in the East Shoreline fault zone (see below) and the San Andreas fault zone.

It is estimated that the Brawley Formation is 1,520 meters thick at Durmid Hill based on the compilation of cross-sections in figure 22. Calculations provide a total

thickness of roughly 1.5 km. This revised value is 400 meters more than Babcock's measured thicknesses but are in line with Dibblee's original estimates (Table 2). Similar thicknesses of latest Cenozoic sediment occur in the Mecca Hills (~1.3 km, McNabb, 2014), and in the same age units above the Arroyo Diablo Formation west of the Salton Sea (~2.3 km; Steely et al., 2009; 2.3 km in Borrego Badlands of Dorsey and Housen as reported in Kimbrough et al. 2015; 1.5 km in an abbreviated section in the Fish Creek-Vallecito basin (Dorsey et al., 2011).

The Brawley Formation in the study area consists of beds with varying compositions, provenance and grain size, bed thickness, and presence of gypsum rich beds. These differences provide unique color differences in the rocks and especially in the imagery. The most important characteristic that affects color is the composition. Colorado River derived sediments or C-suite sediments are red to brown whereas locally derived sediment or L suite sediment consists of mica and typically give the rocks a light blue or green appearance. Key marker units were traced out on the geologic map (Plate b).

In order to learn more about the structural geology of Durmid Hill a composite stratigraphic column was created (Fig. 21). Since there is no complete section that the stratigraphy can be measured at Durmid Hill, piecewise cross-sections were used (Fig. 22). Strategic locations were selected where a majority of the stratigraphy is intact and where no major faults dissect the area (Plate 1). After creating one or more cross sections for each portion of the stratigraphy, it was possible to determine the thickness of the Brawley Formation in the study area of ~1520 meters. The thickness of the Arroyo

Diablo, Olla, and Canebrake were not calculated due to the intense shearing it has encountered northwest of Durmid Anticline (Fig. 17). Thickness of the Shavers Well Formation was beyond the scope of this project.

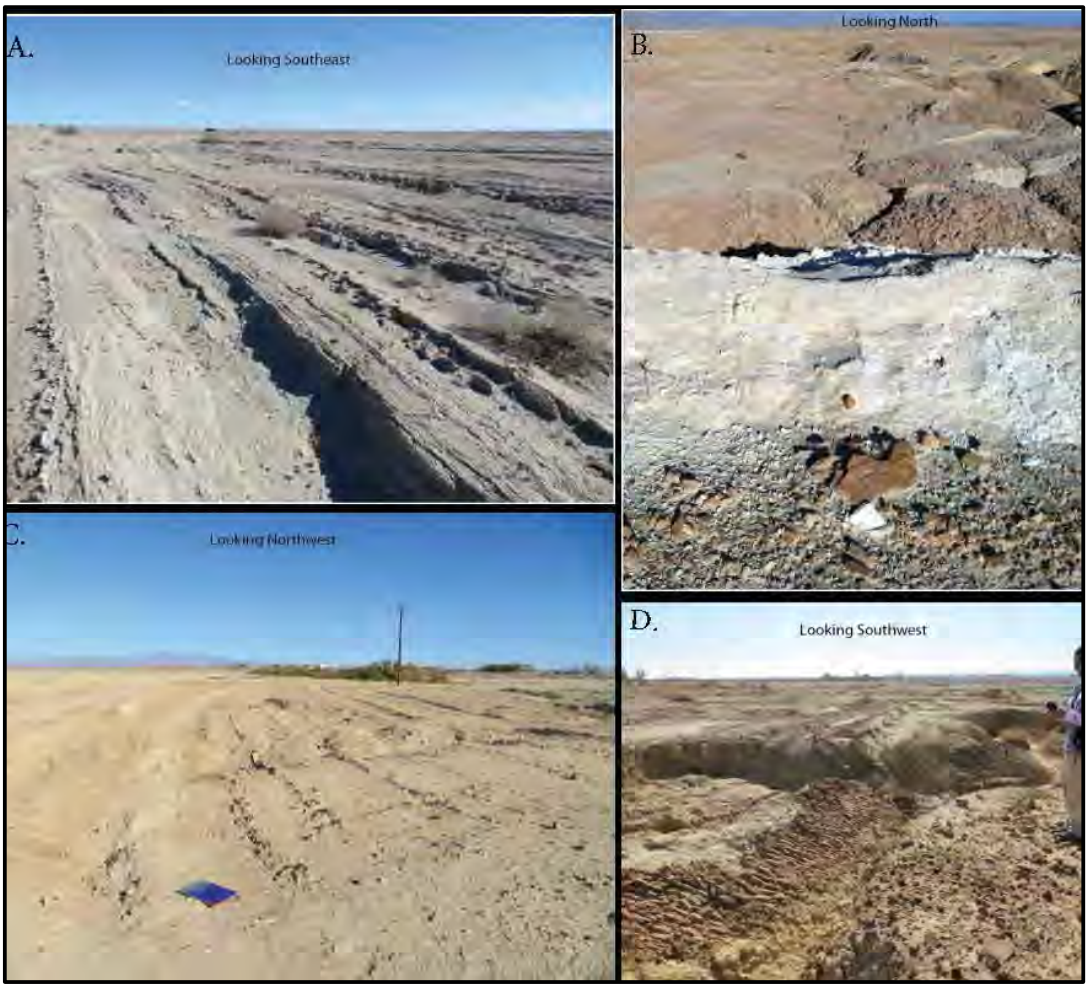

Figure 20. Field photographs of the Brawley Formation at Durmid Hill. A. Upper left photograph (location 3) highlights abundant interbedded thin sandstone beds. B. Upper right (location 4) highlights the Bishop Tuff marker bed. C. Bottom left (location 5) highlights mud-rich sediment with interbedded gypsum. D. Bottom right (location 6) highlights mostly mud-rich sediment with interbedded sandstone and siltstone bedding. Locations of photographs can be found on Fig. 17.

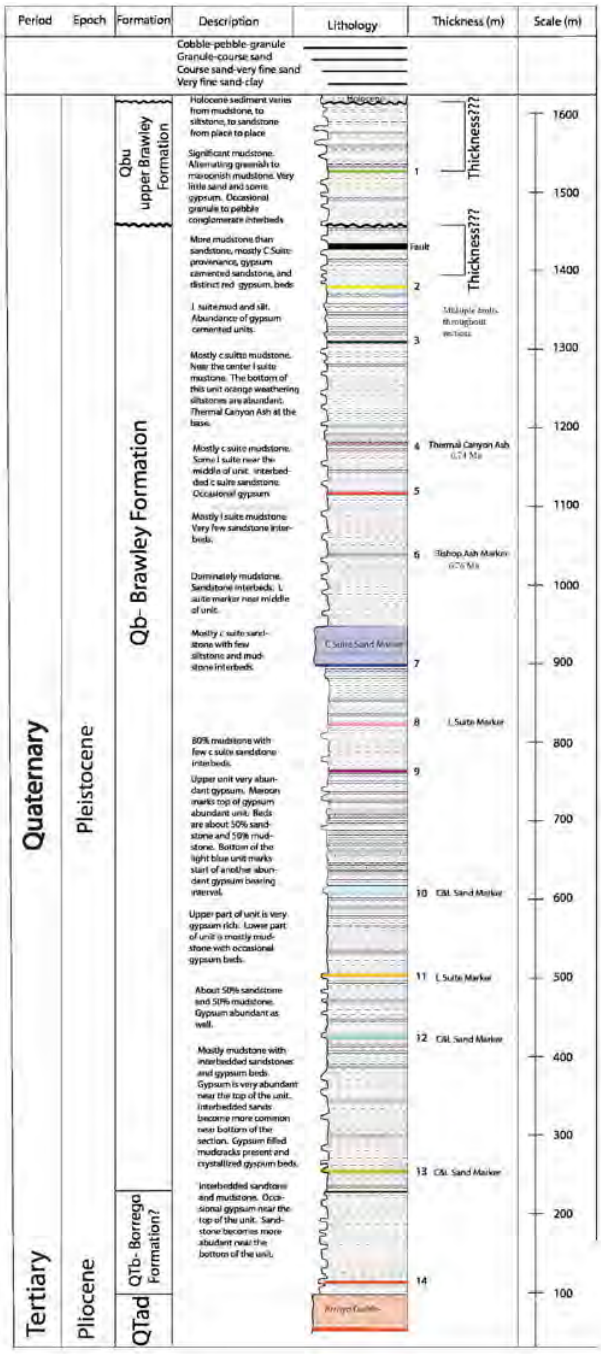

Figure 21. Stratigraphic column of the Upper and Lower Brawley formations. The stratigraphic column also shows the basal contact of the Lower Brawley Formation where it is underlain by the Arroyo Diablo Formation. Thicknesses were determined using cross-sections between the colored marker units. See Table 2 for more data.

Table 2a. Thicknesses of different stratigraphic intervals in the Borrego and Brawley formations.

MARKER BED, YOUNGEST AT THE TOP	Formation or member	Number of cross sections used to constrain the thickness	Thickness of the interval below this marker unit (m) #
Lime Green (1) to the highest unit in cross section	Upper Brawley Formation	1	185?
Base upper Brawley To Lime Green	Lower Brawley Formation	1	70?
Yellow (2) to Forest Green (3)	Lower Brawley Formation	1	70
Forest Green (3) to Purple (4)	Lower Brawley Formation	1	130
Purple (4) to Red (5)	Lower Brawley Formation	1	60?
Red (5) to White/Grey (6) (Bishop)	Lower Brawley Formation	2	70
White/Grey (6) (Bishop) to Blue (7)	Lower Brawley Formation	1	140
Blue (7) to Pink (8)	Lower Brawley Formation	1	75
Pink (8) to Maroon (9)	Lower Brawley Formation	1	60
Maroon (9) to Light Blue (10)	Lower Brawley Formation	2	155
Light Blue (10) to Orange (11)	Lower Brawley Formation	2	105
Orange (11) to Green (12)	Lower Brawley Formation	4	80
Green (12) to Gold (13)	Lower Brawley Formation	2	170
Gold (13) to top of the red marker above the top of the Arroyo Diablo (14)	Borrego Formation ?	1	140
Total thickness	Borrego and Brawley formations		1,510 m

Thicknesses were calculated from short cross-sections in locations of minimal faulting and were rounded to the nearest five meters. Bottom portion of the table compares the difference in thickness between the Bishop Tuff and Arroyo Diablo Sandstone from my study and Babcock (1974). See Fig. 22 and plates 1 and 2 for the map pattern of units.

Table 2b. Comparison of the prior stratigraphic column and that constructed in this study.

	Thickness of the interval between the Bishop ash and the top of Arroyo Diablo Fm (m)
This study	925
Babcock (1974)	710
Difference (m)	215 m more in this study
% Difference	+23%

The age of the lower Brawley Formation at Durmid Hill is well constrained to be lower to middle Pleistocene because it contains the 0.76 Ma Bishop ash near the middle of the formation (Figure 21 and plate 1). This ash was identified and correlated to equivalent units elsewhere in the Salton Trough, including the Palm Spring Formation in the Mecca Hills (Fig. 20)(Hildreth, 1979; Herzig and Elders, 1988; Sarna-Wojcicki et al., 2000; French et al., 2006; Lutz et al., 2006; Crowley et al., 2007; Dorsey et al., 2007; Kirby et al., 2007; Schmitt and Hulen, 2008; Steely et al., 2009; Dorsey et al., 2011; McNabb, 2013).

The Thermal Canyon ash is also exposed elsewhere in the Salton Trough such as the Mecca Hills and was first discovered at Durmid Hill during this study. It is younger than the Bishop ash, dates to about 0.74 Ma, and was deposited about 150 meters above it (Merriam and Bischoff, 1975; Sarna-Wojcicki et al., 2000; Crowley et al., 2007; Rivera et al., 2011). Samples were analyzed and correlated by Dr. Barbara Nash from the

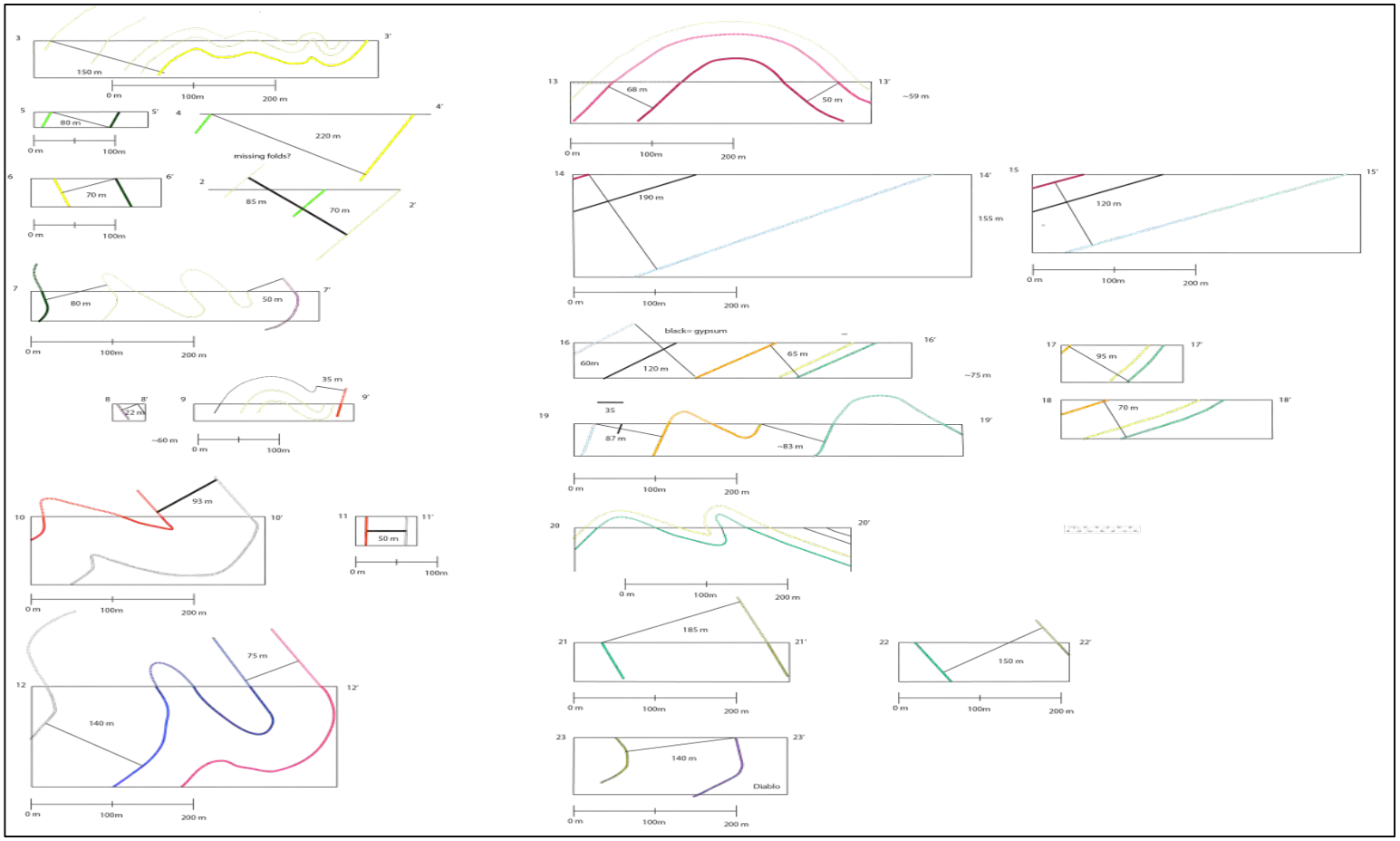

Figure 22. Compilation of short cross sections through fairly intact stratigraphy of the Brawley Formation at Durmid Hill that were created to estimate the thickness of the units. The thickness of the interval between selected marker units is shown on the cross sections. There is no vertical exaggeration and the colors of the lines correspond to the stratigraphic column (Fig. 20). These data were used to determine thickness intervals between units (Table 2). See Plate 1b for locations of the cross sections

University of Utah. The results of sample DM-17 yielded two glass shards in the aliquot that was mounted and matches the type Thermal Canyon Ash sample.

Gypsum is abundant at Durmid Hill and is manifest in a variety of forms within the Brawley Formation. By definition gypsum is found only in the Brawley Formation. Field observations assessed the presence of bedded gypsum, gypsum-cemented sandstones, rose gypsum, recrystallized gypsum in fractures and deformed mudstone (bladed), and various pieces of gypsum in the upper veneer on the surface (Fig. 23).

I do not correlate any units with the deep water Borrego Formation except for rocks of a narrow fault-block of highly sheared red mudstone within the San Andreas fault zone at Salt Creek (Fig.17).

Holocene Deposits

Holocene deposits in the study area include lacustrine, fluvial and eolian sediment. They are less deformed than the underlying units, thin, and in angular unconformity with more tilted folded and faulted sediment. The recent dating of late Pleistocene to 2,500 year old volcanic rocks in the Salton Trough (Schmitt et al., 2013) makes it possible to separate the youngest, volcanic bearing gravels from underlying older barren deposits. Clasts of transported pumice in some of the sediment on Durmid Hill allow Holocene deposits to be definitively discriminated from middle Pleistocene and older lacustrine sediment. Other distinctive features of the Holocene sediments are the presence of contain molluscan shells and are excellent indicators because both of the above are missing in the older, more deformed bedrock. These deposits are typically

dark in the field and on satellite imagery.

Figure 23. Field photographs of the different types of gypsum observed in the field. A. Gypsum filled fractures within a mudstone. B. Recrystallized bladed gypsum within a mudstone. C. Bedded gypsum. D. Rose gypsum float atop the surface.

Field work assessed that most of these Holocene deposits in the field area are flat and overlie the older stratigraphy unconformably. These angular unconformities usually help distinguish the highly deformed Pleistocene rock from the Holocene. In other areas, where deformation is more active, Holocene deposits have been tilted and dragged in fold and fault zones. Faults that cut Holocene sediments can be used to determine active vs. inactive (non-Holocene faults).

Structural Geology

In this study, observations are made about the nature of the southern tip of the main strand of the San Andreas fault at Durmid Hill, where it nears the Brawley seismic zone and other normal-oblique and transrotational structures of the Gulf of California-Salton Trough plate boundary system (Fig. 2). Results for the presence and orientation of the main strand of the San Andreas fault, East Shoreline strand of the San Andreas fault, east-west left-lateral faults, and other subsidiary faults are presented here.

The three dominant fault zones at Durmid Hill presented above are similar in that they all lack a principal slip surface. Instead of the traditional fault core and surrounding damage zone, they are manifest as wide fault zones up to 500 meters wide at the surface. These are characterized by highly disrupted bedding often with very steep to vertical dips. Within the disrupted bedding contain dozens of faults, fractures, deformation bands, and gypsum.

The San Andreas fault is located near the crest of Durmid Hill (Plate 1). The East Shoreline strand of the San Andreas fault is located near the Shoreline of the Salton Sea and the east-west left-lateral faults are located in a domain between these two faults (Plate 1). The fault geometry resembles that of a ladder in which the main strand of the San Andreas fault and the East Shoreline fault are the side rails of the ladder that strike roughly northwest and the East-West left-lateral faults are the rungs of the ladder. In between the dextral side rails are coherent blocks that contain abundant folds and subsidiary faults (Plate 1). To the northwest of Durmid Anticline (Fig. 17), the east-west

left-lateral faults change orientation to a northwesterly strike (Plate 1 b). Here, it is not entirely clear where the boundary between the main strand of the San Andreas fault and the East Shoreline fault is located. Instead, a series of synthetic connecting faults appear to connect the two major structural elements (Plate 1 b).

The field area was split up into four different structural domains based on the information discussed above (Fig. 24). The folds in the field area are very closely related to faulting and generally fold axes are parallel to sub-parallel to the strike of faults in each specific domain.

Folds at Durmid Hill

Four structural domains were identified on the basis of orientation of bedding planes, fold axial planes, and fault orientations (Fig. 24). The numbered domains are also color color-coded to further distinguish them (Fig. 24). Domain one is the San Andreas domain, domain two is the east-west domain, domain three is the transitional domain, and domain four is the Shoreline domain (Table 3).

The San Andreas domain includes primarily dextral strike-slip fault (Fig. 24). The transform plate boundary fault, the San Andreas fault is the northeast boundary of this domain, that narrows to the southeast toward Bombay Beach (Fig. 1 and 24). The open to

tight folds within this domain are generally the tightest of all of the structural domains with an average interlimb angle of about 58°±32°. The southwest limbs of the folds are the steeper limbs by about 8°. The dominant fold axial plane is 295°/86°N and is oblique to the strike of the San Andreas fault by about 15°.

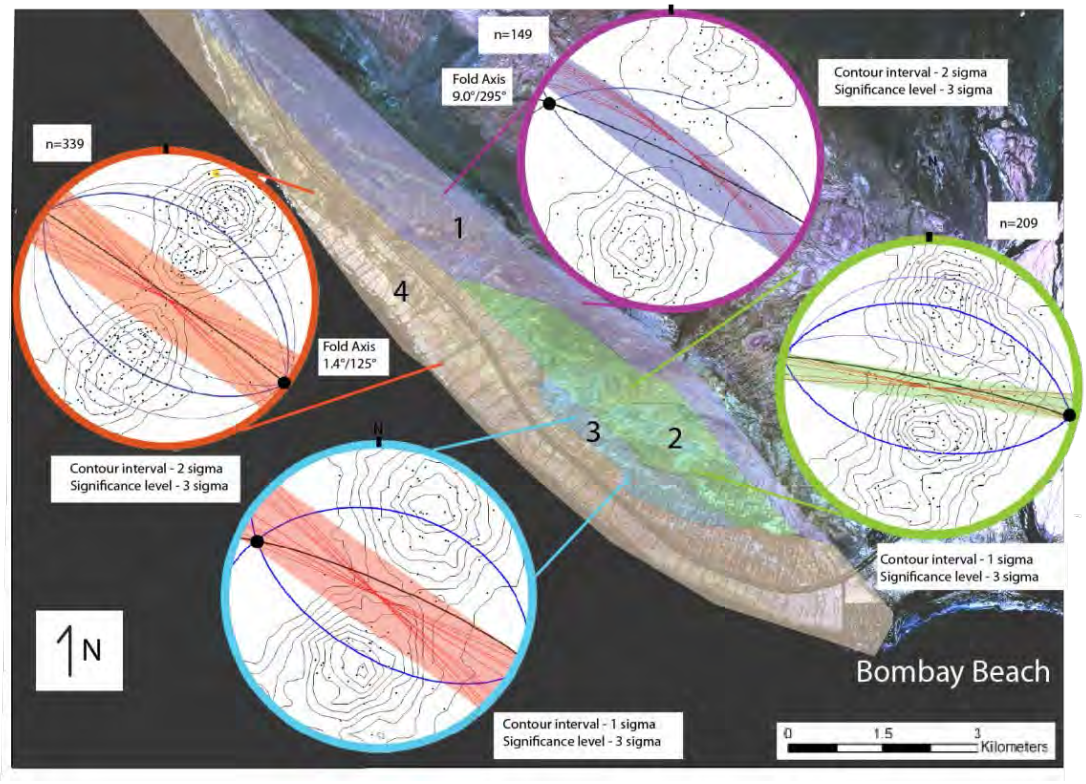

Figure 24. A map of the field area showing the spatial relationship of the four different structural domains at Durmid Hill. The stereonet's outer ring is color coded to match the color of its respective domain on the map. Each stereonet is an equal area lower hemisphere plot. Closed circles are poles to planes of bedding orientation and magnitude of dip. Opened circles are that of overturned bedding. The blue planes are the orientations of the dominant limbs within that domain. Red planes are orientations of the major fault zones within or adjacent to that domain. Shaded red is domain 4 and the East Shoreline fault zone orientations. Shaded green is domain 2 and the cross-over fault orientations. Shaded blue is domain 3 and the transitional domain. Shaded purple is domain 1 and the San Andreas domain. The black plane is the dominant fold axial plane for that domain. Finally, the black contoured lines are Kamb contours. The contour interval and significance level are noted on the figure.

The east-west domain includes primarily east-west left-lateral strike-slip faults (Fig. 24). The faults in this domain are similar to the average orientation of the folds but are oblique by about 5°. This domain is one of the multimodal domains where there is more than one dominant fold limb within the data. The two dominant northern dipping

limbs are 286°/68° N and 279°/26° N. The dominant southern dipping limb is 100°/54° S. The dominant fold axial plane is 281°/78°N. The interlimb angles vary from 59° to 101° but 101° is more dominant. The average dip of the rock is generally the least within the east-west domain. The northern limb averages 50° and the southern limb averages 43°.

The transitional domain includes right-lateral and left-lateral strike-slip faults (Fig. 24). It is located southwest of the east-west domain and is adjacent to the Shoreline domain. Here, the two dominant limbs are 282°/43° N and 121°/58° S. The average fold axial plane is 293°/82°N and is about 10° oblique from the average orientation of the East Shoreline fault zone. The average interlimb angle of the folds are 82°±38° in this domain. The average dip for the southwest limb is 53° and average dip for the northeast limb is 49°.

The Shoreline domain is adjacent to the Salton Sea and is thus the farthest to the southwest (Fig. 24). This domain includes primarily right-lateral strike-slip faults, steep beds, and many folds of the East Shoreline fault zone. The dominant attitude of axial planes is 305°/88°N in folds and faults. This domain is also multimodal and the dominant interlimb angle ranges from 64° to 125° but the average is 92°±15°. The two dominant northeast dipping limbs are 307°/54° NE and 305°/31° NE. The two dominant southwest dipping limbs are 125°/62° SW and 124°/29° SW. The average dip for the southwest limb is 52° and the average dip for the northeast limb is 47°.

East Shoreline Strand of the San Andreas Fault

Results of remapping structures at Durmid Hill suggest a secondary strand of the

San Andreas fault which is southwest of the main strand of the San Andreas fault and in part parallel to highway 111. The fault was not previously mapped and persists southwest of highway 111 to the northeast edge of the Salton Sea (Fig. 17). This fault is named the East Shoreline fault here to distinguish it from the Shoreline fault near the Diablo Canyon Power Plant in San Luis Obispo County, California. The East Shoreline fault is at least partly onshore and could have multiple branch points. Mapping in this study shows traces of the East Shoreline fault that are laterally continuous and are up to 2 kilometers long (Plate 1 b). These traces come onshore near Salt Creek and continue as far south as Bombay Beach (Plate 1 b). The existence and character of the fault is a critical component of our geometric and kinematic model.

Eight key pieces of field data provide evidence for the East Shoreline strand of the San Andreas fault at Durmid Hill. These are: 1) Direct mapped of many tens of traces of steep, northwest-striking dextral faults within the East Shoreline fault zone; 2) Stratigraphic units cut out by the dextral faults within the fault zone 3) High intensity of folding in and adjacent to faults; 4) The near perfect parallelism fold axes and mapped dextral faults. 5) Misaligned sinistral strike-slip faults (east-west left-lateral faults). Other pieces of evidence show that it is an active structure include: 6) Late Pleistocene to Holocene sediment dragged into fault zones; 7) An escarpment and modern fractures in beach deposits within the fault zone; And 8) Growth folds. Multiple fault traces with orientations similar to that of the San Andreas fault (N50˚W) were found within domain 4 (Fig. 25, 26, 27, and Plate 1 b). This domain extends west and northwest of Bombay Beach as far north as Salt Creek (Fig. 24). These faults are typically short, discontinuous,

Table 3. Fold analysis data for each domain

Domain	Number of data	Average S or SW limb	Average N or NE limb	Fold axial plane	Fold axes	Multimodal folds interlimb angle	Average interlimb angle	Strain, fold classification
1. San Andreas	149	58°	50°	295°/86°N	295°/9.0°	58°	58°±34°	Highest average strain Close folds
2. East-West Folds	209	50°	43°	281°/78°N 103°/84°S	279°/1.0° 103°/4.0°	101° 59°	82°±31°	Medium strains Open folds
3. Transition	73	53°	49°	293°/82°N	295°/11°	82°	82°±34°	Medium strains Open folds
4. Shoreline#	339	52°	47°	305°/88°N	125°/1.4°	64° 125°	92°±16°	Lowest average strain Open folds

#Upper Brawley Formation in the East Shoreline domain lies in angular unconformity on structures and dips less steeply than the underlying units. The somewhat lower strains in this domain could reflect the presence of less deformed Upper Brawley Formation units.

.and appear to interact with the east-west fault domain (domain 2); (Fig. 25, 26,27, and Plate 1 b). In areas where the East Shoreline strand of the San Andreas fault deforms upper Brawley Formation, a ladder structure describes the geometry at the surface with part of a leg of the ladder possibly slightly offshore (Plate 1 b). The overall width of the East Shoreline fault zone is about one kilometer but individual damage zones are much narrower and range from a few meters to tens of meters wide (Fig. 25, 26, and Plate 1 b).

The stratigraphy at Durmid Hill is another key indicator of the presence of a major secondary shear zone boundary (Fig. 28). There is about 500-1000 meters of the stratigraphy of the Brawley Formation that has been cut out by the dextral fault (Fig. 27 and 28). This is a gross estimate because in addition to faulting, there are several unconformities in the Brawley Formation that make it difficult to determine the total amount of stratigraphic section missing because of faulting.

Folds parallel faults throughout the map area. In the east and west folds parallel the dextral main strand and East shoreline strands of the San Andreas fault (Figure 24)(Table 3). In between, folds parallel the strikes of the left-lateral faults. Near the shoreline and throughout the field area, folds range from gentle, open, close, tight, to isoclinal, and hinge zones are typically narrow, with the limbs of fold changing abruptly from nearly horizontal to vertical in a matter of meters (Fig. 29 and 30). Overturned folds are common in the East Shoreline fault zone (Fig. 29) and there are many fault-fold pairs there. Faults of the East Shoreline strand of the San Andreas fault often strike parallel to the steep limbs of folds (Fig. 29 and 30). Faults die out into folds and sometimes step lateral through a folded area. Faulted step-overs also occur in the fault zone.

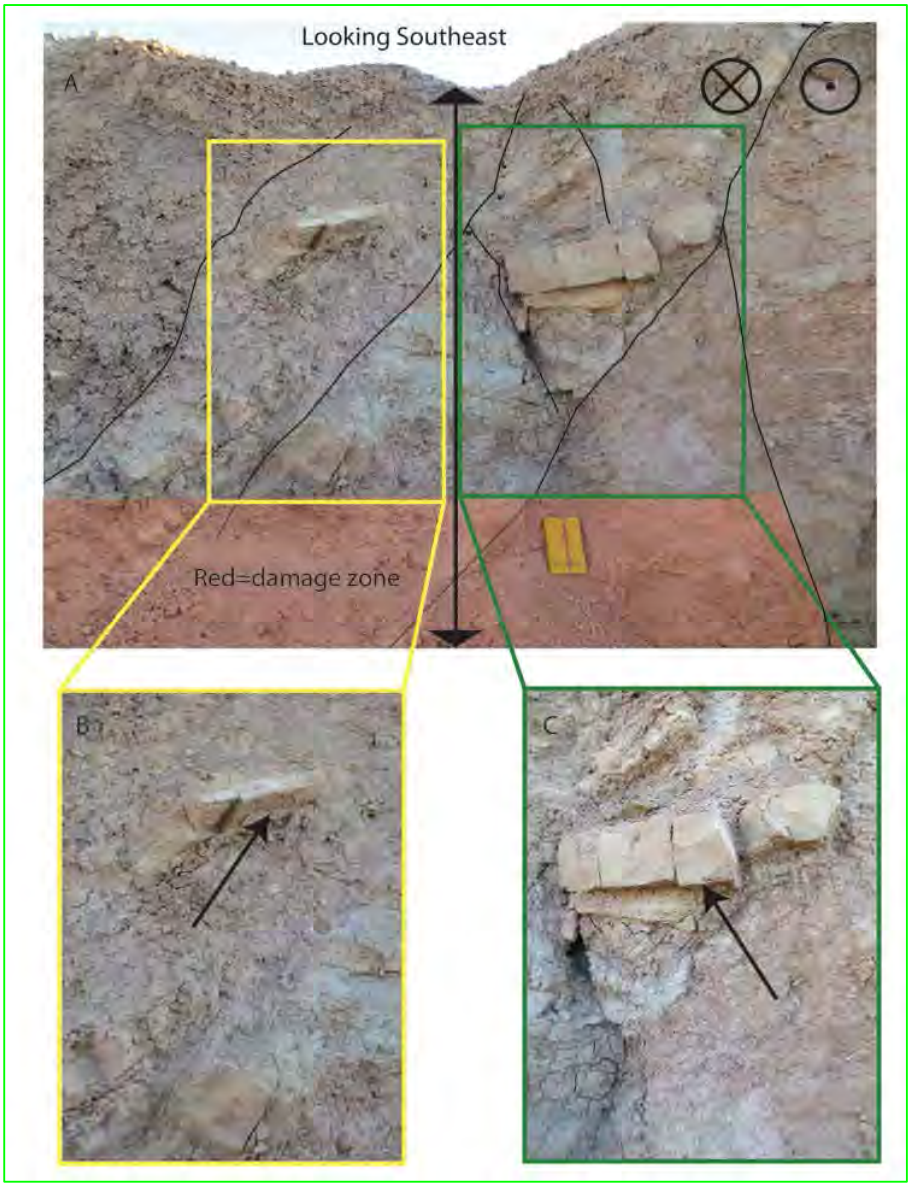

Figure 25. Field photographs of the East Shoreline fault damage zone. Location of this photograph is number 8 and shown in Fig. 17. A) Field photograph of the damage zone of a fault along the East Shoreline Fault. The arrow shows the vertical extent of the damage zone and the ~ 2m width of the damage zone is highlighted in red. The central fault is bounded by the two faults on either side. The red damage zone is only highlighted on the bottom of the image so that details of the photograph remain clear. B) Close up of blocks of sandstone (arrow) floating in a faulted matrix of mudstone within the damage zone. C) Another close up of an even larger block of sandstone (arrow) in the faulted matrix within the damage zone. This is the Brawley Formation.

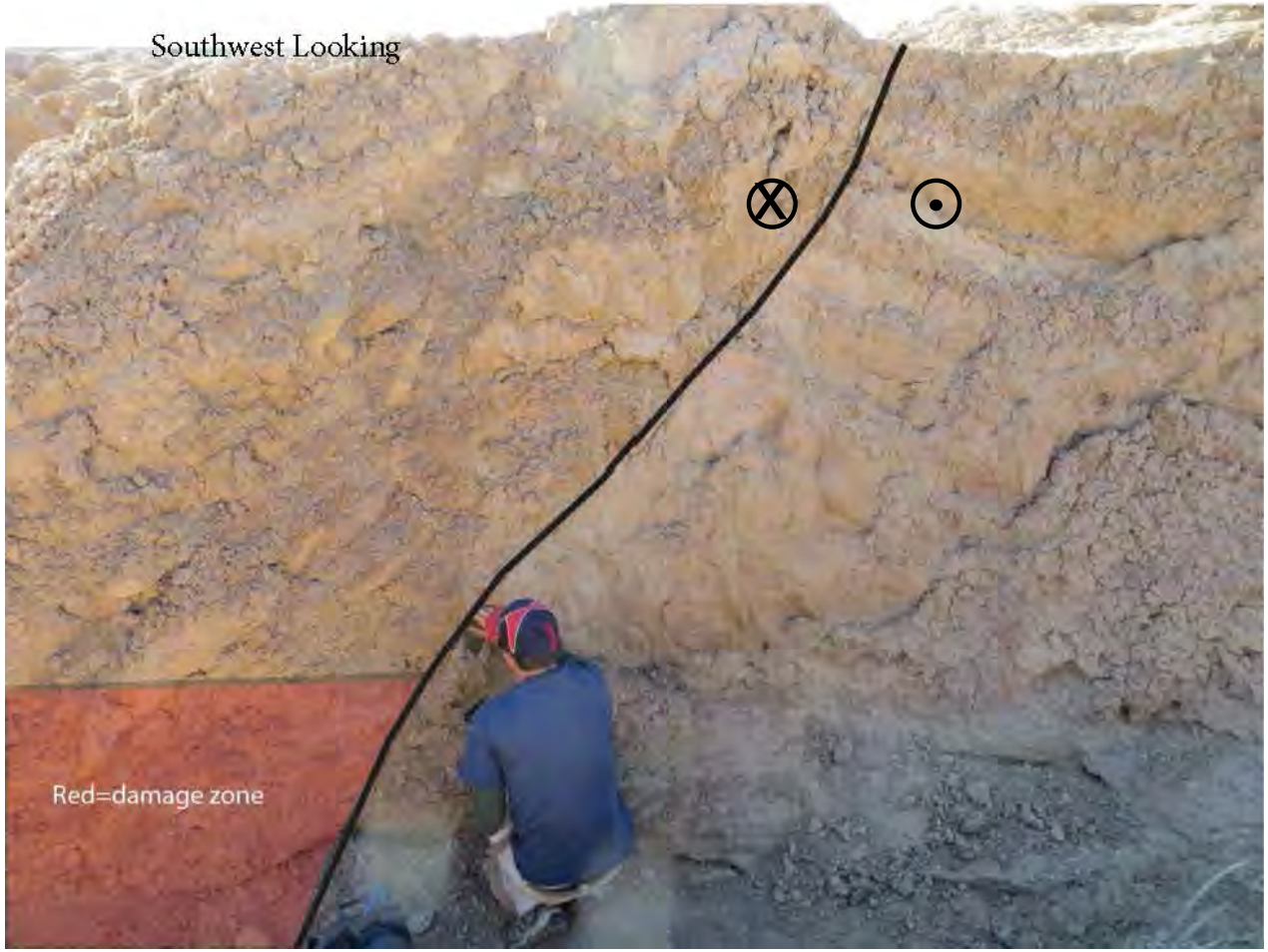

Figure 26. Field photograph of the damage zone of a dextral fault in the East Shoreline fault zone. The width of the damage zone in this photograph is ~1 meter wide. The fault is oriented about 298°/ 75° NE. This is the Brawley Formation.

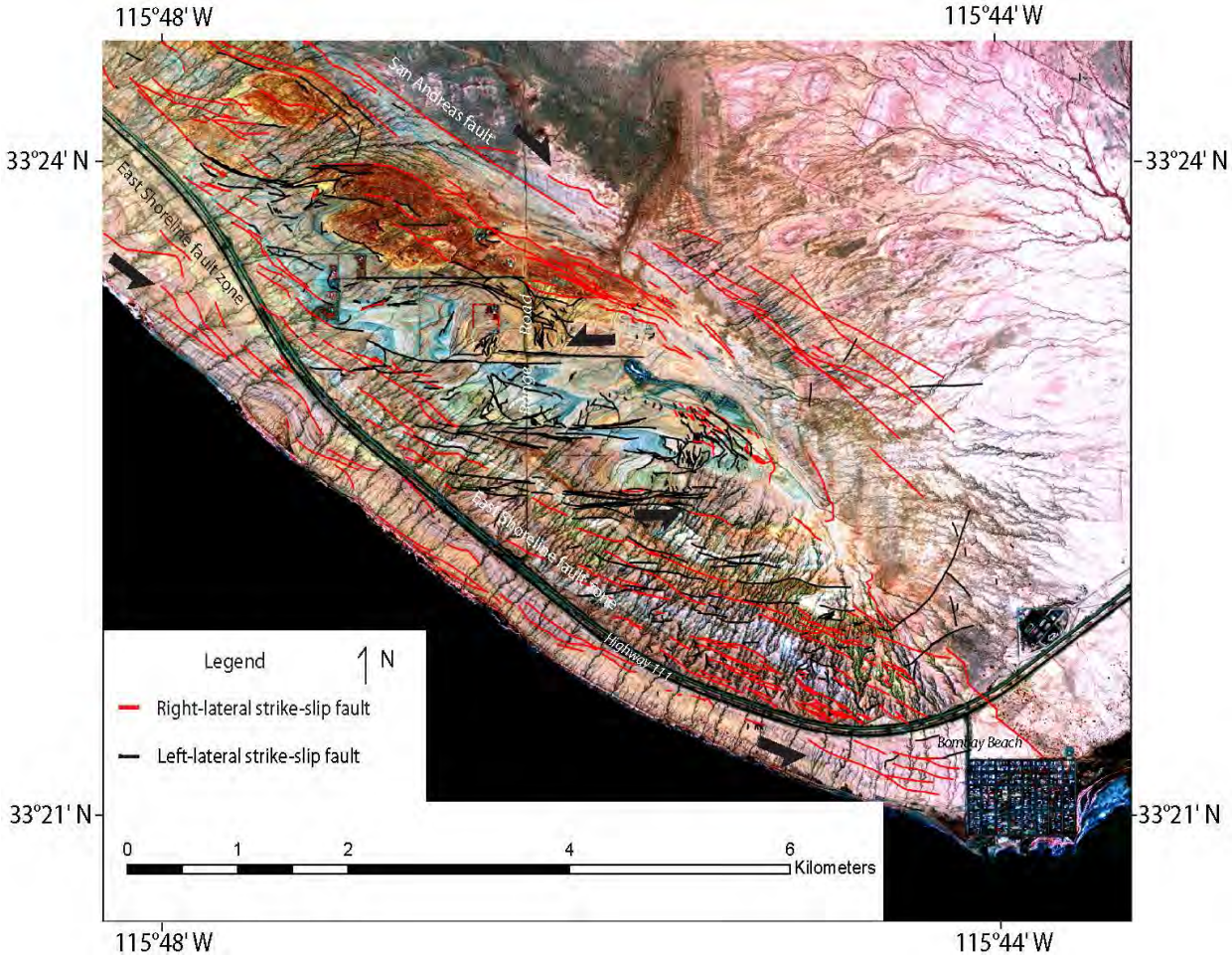

Figure 27. Geologic map of Durmid Hill highlighting the right-lateral strike-slip faults (red) and left-lateral strike-slip faults (black). The basemap is NAIP imagery that I processed to highlight structural features. See plate 1 for the full view.

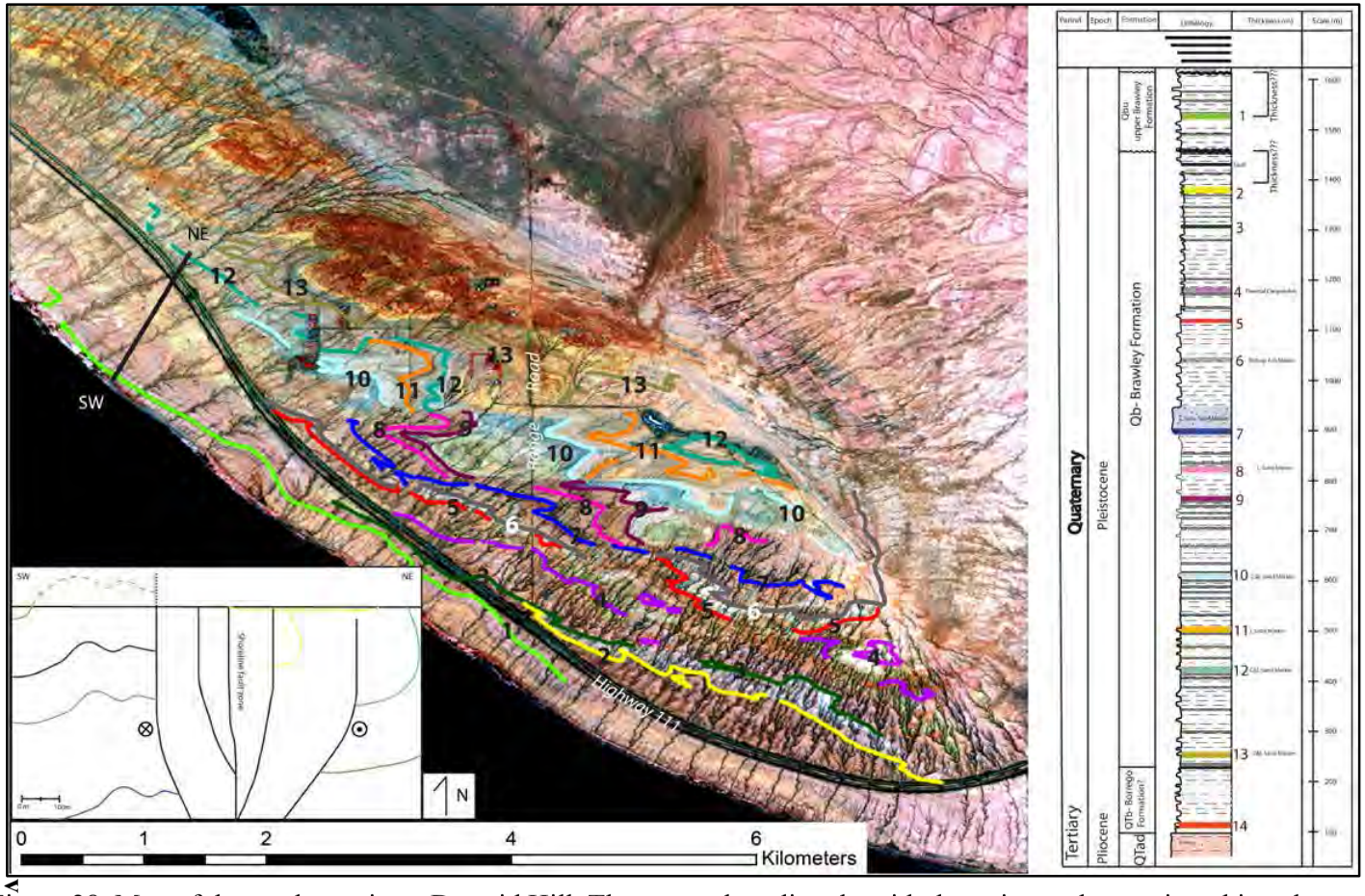

Figure 28. Map of the marker units at Durmid Hill. These correlate directly with the units on the stratigraphic column on the right and are color coded. The cross-section used in this calculation highlights a line from the southwest near the Salton Sea that starts at the lime green marker bed to the turquoise green marker. The basemap is NAIP imagery that was processed in false color to highlight structural features.

The orientations of the folds provide further evidence for the East Shoreline strand of the San Andreas fault. The folds at Durmid Hill trend towards parallelism with the main strand of the San Andreas fault and trend toward parallelism near East Shoreline fault as well (Fig. 7, 9, 24, and 29; Bürgmann, 1991). The intensity of folding should dramatically decrease southwestward and the orientation of folds should continue to diverge with distance away from the main strand of the San Andreas fault if it were the only significant fault strand in the area. Neither prediction holds true and the presence of the numerous northwest-trending folds near the Salton Sea is additional evidence for the East Shoreline strand of the San Andreas fault (Table 3) (Fig. 29). Folds in the East Shoreline fault zone trend subparallel to the fault zone, just as folds within the damage zone of the main strand of the San Andreas fault parallel that fault (Figs. 9, 10,24, and 29).

The presence of misaligned left-lateral strike-slip faults provides evidence for the East Shoreline strand of the San Andreas fault (Fig. 27). Sinistral faults coordinated with the San Andreas fault should have northeast strikes (Wilcox and Hardy, 1981). The San Andreas fault strikes ~310^{o} at Durmid Hill and the left-lateral faults are oriented roughly east-west striking (~90°), instead of roughly northeast-striking (45°). They are 40-50° clockwise of their expected strikes. It is likely that this domain experienced clockwise rigid body rotation (Fig. 27).

Three pieces of evidence also show that the East Shoreline fault may be currently active at Durmid Hill. The activity of the East Shoreline strand of the San Andreas fault can be observed indirectly by the presence of growth folds (Fig. 31). An excellent

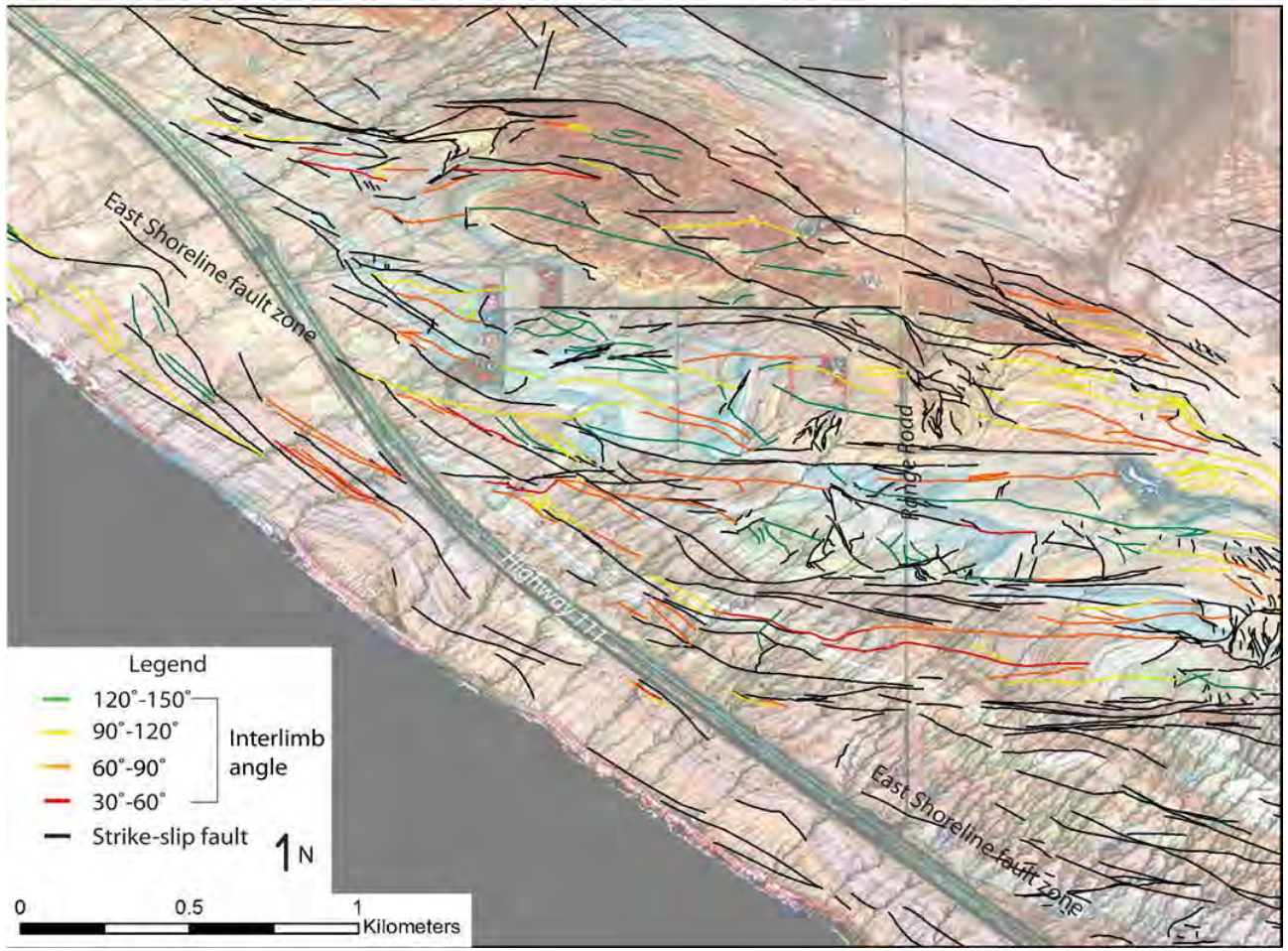

Figure 29. Map of the distribution of fold interlimb angles at Durmid Hill. The interlimb angles are color coded where red is the tightest and green are least tight in terms of interlimb angle. The basemap is NAIP imagery that I processed to highlight structural features.All faults ion this map are black regardless of the direction of movement.

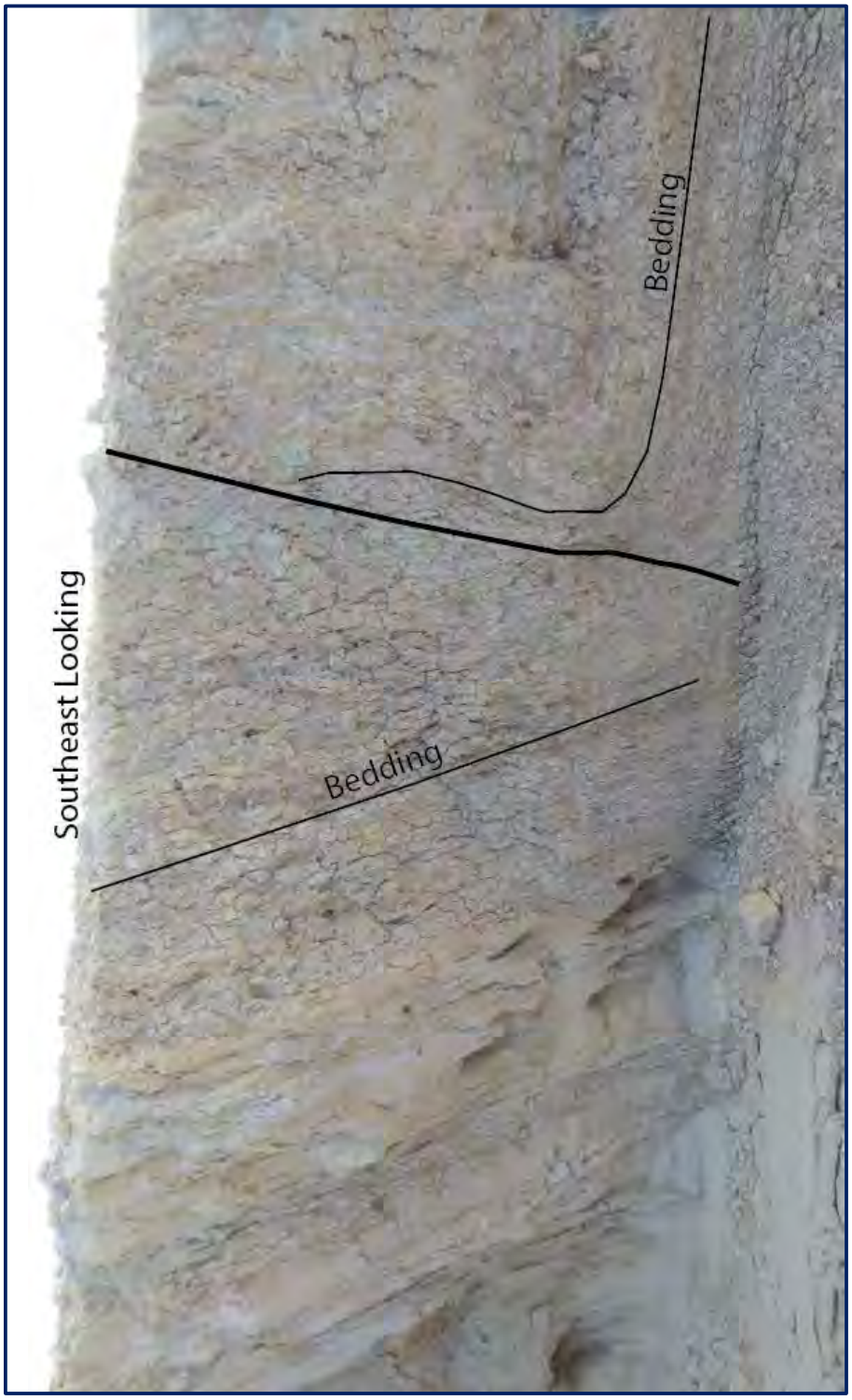

Figure 30. Field photograph of an abrupt fold adjacent to a fault strand of the East Shoreline fault zone. Notice the backpack in the bottom left corner for scale. Photograph number 9 is shown on Fig. 17. This is the Upper Brawley Formation.

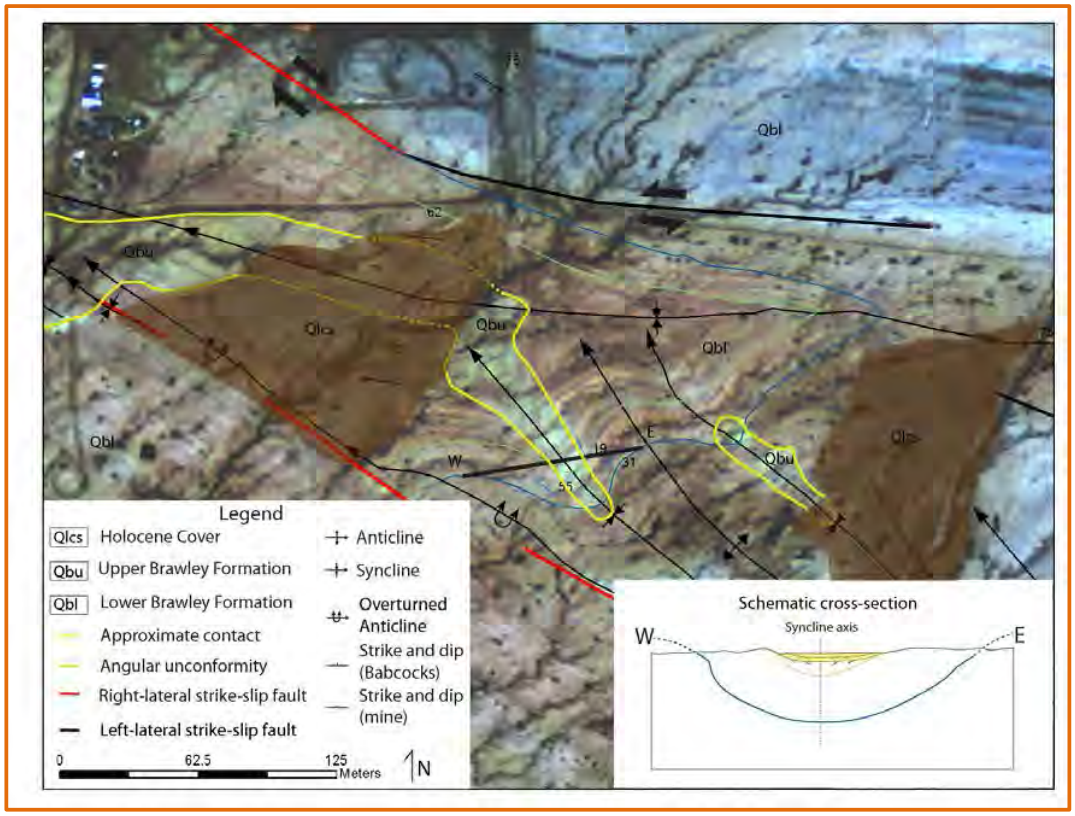

Figure 31. A map of a growth folds within the East Shoreline fault zone. Location of this area is located on Fig. 17 number 10. This presents evidence for progressive deformation and sedimentation. It also suggests the East Shoreline fault being active during the deposition of upper Brawley Formation.

about 150 meters long and 40 meters wide (Fig. 33). These were first thought to be expansion cracks due to the evaporation of water but upon further inspection, the fractures persist through different types of sediment, parallel mapped dextral faults, strike into them, and rarely have vertical separation. They cut sandy beach ridges, lagoonal mud, and barnacle deposits (Fig. 33). It is unlikely that the fractures would form in different types of sediment, including many that lack clay particles, if they are

desiccation cracks. These fractures are likely to be tectonic and related to the activity on the East Shoreline fault.

An escarpment up to 2.5 m high coincides with the uppermost edge of the modern beach deposits where fractures deform the modern beach sand and mud. The escarpment disappears north and south of the roughly 6 km long zone of fractures and is closely linked in space.

Late Pleistocene to Holocene sediment cut by faults are another important indication that the East Shoreline strand of the San Andreas fault is currently active. In the southern extent of the East Shoreline fault zone adjacent to Bombay Beach, faults cut the upper Brawley Formation. Holocene sediment is faulted along with the underlying Brawley Formation in several places (Fig. 34). InSAR also provides evidence of the activity of the East Shoreline Strand of the San Andreas fault and is presented in a later section.

The Southern San Andreas Fault

Janecke's analysis shows that bends in the San Andreas fault do not correlate all that well with the locations of contractional deformation and may not explain all of the uplift. For example, uplifted basin fill in the Mecca Hills and Indio Hills persist beyond the contractional sections of the San Andreas fault (Fig.7 and 8). In other localities, uplifted sedimentary rocks do not fit the sawtooth-model (Fig. 8). In the northern, southern Mecca Hills. and southern Durmid Hill, uplifted and folded sedimentary rocks should not be observed according to the sawtooth model (Fig. 8).

Figure 32. The Shoreline escarpment near the Shoreline of the Salton Sea. Field photographs A and B are in area 11 and can be located on Fig. 17. In this location, the escarpment was 1 to 2 meters high and vertical. The Salton Sea is barely visible in the middle right of photograph. The escarpment is eroded into beds of the Upper Brawley Formation.

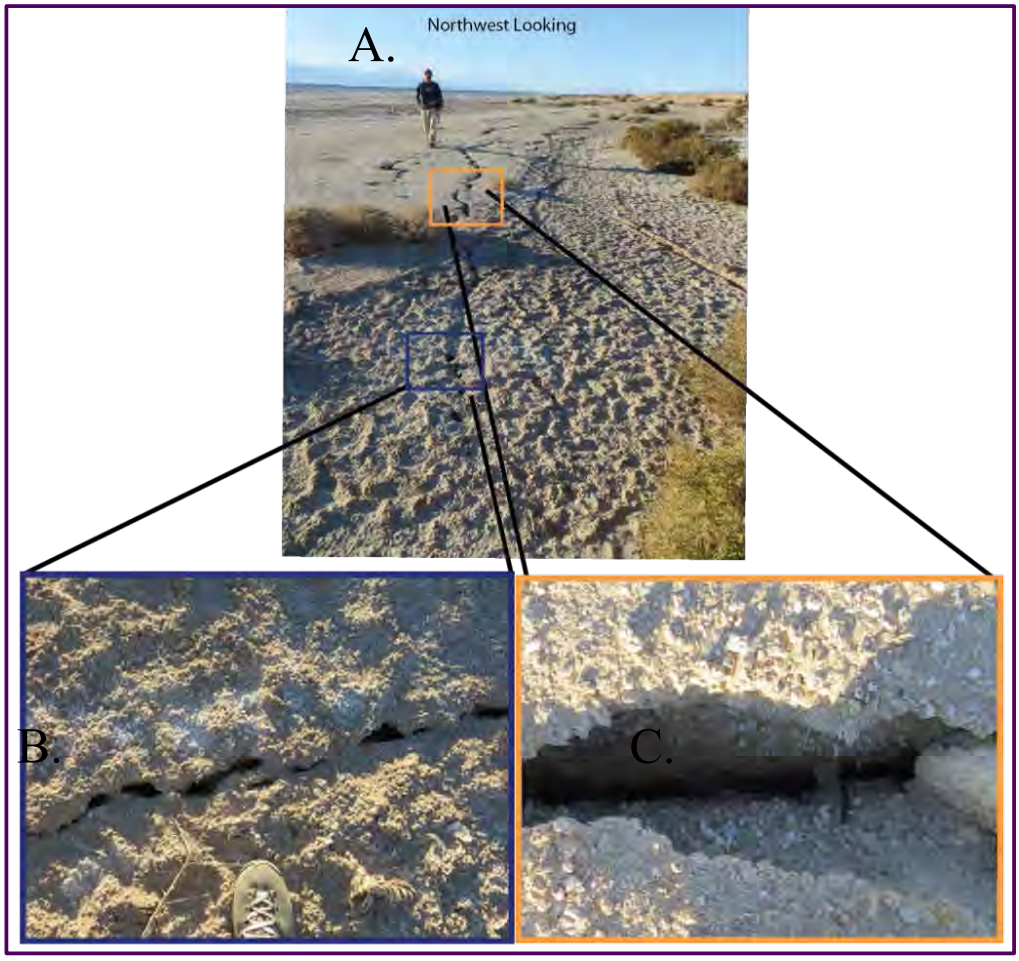

Figure 33. Field photographs of fractures in the East Shoreline strand of the San Andreas fault zone. Field location number 11 is shown on Fig. 17. Photograph A shows these fractures cutting across different sedimentary facies and developed in both sandy and muddy facies. Barnacle-bearing sand, like that shown here, cannot undergo shrink-and-swell to form desiccation fractures. The photographs below (B and C) are close-ups of the fractures in muddy (B) and sandy facies (C). Notice the foot for scale.

Larger scale maps by Dibblee in the Mecca Hills help confirm that there is also contractional deformation and uplift north and south of the contractional section of the San Andreas fault (southeast of bend 4)(Fig. 8 and). At Durmid Hill near Bombay

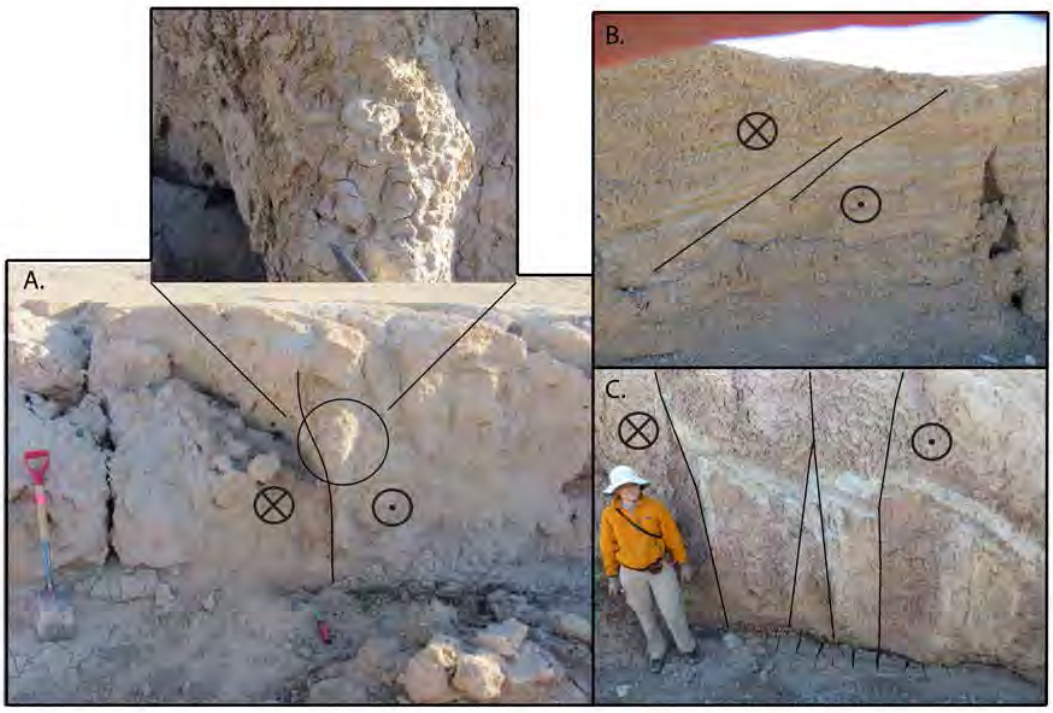

Figure 34. Faults that cut Upper Brawley Formation and the overlying Holocene sediment. A. Fault cuts Holocene sediment with an inset close-up that shows upper Holocene pumice clasts within the Holocene sediment. The location of this photograph can be found on Fig. 17 is at location 12. B. A fault cuts Pleistocene to Holocene mudstone. The location of this photograph is at location 13. C. Upper Brawley Formation lying unconformably above nearly vertical Lower Brawley Formation. Both units are cut by the vertical strands of the East Shoreline fault zone. The location of photograph C is at location 14. All photographs are looking southeast.

Beach, previous maps show there is a large amount of contractional deformation south of the more westerly-striking San Andreas fault (South of bend 1)(Babcock, 1974; Bürgmann, 1991; Dibblee and Minch, 2008a, b and c)(Fig.).

The broad geomorphology of Durmid Hill is an anomaly when compared to the other areas of uplifted basin fill in the Salton Trough (Indio and Mecca Hills). Other uplifted sites are concentrated on the northeast side of the San Andreas fault zone

whereas Durmid Hill is on the southwest side (Fig. 7). Where the Indio and Mecca Hills have topographic relief of about 900 meters and 450 meters respectively, Durmid Hill is subdued and only about 10 meters above the surrounding landscape and resides mostly on the southwest side of the San Andreas fault. Durmid Hill is a subtle hill but contains of significant contractional deformation within the young mudstone and sandstone units.

From Salt Creek to the southeast, the main strand of the San Andreas fault can be traced to about 0.8 km southeast of Bertram Mine to a point that we call bend 1 in figure 35 (Figs. 17, 35). There, the main trace of the San Andreas fault has been mapped by most prior researchers as bending southward. We found that the damage zone of the main strand of the San andreas fault on the more northerly striking part south of bend 1 is overlapped by the Brawley Formation. Several subsidiary traces continue within Pleistocene and Holocene sediment to the southeast from bend 1 along the same strike as north of the bend (Fig. 33 and Plate 1 b). Field observations and mapping on aerial photography suggest that the actives trace of the San Andreas fault projects straight (N50^{o}W) and bypasses the older bend 1 in the fault (Fig. 17,). Observations from a mapping field reconnaissance assessed that the strands are arranged in an en echelon pattern and cut both upper Brawley Formation and Holocene deposits. Further field work is needed to fully evaluate and map this complex area.

The southern San Andreas fault in the overlap area (Figs. 17 and 36), exhibit important cross cutting relationships that explain the development of the fault zone. Mapping results indicate that at the southern San Andreas fault there is an overlapping geometry (Fig. 17 and 36). Here, there are fault traces that lap onto beds that are folded

but are not cut by the older strand of the San Andreas fault south of bend 1 (Fig.36). The folded beds adjacent to the San Andreas fault include a prominent C suite sandstone marker bed and volcanic tuff deposit slightly up section (Fig. 36 and Plate 1 b). Characterization of the southern San Andreas fault south of bend 1 at Durmid Hill is difficult because of subsidiary strands, the distribution of depositional cover, and its unusually wide damage zone.

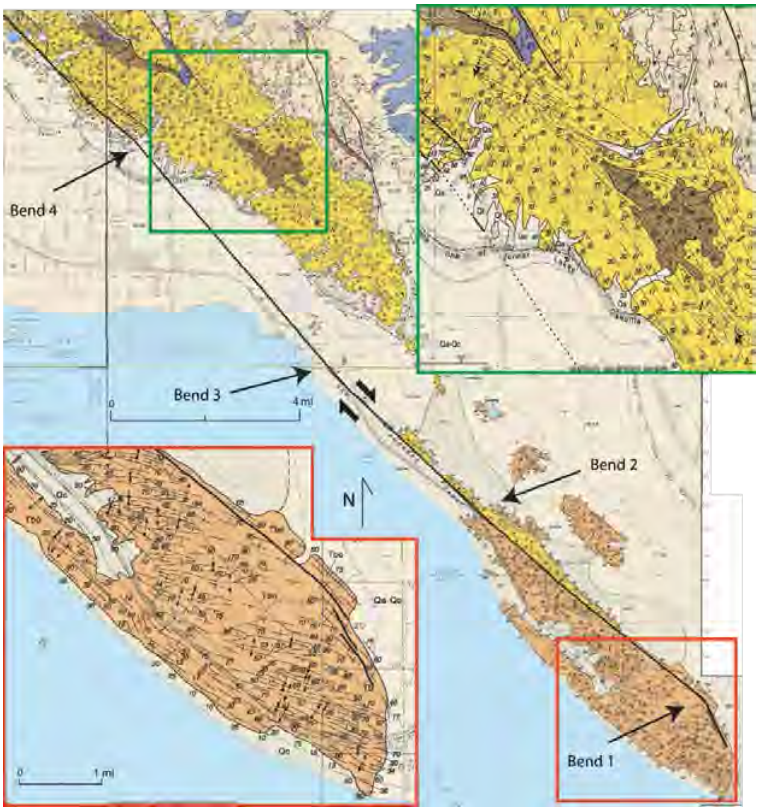

Figure 35. Geologic map of Durmid Hill and the Mecca Hills near the northeast corner of the Salton Sea. The solid black line is the trace of the southern San Andreas fault. The arrows point toward our observed bends in the fault where uplift and or deformation anomalies exist. The red inset is a closeup of southern Durmid Hill and the green inset is a closeup of the southern Mecca Hills. Modified from Dibblee and Minch (2008a, b and c).

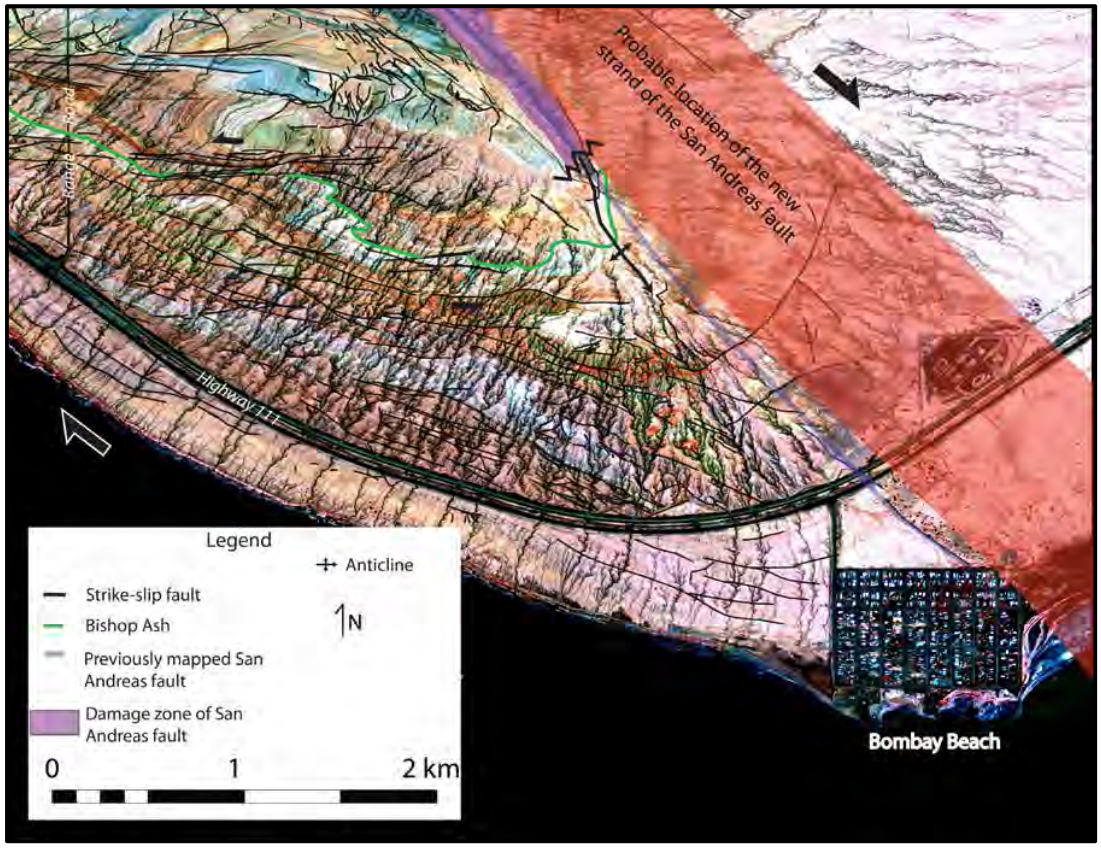

Figure 36.The deactivated southern end of the San Andreas fault, its damage zone in purple, and its overlapping Pleistocene sediment are south of the black lines. The location of this map can be found on Fig. 17 as location 15. The overlapping sediment contains the 0.78 Ma Bishop ash, in green, near the base of the overlap succession. Note that the attitudes of the overlapping deposits define a SSE-plunging anticline along the trend of the underlying, buried San Andreas fault zone. The location of the ash is from Babcock, 1974 and this study.

The San Andreas fault's damage zone is defined here as the area of very high deformation and disturbed bedrock in which bedding cannot be traced laterally. The damage zone consists of sandstone, mudstone and gypsum blocks up to 160 meters that lie in a matrix of mudstone and gypsum rich mudstone where a consistent bedding orientation cannot be resolved. Based on field observations and analysis of imagery, the

damage zone of the San Andreas was resolved and mapped. The most intense and disrupted damage zone with a block-in-matrix deformational style is localized on the southwest side of the main fault trace (Plate 1). However, from about bend 1 to the southeast, the damage zone may exist on both sides of the main trace of the San Andreas fault. It is unclear exactly where the main strand of the San Andreas fault is located in a zone of numerous branch-fault type splays (Figs. 13, 17 and Plate 1 b).

The overall damage zone of the San Andreas fault at Durmid Hill is about 0.5 km wide where the main strand is easily distinguishable, north of bend 1. The damage zone of the San Andreas fault has a different character elsewhere and is not fully resolved (Fig. 17 and 36).

East-west Striking Left-lateral Faults at Durmid Hill

A domain of roughly east-west striking faults lie in between the San Andreas fault and the East Shoreline strand of the San Andreas fault at Durmid Hill (Fig. 17 and Plate 1). My results suggest that they are a group of strike-slip faults that are kinematically sinistral. Offset marker beds and the steeply dipping damage zones show that the fault zones are left lateral. The faults rarely preserve slickenlines, thus, it is nearly impossible to determine the vertical component of motion if any. The orientation of these faults changes about 15°-20° at the edge of structural domain 2 to a more northwesterly strike (Fig. 24).

Five major east-west left-lateral fault zones were discovered and mapped in this research. These faults are both regularly spaced, and uniformly wide fault zones. Their

orientations are roughly 274° and have left separations of 250 meters to 1000 meters. Damage zones along these faults are very broad and they range from about 120 meters up to 250 meters wide in this domain (Plate 1 b). Numerous branching, en echelon, and subparallel strands comprise each left-lateral fault zone. Spacing between fault zones are roughly 475 ± 75 meters apart and fault-parallel folds separate these fault zones. Each fault begins and ends a short distance farther west relative to its southern neighbor, forming a gross left-stepping array from south to north (Plate 1 b). All of these fault zones lack a distinct fault core but instead, manifest as large damage zones and adjacent folded Pleistocene beds. Bedding is highly disrupted and often steep when intact. Some areas previously described as large boudins structures (Babcock,1974; Bürgmann, 1991) are better described as fault zones that have been sheared by block in matrix deformation (French et al., 2006; and this study).

Gravity and Magnetic Maps

Gravity data and magnetic data were used to constrain the presence of faults, folds, to indicate dip direction of structures in the subsurface, and to estimate the depth of buried or covered structures in the Salton Trough. Detailed gravity and magnetic data suggests that from Indio to Salt Creek higher density rocks occur all along the northeast side of the San Andreas fault (Langenheim et al., 2007; Langenheim et al., 2011; Langenheim et al., 2012). This indicates a northeast up vertical component of slip on the fault that places lower density basin fill on the southwest beneath higher density bedrock on the northeast side. In the Salt Creek and Durmid Hill area the dip direction of the main

strand of the San Andreas fault cannot be resolved unequivocally, but there is a change in the component of vertical displacement southward along the fault trace. At Salt Creek, the northeast side of the main strand of the San Andreas fault is up relative to the southwest side, based on a gravity high on the northeast side. Farther south, at Durmid Hill, the opposite is true (Babcock, 1969; Langenheim et al., 2007; Langenheim et al., 2011; Langenheim et al., 2012; Langenheim et al., 2014). Such behavior is called porpoising and occurs along major strike-slip faults. No clear signature of the East Shoreline strand of the San Andreas fault appears on either the gravity or magnetic datasets near Durmid Hill.

InSAR

Interferometric Synthetic Aperture Radar (InSAR) is a type of geophysical method to record changes in the Earth's surface. It works by combining two images of different times to measure differences in x, y, and z coordinates.. InSAR studies following the 1992 Landers earthquake show an interseismic creep rate of 5-7 mm/year in the Durmid section of the San Andreas fault from 1993- 1999 (Lyons and Sandwell, 2003). This is significantly higher than the 2 mm/year slip rate observed from 1967-1984 by Bilham and Williams (1985). This discrepancy could be either due to an underestimation of creep rates with creep meters and/or a longer term increase in the average creep rate since the Landers earthquake (Lyons and Sandwell, 2003).

In the Salton Trough, an InSAR dataset by Tong et al. (2012) measured ground motion throughout California. We examined the data from the southern Salton Trough as

far north as San Gorgonio Pass (Fig. 37). Results of this interferogram show a signal of creep along the southern San Andreas fault as far south as Durmid Hill (Fig. 37). Furthermore, sharp, northwest trending boundaries of extremely rapid subsidence were detected about 5 miles southeast of Palm Springs (Fig. 37). Using InSAR in southern California, boundaries of subsidence are typically interpreted as marking areas of high water withdrawal from the basin (Wisely and Schmidt, 2006; 2009). The data show strong, sharp boundaries of subsidence suggesting the presence of an impermeable northwest-striking fault southeast of Palm Springs that appears to project to the East Shoreline fault zone in Durmid Hill (Fig. 37).

At Durmid Hill the InSAR signal is strong along the main strand of the San Andreas fault and variable along the East Shoreline strand of the San Andreas fault (Fig. 37). Field observations assessed the presence of faults that strike parallel to highway 111 eases some doubt on the variable signal but perhaps the signal there is a combination of both of fault creep and cultural features such as roads and railroad construction.

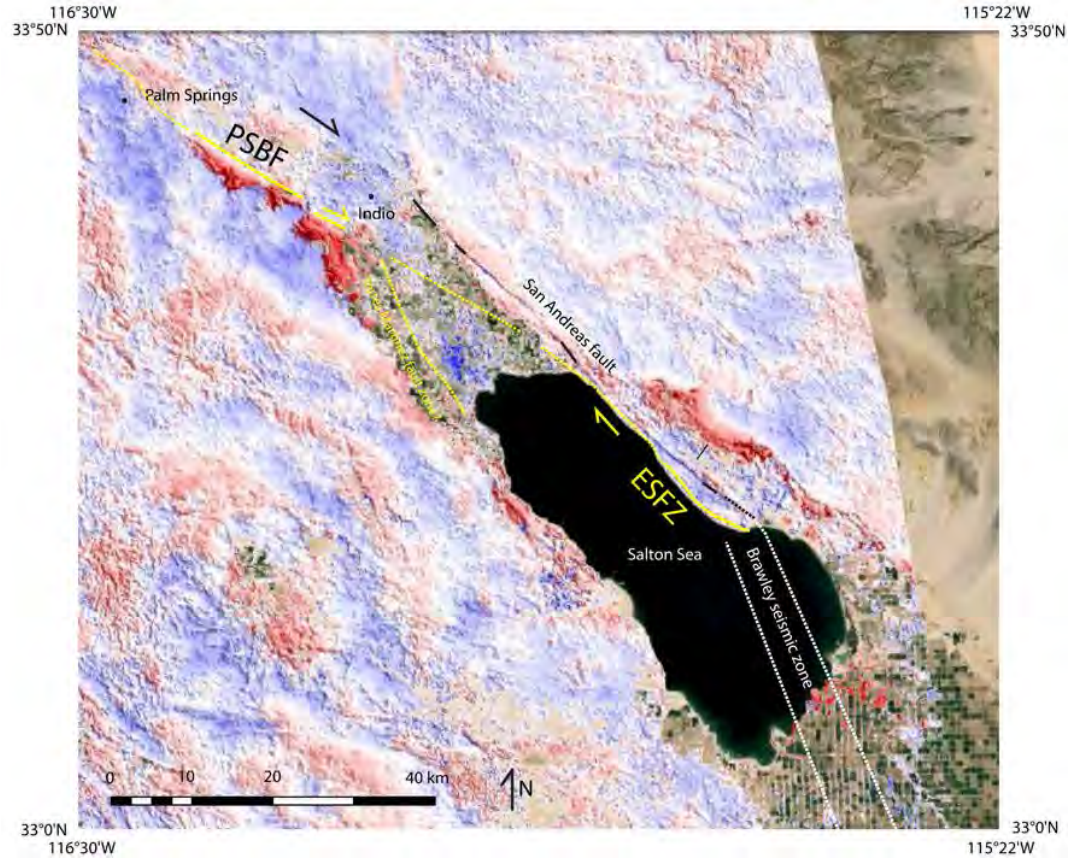

Figure 37. ALOS radar interferogram of Tong et al. (2012) showing ground motion along across probable dextral faults. between Palm Springs, California and the Salton Sea.ESFZ- East Shoreline fault zone, PSBF- Palm Springs branch fault. Reds fields depict motion away from the satellite and blue fields represent motion towards the satellite. Notice the subsidence just southeast of Palm Springs across a linear and abrupt boundary (Wisely and Schmidt, 2006 and 2009; Wisely, 2012; Sneeds and Brandt, 2011; Tong et al. 2012). The East Shoreline fault is nearly parallel to the northeast margin of the Salton Sea and dies out in the south, or merges with other faults beneath the Salton Sea. Black lines highlight creep across the main strand of the San Andreas fault zone and yellow lines highlight strains across the East Shoreline fault. The composite East Shoreline fault zone projects northwest toward the San Gorgonio Pass area and cuts more directly past a bend in the San Andreas fault zone. I interpret the East Shoreline fault as a strand of San Andreas fault system.

DISCUSSION

Regional Continuation of the East Shoreline Fault

In light of the evidence presented here for the East Shoreline strand of the San Andreas fault at Durmid Hill, we first discuss the possibility of a continuation elsewhere in the Salton Trough and what it would mean. The gravity maps and InSAR data suggest the presence of a buried fault near Palm Springs north of Cathedral City and La Quinta that is oriented northwest southeast (Fig. 37).

In addition to these data, other gravity data agrees with the presence of the East Shoreline strand of the San Andreas fault near Palm Springs. The data suggest that a buried fault trace lies near the Palm Springs International Airport (Sneed and Brandt, 2011). An isostatic gravity map of Joshua Tree National Park also shows similar gravity anomalies along a line north of Cathedral City, Palm Desert, and La Quinta (Langenheim et al., 2005; Langenheim et al., 2007; Langenheim and Powell, 2009). Interpretations of InSAR from Tong et al. (2012) show evidence for a partitioned aquifer there.

We suggest that the East Shoreline fault mapped in the study area continues northwest and connects with the fault detected by subsidence that cuts through the Palm Springs airport (Fig. 37). The southwest boundary of this subsidence is fairly irregular and we interpreted this as subsidence related to water withdrawal in the general vicinity. The sharp boundary on the northeast side may represent a fault-bounded aquifer that is sealed by the fault on the northeast side. In a few locations, this boundary is not as sharp indicating the possibility of the fault barrier being leaky in the subsurface.

About 5 kilometers south of Indio, the East Shoreline fault has a branch point (Fig. 37). A strand bends south to the Torres Martinez fault zone and a strand continues towards the northern end of the Salton Sea (Fig. 37). If this fault strand connects to the East Shoreline strand of the San Andreas fault and it is slightly offshore where it comes on land near Salt Creek, there is a good possibility that shallow seismic surveys could have missed this strand of the the San Andreas fault since it is located so close to the shoreline. The wave action of the Salton Sea can disturb the seismic surveys.

Seismic Hazard of the Southern San Andreas Fault

Cross-fault Trigger

The Coachella segment of the southern San Andreas fault has not experienced a major earthquake since A.D. 1680 and it is implied that the seismic hazard is high there (Weldon et al., 2004; Fialko, 2006; Olsen et al., 2009). This lack of seismicity suggests that it is a locked southern strand and has a high potential for rupture in the future. The ShakeOut scenario earthquake and predictions by Brothers et al. (2009, 2011) suggest a northwest propagating rupture nucleating on the southern tip off the Coachella segment (Fig. 6). With the discovery of another strand of the San Andreas fault and the absence of a direct connection of northeast striking faults under the Salton Sea, the southern San Andreas fault is under less risk of a triggered slip event than originally estimated by the modeled earthquake in ShakeOut (Fig. 5). Although, the fault is well overdue for an earthquake, there is no clear indication to the rupture directivity and based on field

mapping, there is no direct connection at the surface between the main strand of the San Andreas fault and the Extra fault array (i.e. there is no evidence that the Extra fault array extends as far northeast as Durmid Hill). In fact, the East Shoreline strand of the San Andreas fault may buffer the main strand San Andreas fault from the Extra fault array at Durmid Hill.

It is possible that the East Shoreline strand of the San Andreas fault can be triggered by the cross-fault mechanism, especially because it appears that the East Shoreline fault zone extends southwest under the Salton Sea. Therefore, may be possible that the East Shoreline strand of the San Andreas fault could experience a triggered-slip event like the Elmore Ranch and Superstition Hills event in 1989 (Fig. 5).

At Durmid Hill, there are faults that have a similar geometry to that of the cross-fault model (Fig. 5). The east-west left-lateral faults strike roughly east-west oriented about 95° and the San Andreas fault is northwest striking about 130° (Plate 2). At the surface, these two faults are not connected but they curve at each end toward the orientation of the San Andreas fault and the East Shoreline strand of the San Andreas fault. At most, there is about 35° difference between the orientations of the two fault zones.

Therefore, the east-west left-lateral faults are not likely a source for a triggered slip event on the San Andreas fault for two reasons. First, as discussed above their orientation is not orthogonal. In the cross-fault model (Fig. 5)(Hudnut et al., 1989), the fault zones are perpendicular to each other, but in this situation they are not. Second, the faults are much shorter in length than the Extra fault array. The relatively short length of

the east-west left-lateral faults compared to the Extra fault array could not likely create enough stress change to trigger a northwest propagating rupture on the San Andreas fault.

Ground Motions From a Rupture on the San Andreas Fault

Most recent geophysical models have not taken into account the East Shoreline strand of the San Andreas fault but do account for yielding close to the fault during a future rupture event. Roten et al., 2014 suggest that current simulations are over predicting ground motions by assuming linear elastic rock response during a future large earthquake along the San Andreas fault. While the southern San Andreas fault is largely overdue, they show that nonlinear material behavior could reduce the earlier predictions of large long-period ground motions in the Los Angeles Basin by up to 70% if cohesion of the rocks are close to zero (Roten et al., 2014). At Durmid Hill, there are many rocks within the Pleistocene Brawley Formation with cohesions close to zero. In addition, the combinations of the wide San Andreas fault and East Shoreline fault damage zones create an even larger deformational area than previously thought which may reduce the hazard of a triggered-slip event on the southern tip of the San Andreas fault.

Folds

Folds associated with strike-slip faults are typically arranged in en echelon patterns, oblique to the principal direction of shear (Harding, 1974; Dibblee, 1977; Harding and Lowell, 1979; Harding and Tuminas, 1988; Sylvester, 1988). En echelon

folds may form in a narrow zone in between two master faults in contractional stepovers, however, the presence of folds that parallel a zone of right or left-lateral deformation is possible, but much less common (Sherill, 1929; Campbell, 1958; Christie-Blick and Biddle, 1985; Sylvester, 1988).

The folds are sigmoidal in their map pattern at Durmid Hill that suggest evidence for a secondary shear zone boundary (Fig. 9). Fold tightness does not appear to have a definite spatial pattern at Durmid Hill (Fig. 29) but abrupt changes in dip and overturned stratigraphy on the southwest side of highway 111 are evidence that there must be another large strand of the San Andreas fault close by. It would be expected that intensity of folding should decrease and the orientation of folds should remain consistent with increasing distance from the San Andreas fault if it was the only major structure there.

The intensity of folding about 2 km southwest of the San Andreas fault at Durmid Hill is often just as high, if not more intense than near the main strand of the San Andreas fault. Also, the orientation of the folds 2 km southwest of the San Andreas fault tend to be closer to parallelism to the strike of the San Andreas fault than to the folds right adjacent to the San Andreas fault (Fig. 10).

The results of stereonet analysis show that the folds in the San Andreas domain have the highest average interlimb angle, and that the Shoreline domain has the lowest (Table 3). Upper Brawley Formation in the Shoreline domain is in angular unconformity on structures and dips less steeply than the underlying units. The lower average strains in this domain could reflect the presence of both units because other field evidence show that this domain includes some of the most intense and abrupt deformation.

Qualitative analysis shows that the East Shoreline domain contains many tight, overturned, and abrupt folds. Yet, the East Shoreline domain is multimodal and has two dominant fold interlimb angles. This may be because of tight, overturned, and abrupt folds in addition to younger stratigraphy lying unconformable atop. As discussed above, the folds that above are generally less deformed and may be the reason for the multimodal behavior (Table 3).

East Shoreline Strand of the San Andreas Fault at Durmid Hill

Several pieces of evidence were presented that support the existence and character of the East Shoreline fault at Durmid Hill. The pattern of the East Shoreline strand of the San Andreas faults multiple strands and branching pattern could be the result of several different scenarios. One explanation is that the East Shoreline strand of the San Andreas fault is further offshore and we are only seeing subsidiary faults of the structure. Another scenario may be that the fault is less active today than it was in the past. This would effectively bury the surface trace and make it difficult to identify. On the contrary, evidence of folded and faulted Upper Brawley and Holocene rock and recent shoreline fractures suggest that it is very active today.

It is possible that the East Shoreline strand of the San Andreas fault hasn't fully developed and obtained a continuity and character similar to that of the main strand of the San Andreas fault yet. The East Shoreline fault could be younger and through-going in the subsurface that has accommodated much less slip than the San Andreas fault.

Cross-cutting relationships point to initiation of the East Shoreline strand after initiation of the main strand of the San Andreas fault and before the weakly expressed part north of Bombay Beach (Plate 1). This weakly expressed fault north of Bombay Beach may be a poorly expressed portion of the newer East Shoreline fault.

San Andreas Fault Overlap

Another discovery in this work that has important implications for the Salton Trough is the possible presence of a buried strand of the San Andreas fault under southeastern Durmid Hill. Using Google Earth imagery, the original trace of the San Andreas fault was mapped and it is overlapped by part of the Brawley Formation (Fig. 17 and 36). The fault is overlain by Brawley sand, mud, and ash that are folded into a southeast plunging anticline.

The replacement for the inactive part of the San Andreas fault is multi-stranded, lacks a well-developed central damage zone because it is only ~1 to 1.3 Ma, and is dispersed across a large area (Fig. 36). A single strand of the San Andreas fault here is difficult to identify in the field due to a wide damage zone and muddy stratigraphy that result in the fault being obscured. En echelon fault geometries further complicate identification of this new piece of the main strand of the San Andreas Fault. The fault zone seems to narrow to the south as it approaches the overlapped Brawley Formation, which may be a result of the unconformity between the two.

The change in fault geometry from the paleo-San Andreas fault to its newer

Pleistocene piece is probably a manifestation of the early Pleistocene reorganization of the Gulf of California and Salton Trough (Janecke et al., 2010; Janecke and DeMets, 2010). This overlap and presence of reorganizations elsewhere in the Salton Trough around~1 Ma could point toward the initiation of the East Shoreline fault near that time.

We suggest that the San Andreas fault is therefore no longer active in its original trace at its southern tip near Bombay Beach. A new strand may have formed before the Bishop ash was deposited at 0.76 Ma (Rivera et al., 2011). Down section, a highly folded sandstone unit is present and may contain a reliable date for the age of structural reorganization of the San Andreas fault here. Structural reorganizations seen elsewhere in the Salton Trough have been documented and could possibly be correlated to the same major event. Major adjustments of the San Felipe, Coyote Creek, and Clark faults after ca. 0.6- 0.5 Ma have been found and could be related to the reorganization of San Andreas fault (Janecke et al., 2010). It is possible that the structural reorganization at ~1 Ma could have been the initiation of the East Shoreline fault and the 0.6- 0.5 Ma reorganization may or may not have affected the East Shoreline strand of the San Andreas fault.

Bends in Strike of the San Andreas Fault

Examination of the marked spatial mismatch between contractional strains along the main strand of the San Andreas fault and more northwest-striking parts of the fault zone show that the saw tooth model is not a good general model to explain the

contractional deformation at the Indio Hills, Mecca Hills, and Durmid Hill (Fig. 7). There are bends along the fault where topographic highs should exist according to the saw tooth model but topographic lows occur (Fig. 8), and vice versa. Theoretically, deformation should occur on both sides of contractional segments of the San Andreas fault but it is only observed on one side of the fault.

An extension of influence from the Eastern California Shear Zone as the origin of contractional deformation and uplift in the Indio and Mecca Hills fits better than the saw-tooth model. At Durmid Hill maybe a slight influence from the Eastern California Shear Zone but it is best explained by a contractional ladder-like geometry.

Origin of Rotation for the East-West Left-Lateral Faults

The east-west left-lateral strike-slip faults are presented as evidence for the East Shoreline strand of the San Andreas fault (Fig. 27). Cross-faults in between large strike-slip systems can be very important because they can accommodate a compressional step and facilitate block rotation (Nicholson et al., 1986; Sylvester, 1988; Schreurs, 1994). With the north-south oriented maximum horizontal stress, it would be expected to find that these should be primarily reverse faults. In addition, their orientation is not predicted by clay models, strain ellipses, or a step-over models of strike-slip deformation (Wilcox and Hardy, 1981; Schreurs, 1994). Expected orientations for antithetic faults to the San Andreas fault would be at roughly 100° from the strike of the San Andreas fault to the east-west left-lateral faults (Wilcox and Hardy, 1981). Instead we observe a much smaller

angle of 40º between the east-west left-lateral faults and the main strand of the San Andreas fault. Below are three interpretations of how the east-west left-lateral strike-slip faults formed. Two of which involve one episode of deformation and one that at least two events of deformation have occurred.

Two scenarios can be proposed to explain just one event that all deformation occurred (folding, faulting, and rotation) these are the two scenarios. 1. The faults and folds could have a relationship like the East Shoreline fault domain where folds parallel faults. 2. Left-lateral faults and folds formed each with different orientations.

For the first scenario to be valid there must be many left-lateral faults near each east-west oriented fold. Results discussed above describe the left-lateral fault domains as wide fault zones that are evenly spaced apart about 475±75 meters (Fig. 27). Between these fault zones there are folds and not many significant faults. Unless there are several buried faults that created the east-west folds between the left-lateral faults, this scenario is highly unlikely.

The second scenario with one deformation event, we would expect structures predicted by the strain ellipsoid. With a north-south oriented sigma 1, structures produced originally would include antithetic sinistral faults to the San Andreas fault oriented southwest northeast and east-west oriented folds. Upon coherent rotation, the left-lateral faults would be rotated to an east-west orientation and the folds should be rotated to a northwest-southeast orientation (Fig 38). This type of relationship is not observed.

It is unlikely that one event of deformation created the misaligned sinistral faults and east-west folds because of the observations stated above, however, if block rotation is

an active mechanism at Durmid Hill there must have been multiple deformation events. For this third scenario to be valid, the left lateral faults would have to form first with a southwest-northeast orientation. These faults later would become rotated clockwise followed by later N-S contraction. Broad east-west oriented folds were created late after rotation of the left-lateral strike slip faults (Fig. 39). A way to test this two stage deformation idea would be find evidence for folded faults. Another test would be to use paleomagnetic data to test if the rocks were rotated. If a one-stage or two-stage sequence of events did not create this configuration then perhaps they just formed this way.

Stratigraphic Interpretations

Our working stratigraphic reinterpretation suggests that the oldest formation, the Late Miocene?-Pliocene Shavers Well Formation, that is concentrated in fault-bounded blocks on the northeast side of the San Andreas fault, may be correlative with the Mecca Formation of the Mecca Hills. The discovery of large burrows by Janecke in some green weathering beds of the Shavers Well Formation suggest that it may even be partly correlative with the marine, late Miocene to Pliocene, Imperial Formation (Fig.14)(Dibblee, 1954; Dibblee, 1986; Dibblee 1996, 1997; Dorsey et al., 2011). We further propose that the Borrego Formation in the Durmid Hill area (Dibblee, 1954; Babcock, 1979; Bürgmann, 1991) should be reassigned to six different formations (Fig. 14). From base to top these are: 1) The Pliocene Arroyo Diablo Formation and its lateral equivalents in the Olla Formation, and Pliocene-Pleistocene Canebrake Conglomerate; 2)

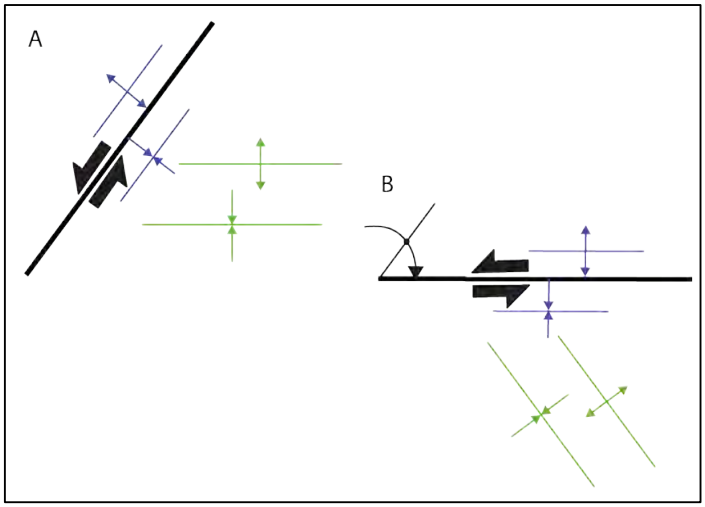

Figure 38. Schematic drawings of a left-lateral cross-fault and folds adjacent to them. Blue folds are the folds associated with the fault and green are folds produced away from the major left-lateral fault from N-S sigma one. A) Original orientation of left-lateral fault. B) Orientation of left-lateral fault and folds after clockwise rotation.

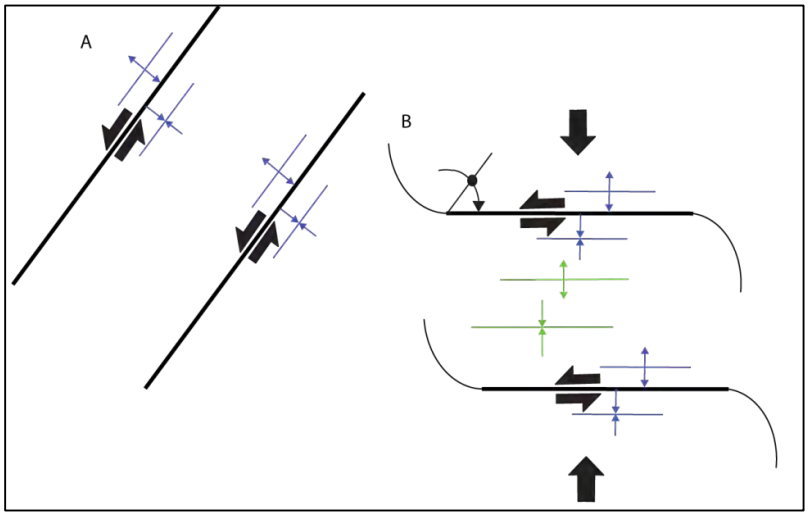

Figure 39. Schematic drawing of two stages of deformation in the cross-fault domain. Blue folds are folds associated with the fault and green folds are broad folds created later. A) Original orientation of left-lateral faults and folds. B) Orientation of left-lateral faults and folds after clockwise rotation. The green folds form after clockwise rotation of the left-lateral faults and blue folds.

the overlying Plio-Pleistocene Borrego; 3) capped by the Pleistocene conglomeratic

the overlying Plio-Pleistocene Borrego; 3) capped by the Pleistocene conglomeratic Ocotillo Conglomerate and its basinward finer equivalents in the Lower and Upper Brawley Formations, as well as; and 4) several overlying Holocene alluvial, eolian, to lacustrine deposits (Dibblee, 1954; Babcock, 1974; Dibblee, 1984; Dibblee, 1996; Winker and Kidwell, 1996; Kirby, 2005; Kirby et al, 2007; Steely, 2006; Steely et al., 2009; Dorsey et al., 2011; this study).

Paleomagnetic results of a study done in the Mecca Hills show that the Mecca Formation is younger than previously thought and suggest a Guass-Matuyama reversal at 2.58 Ma (McNabb, 2013). These results suggest that the Mecca Formation is possibly as young as Pleistocene in age. These results are not only young compared to results of ages from other studies, but if true there is much less control on age of the current main strand of the San Andreas fault. The Mecca Formation is one of the oldest sedimentary rocks that the San Andreas fault cuts an if it is Pleistocene in age than we know much less about the history of the San Andreas fault.

The resistant yellow-brown to tan, medium to coarse grained sandstones with interbedded claystones exposed at Durmid Anticline (Fig. 17) are interpreted as being equivalent to the Arroyo Diablo Formation. This rock is correlated with the Arroyo Diablo Formation because the there is more sandstone than mudstone within the stratigraphy here and because the sandstone is of Colorado River provenance. This rock is also much more resistant than the surrounding Brawley Formation and produces the crest of the subtle hill at Durmid Hill. In areas northwest of Durmid Anticline, Olla Formation and Canebrake Conglomerate interfinger with the Arroyo Diablo Formation

(Plate 1). It was not possible to resolve stratigraphic contacts between these units due to the intense shearing observed in these areas.

It is interpreted that the Brawley Formation exists directly above the Arroyo Diablo Sandstone between a possibly very thin layer of Borrego Formation at Durmid Hill (Plate 1). Evidence for this interpretation includes volcanic ash layers such as the Bishop Ash and Thermal Canyon Ash and the abundance of gypsum throughout these rocks (Fig. 21). My calculation of the total thickness of the Brawley Formation to be about 1,520 meters is consistent with Dibblee's (1954) estimate of roughly 1,495 meters. See Figure 21 for the revised stratigraphic column. With a new stratigraphic column and traced marker beds throughout Durmid Hill, it is now possible to create new cross-sections of Durmid Hill with these data (Fig. 21).

The lake beds that drape across the Durmid Hill area commonly contain clasts of pumice. Volcanic rocks in the southern Salton Sea have recently dated as late Pleistocene and Holocene and is an indication that the eruption of obsidian flows may have coincided with human presence in the region (Schmitt and Vazquez, 2006; Schmitt and Hulen, 2008; Schmitt et al., 2013; Wright et al., 2015). It also allows us to interpret a relative age of sediment that has clasts of pumice imbedded within it.

Cut Out Stratigraphy

Missing stratigraphy is presented as the second strongest piece of evidence for the existence of the East Shoreline fault. About 500-1000 meters in the middle of the Lower Brawley Formation is missing along the boundary between the East Shoreline and East-

West domains at about 33.39° N latitude (Fig. 28). We suggest this is due to the East Shoreline fault cutting out the stratigraphy there. The Lower Brawley Formation is likely thinned significantly from faulting along the East Shoreline fault. The younger Upper Brawley Formation is folded and faulted and lies unconformably on the thinned and faulted Lower Brawley Formation (Fig. 34 and Plate 1). Even Holocene deposits are faulted in many places and provides significant evidence of the continuing deformation and activity in the East Shoreline fault zone.

Instead of the Shoreline Strand of the San Andreas fault removing stratigraphy, there is also the possibility that the stratigraphy pinches out or that it is covered entirely by Upper Brawley Formation. The Upper Brawley Formation blankets the area in places and there are multiple unconformities within Durmid Hill. With the deposition of these rocks coeval with tectonic activity there, it is likely that the missing stratigraphy is a result of both faulting and syntectonic deposition.

Gypsum and Rheology at Durmid Hill

Bedded gypsum is an unusually common occurrence and thick in the Durmid Hill field area. In general, bedded gypsum may be sedimentary or hydrothermal in origin (Sharpe and Cork, 2006; Mazzini et al., 2011). In fault zones, it can promote ductile slip rather than narrow brittle deformation (Brantut et al., 2011). It also may explain the unusually thick damage zone of faults in the area and may have localized structures.

The abundance of gypsum at Durmid Hill presents a few problems: 1) If we are at the margin of the basin you would not expect an abundance of evaporates, because dilution by clastic inputs would inhibit the precipitation of evaporates and 2) Gypsum is

only known from the Brawley formation and the basal Imperial Group and is not expected in the Borrego Formation because that formation was deposited by perennial lakes fed by the Colorado River, and it has persistent open water conditions (Dibblee, 1954; 1984; Dorsey, 2002; Dorsey et al., 2007; Dorsey et al., 2011). Perhaps the Borrego Formation is not present at Durmid Hill and the Brawley Formation was deposited directly over sediments of the Colorado River delta (Arroyo Diablo Formation).

Evidence for active high heat flow and geothermal fluids is absent in the Durmid Hill study site but it may have been more active in the past. About 20 km south of Durmid Hill these processes are active today. Low-grade metamorphic rocks have been discovered from scientific boreholes drilled to assess the geothermal potential of the area (Herzig and Elders 1988; Elders and Sass., 1988). Other signs of activity are mud pots and very young volcanic rocks in the region.

Gryphons may enable upward moving geothermal fluids debouching it at the surface. A mud volcano (gryphon) is a surface expression of mud that originated at depth (Kopf, 2002). Perhaps the discovery of an extinct mud volcano may explain some of the authogenic gypsum in fault zones (especially in the San Andreas fault zone). Currently, at Durmid Hill there is no evidence of active gryphons there but it is possible they were active in the past. Furthermore, mud volcanoes or gryphons have showed to increase in activity immediately following large earthquakes (Rudolph and Manga, 2010). On the contrary, most of the gypsum observed at Durmid Hill is bedded gypsum and appears very laterally continuous. This would then rule out the possibility of authogenic gypsum being the sole case for an abundance of gypsum at Durmid Hill.

Comparison of Durmid Hill and the Ocotillo Badlands Step-over

Mapping of folds at Durmid Hill shows a comparable relationship to that of the Ocotillo Badlands (Sharp and Clark, 1972)(Fig. 2). The fold axes at Durmid Hill have a sigmoidal map pattern and strike and dips are variable in both orientation and magnitude (Fig. 9). The folds at Durmid Hill are similar to those at the Ocotillo Badlands. There is a domain near the main fault strand of the Coyote Creek fault where folds trend northwest and a central domain where folds trend east-west (Fig. 12) A third domain near the left-stepping fault is faint but the domain appears to be mostly covered by Quaternary alluvium (Fig. 12).

Rocks in the core of the Ocotillo Badlands step-over are uplifted and older than the surrounding rocks. Borrego Formation and Ocotillo Formation are exposed here (Fig. 12). A similar relationship is observed at Durmid Hill, where complex folding and faulting expose older rocks of the Pliocene (?) Arroyo Diablo Formation and younger rocks of the Pleistocene Brawley Formation at the perimeter. Even older rocks the Miocene-Pliocene (?) Shavers Well Formation are uplifted in a narrow fault block on the northeast side of the main strand of the San Andreas fault for ~10-15 km (Dibblee and Minch, 2008a, b and c) but their uplift is not related to the ladder-like zone between the East Shoreline strand of the San Andreas fault and main strand of the San Andreas fault.

The nature of the main fault strands for both the Ocotillo Badlands and Durmid Hill examples differ greatly. The Ocotillo Badlands reflects the typical geometry of a

strike-slip left step-over where uplift and deformation is constrained to the core of the step-over (Fig.11 C). The secondary fault does not connect up with the main strand and continues to the northwest without the continuation of the other fault (Fig. 12).

At Durmid Hill, the geometry is more complicated. Faults of the East Shoreline strand of the San Andreas fault appear to connect to previously mapped traces of what were thought to be the San Andreas fault near Bombay Beach. In the Durmid Hill ladder-like geometry, many structures within the transfer zone are observed including connecting faults, antithetic faults, and rotating blocks (Fig. 13 and 11 C,D, and E). The development of Durmid Hill represents a more complicated fault system and history of the San Andreas fault rather than a simple left-step in a dextral strike-slip fault like the Coyote Creek fault at the Ocotillo Badlands. Nonetheless, the implications of Durmid Hill to the simple contractional step-over model of the Octotillo Badlands provide more evidence that it can be a transitory feature where slip along the San Andreas fault is being transferred across this contractional strain.

FUTURE WORK

East Shoreline strand of the San Andreas Fault

A detailed analysis of the stratigraphy at Durmid Hill may help in determining amount of displacement of the East Shoreline strand of the San Andreas fault. An important observation in the stratigraphy is that the bishop tuff seems to be absent after it crosses highway 111. It could be displaced further north or it is also possible that the ash deposit pinches out. Looking at adjacent stratigraphy and determining if they are also displaced or continuous is key in answering this question.

The installation of creep meters along the East Shoreline fault would be a great dataset to provide more evidence for its existence and to also provide an estimate of how active it is deforming today. In specific, a good place to install a creep meter would be in the area of discovered fractures along the Shoreline of the Salton Sea.

The Southern San Andreas fault

Future research should address if the overlapping upper Brawley Formation was deposited in an angular unconformity across an inactive older trace of the San Andreas fault or if it was faulted into place. Future work should also map the new traces of the San Andreas fault at a smaller scale to assess more detail.

Some important questions arise with the discovery of an overlapped buried strand of the San Andreas fault. The first question is what is the timing of reorganization? Does it correlate with the structural reorganization of the San Jacinto fault zone around 1.0 Ma? This makes it important to get a date of the oldest rock that overlaps the San Andreas fault. Another question is where is the unconformity between the fault and overlapped section? Is it a progressive unconformity? More field investigation is needed to answer these questions. If the unconformity is progressive, it may be difficult to identify in the field due to a lack of drainages that cut it.

If the San Andreas fault does not cut this part of the Brawley Formation in the overlapping location, where is it and where does it end (Fig. 17)? More detailed analysis and mapping using satellite imagery, Landsat, and LIDAR is needed to assess the potential locations of the current San Andrea fault and its terminus. Babcock's (1969) dissertation map agrees with our prediction of where the active trace of the southern San Andreas fault is based on satellite imagery interpretation. Future field investigation should start there and build from the overlapped location.

More work is needed on the northeast side of the San Andreas fault in order to get a better comparison of the difference in shortening between Durmid Hill and northeast of the San Andreas fault. High quality strike and dip data will be important there to quantify the data and compare it to my data. The stratigraphy will be another important aspect of this study and confirmation if upper Brawley Formation is exposed on the Northeast side of the San Andreas fault is significant. If upper Brawley is exposed there, where is the contact with the lower Brawley Formation? Near Salt Creek northeast of the San Andreas

fault, there appears to be a band of white sediment within the stratigraphy there. Could this possibly be Bishop Ash from the lower Brawley Formation? Do the Mecca and Shavers Well formations correlate with one another and contain marine trace fossils? Dating the age of the Shavers Well Formation is a critical aspect to answering this question. A coarse look at these areas helped set the stage for a new graduate student to look at these aspects in more detail.

CONCLUSIONS

The region that encompasses the geology of Durmid Hill, southern California reveals structural and stratigraphic relationships related to active deformation due to the southern San Andreas fault. We show that the major structures in the field area are the San Andreas fault, the East Shoreline fault, East-West Left-Lateral faults, and numerous folds within the Tertiary- Quaternary section. Calculations from GPS, InSAR, and measurements of slip deficit from the calculated recurrence interval suggest the San Andreas fault is due for a large earthquake on its southern-most strand the Coachella segment but results of this study suggest that there is no active trigger mechanism for the main strand of the San Andreas fault at Durmid Hill. The ladder-like geometry of the San Andreas fault, East Shoreline fault, and East-West left-lateral faults in between appear to inhibit triggered-slip from the Extra fault zone.

The main San Andreas fault zone has a fairly simple singular trace through much of the field area, with some local complexity. It strikes 130°/ N50°W throughout the field area, except in its southern ~3 km, where its damage zone and an old, partly buried trace bends clockwise and strike 144°/ N36°W instead. The main strand of the San Andreas fault zone has an extremely well developed damage zone that is up to 0.5 km wide and deforms mudstone, sandstone, and gypsum-rich sedimentary rocks. The most intense damage and stratal disruption is localized on the southwest side of the main strand of the San Andreas fault zone in a map scale block-in-matrix damage zone.

Intense shearing, subsidiary faulting, brecciation, and folding in the damage zone persists for about 13 kilometers along the San Andreas fault from north of Salt Creek to ~3 km northwest of Bombay Beach. There, Pleistocene sediment cover the San Andreas fault zone, its entire damage zone, and both sides of the San Andreas fault zone. The ~0.78 Ma Bishop Tuff is near the base of the folded stratigraphic section that overlies a well exposed damage zone of the San Andreas fault zone. Replacement of this piece of the San Andreas fault probably occurred ~1 Ma due to the early Pleistocene reorganization described in Janecke et al (2010) along the San Jacinto fault zone and by Janecke and DeMets (2010) along the entire Salton-Gulf of California plate boundary. The *replacement piece* of the main San Andreas fault is located a few kilometers farther to the east, strikes about northwest, like the rest of the main strand of the San Andreas fault near Durmid Hill, and is incompletely mapped. It is so young, partly covered, and multi-stranded, that it has been difficult to map all of its numerous small-displacement strands.

Field investigations and remote sensing work provide strong evidence for an important secondary strand of the San Andreas fault at Durmid Hill called the East Shoreline fault. The dominant structural style of the East Shoreline fault zone, with its numerous dextral faults that parallel steeply dipping beds and tight folds, is consistently transpressional. It is also somewhat unusual for a strand of the San Andreas fault. Nevertheless, there is compelling evidence for the existence and fairly large strains along the East Shoreline strand of the San Andreas fault in the form of: 1) mapped northwest-striking dextral faults with en echelon geometries in map view, 2) the parallelism of

faults, folds and strikes of beds with the fault zone, 3) the truncated and omission of map units across dextral faults, 4) the reorientation of left–lateral strike slip faults and associated hinge-zones of folds in the vicinity of the East Shoreline fault zone from dominantly east-southeast-striking to southeast-striking, 5) the nearly identical reorientation of left–lateral strike slip faults and associated hinge-zones of folds in the vicinity of the main strand of the San Andreas fault zone from dominantly east-southeast-striking to southeast-striking, 6) the strong deformation within the fault zone, 7) displaced and folded Holocene sediment, and 8) the parallelism of the fault zone with the edge of the Salton Sea, topographic and bathymetric contours. The lack of a single fairly continuous fault core along the East Shoreline strand is probably due many decollements in the mud-rich sediment within it trace, but may also reflect to its young age. Published geophysical data further illuminates the fault zone and show that the East Shoreline fault zone coincides with a magnetic anomaly near Salt Creek, and bounds the southwest edge of an about 5 km long horst block in the southeast part of Durmid Hill. The presence of ~150 m long open cracks in modern beach sands along many dextral faults probably reflect shallow creep and/or triggered slip between 2010 and 2015 within the East Shoreline fault zone.

The multiple surface traces of northwest-striking dextral-oblique-slip faults within this zone range in length, commonly parallel northwest-trending folds, and produces steeply dipping Pleistocene beds on both the northeast and southwest side. Some of the dextral faults produced growth synclines and anticlines that formed angular unconformities between beds of the mud-rich upper member of the Brawley Formation.

Faults in the East Shoreline fault zone have en echelon tendencies, are often centimeters to tens of meters wide, have sheared and faulted damage zones, and contain some block-in-matrix deformational elements. The southwest edge of the fault zone is probably located at the marked break in slope about 5 m below the reference elevation of the Salton Sea a few hundred meters offshore. If so, only a small fraction of the fault zone is beneath the Sea. Shallow seismic data in the Salton Sea of other workers reveal consistent north-northeast fanning dips toward the East Shoreline fault zone beneath the northern 2/3 of the Salton Sea.

The East Shoreline fault zone is different in character to that of the San Andreas fault in that the East Shoreline fault zone is much wider ~1 km and is multistranded. Even though it is not a single coherent fault strand on the surface, it is more likely to be a pitchfork or flower structure. A through going single structure in the sub-surface that pitchforks out into many faults and folds near the surface. The damage zones of individual strands of the East Shoreline fault range from meters to tens of meters while the San Andreas fault has merely one large damage zone about 0.5 kilometers wide. Holocene sediment that is cut, a large one meter escarpment, shoreline cracks, and growth folding all provide evidence that it is still active today. As the East Shoreline fault is still active, it is possible that this strand of the San Andreas fault (East Shoreline fault) could be a nucleation point for a northwest propagating rupture induced by the Extra fault array.

There are many small to medium-displacement left-lateral to oblique slip faults zones between the main and Shoreline strands of the San Andreas fault that connect the

two *side rails*−the dextral faults−together to form a *sheared ladder-like fault zone* in map view. The east-west striking group of left-lateral faults is complex, cuts through genetically related east-trending folds, and consists of approximately five wide fault zones and brittle shear zones. The left-lateral faults are concentrated in the southern part of the field area. Their damage zones vary from about 120 m to 250m wide and are roughly 3 km long. They are much shorter in length than the faults of the Extra fault array and not directly connected to the San Andreas fault. More research is needed in order to determine how these faults formed and if they evolved over time. Some evidence points to these faults being rotated into their current orientation but this requires a complex and unclear history of events to have had occurred over time.

In the north, cross faults strike northwest between the two strands of the San Andreas fault zone and they are dextral faults. All connectors (or cross faults) have damage zones of their own. The Brawley seismic zone, directly south of Durmid Hill, also has this distinctive ladder-like fault geometry but differs in having a north-northwest strike and transtensional kinematic pattern.

The stratigraphy at Durmid Hill include the Brawley Formation, Ocotillo Formation, Arroyo Diablo Sandstone, Olla Formation, and Canebrake Conglomerate. Rocks that match Borrego Formation were discovered and identified at Salt Creek. The Shavers Well Formation may correlate to the Mecca Formation as a finer lateral equivalent. The stratigraphy shows that very young rocks from Pleistocene to Holocene in age have been deformed relatively quickly. It also alludes to the initiation of the East

Shoreline fault via cross-cutting relationships that may reflect large scale changes seen elsewhere in the Salton Trough.

At San Gorgonio pass there may be another branch-point fault that bypasses the main strand of the San Andreas fault along the “little bend” on the “big bend” (Fig. 1). This branch fault called the East Shoreline strand of the San Andreas fault has a possible regional continuation northwest of the Durmid Hill area near Palm Springs that was interpreted from various geophysical datasets such as InSAR, gravity, and magnetic maps. The most likely time of initiation for the East Shoreline fault is about ~1 Ma years ago synchronous to the age of the San Andreas fault overlap and it is also when the San Jacinto fault zone is thought to have initiated.

Several bends in the southern San Andreas fault exist and do not correlate very well with uplifts and depressions in the Salton Trough. Results do not support the saw-tooth model as the key mechanism for uplifts along the southern San Andreas fault at the Indio, Mecca, and Durmid Hills. It is possible that the origin of the uplifts is better explained by the Eastern California shear zone for the Indio and Mecca Hills and an evolved complex ladder-like geometry at Durmid Hill.

REFERENCES

Atwater, T., 1970, Implications of plate tectonics for the Cenozoic evolution of western North America, Geological Society of America, 81, p. 3513-3536.

Axen, G.J., and Fletcher, J.M., 1998, Late Miocene-Pleistocene extensional faulting, northern Gulf of California, Mexico and Salton Trough, California. International Geology Review, 40(3), p. 217-244.

Babcock, E.A., 1969, Structural Geology and Geophysics of the Durmid Area, Imperial Valley California [Ph.D. thesis]: University of California, Riverside.

Babcock, E.A., 1974, Geology of the northeast margin of the Salton Trough, Salton Sea, California, Geol. Soc. Am. Bull., p. 85, 321-332.

Belgarde, B.E., 2007, Structural Characterization of the Three Southeast Segments of the Clark Fault, Salton Trough, California [M.S thesis]: Logan, Utah, Utah State University, 4 plates, map scale 1:24,000, 216 p.

Bennett, R. A., Rodi, W., Reilinger, R. E., 1996, Global Positioning System constraints on fault slip rates in Southern California and northern Baja, Mexico. Journal of Geophysical Research, v. 101, p. 21,943-21,960.

Biehler, S., Kovach, R.L., and Allen, C.R., 1964, Geophysical frame work of the northern end of the Gulf of California structural province, in van Andel, Tj. H., and Shor, G. G., Jr., eds., Marine geology of the Gulf of California — A symposium: American Association of Petroleum Geologists Memoir. 3, p. 126-143.

Biehler, S., 1971, Gravity studies in the Imperial Valley. In: Cooperative Geological Geophysical Investigations of Geothermal Resources in the Imperial Valley Area of California. University of California, Riverside, California., p. 29-41.

Bilham, R. and King, G., 1989, The morphology of strike-slip faults: Examples from the San Andreas fault, California: Journal of Geophysical Research, v. 94, p. 10,204-10,214.

Bilham, R., and Williams, P., 1985, Sawtooth segmentation and deformation processes on the southern San Andreas fault, California, Geophysical Research Letter, 12(9), p. 557-560.

Brantut, N., Schubnel, A., and Guéguen, Y., 2011. Damage and rupture dynamics at the brittle-ductile transition: the case of gypsum, Journal of Geophysical Research, 116, B01404, doi:10.1029/2010JB007675.

Brothers, D.S., Driscoll, N.W., Kent, G.M., Harding, A.J., Babcock J.M., and Baskin, R.L., 2009, Tectonic evolution of the Salton Sea inferred from seimic reflection data. Nature Geoscience, 2, p. 581-584.

Brothers, D., Kilb, D., Luttrell, K., Driscoll, N., and Kent, G., 2011, Loading of the San Andreas fault by flood induced ruptures beneath the Salton Sea, Nature Geosciences, p. 1-7, NGEO1184, DOI: 10.1038.

Bryant, W.A., Lundberg, M., Cluett, S.E., Hart, E.W., and Treiman, J.A., 2002, Fault number 1j, San Andreas fault zone, Coachella section, in Quaternary fault and fold database of the United States: U.S. Geological Survey website, http://earthquakes.usgs.gov/hazards/qfaults, accessed 10/17/2013 11:12 AM.

Bürgmann, R., 1991, Transpression along the Southern San Andreas fault, Durmid Hill, California. Tectonics, 10, p. 1152–1163.

Bürgmann, R., and Pollard, D.D., 1994, Strain accommodation about strike-slip fault disconuities in granitic rock under brittle-to-ductile conditions. Journal of Structural Geology, v.16, p. 1655- 1674.

Campbell, J.D., 1958, En echelon folding: Economic Geology, v. 53, p. 448-472.

Chester, F.M., Evans, J.P., and Biegel, R.L., 1993, Internal structure and weakening mechanisms of the San Andreas fault: Journal of Geophysical Research, v. 98, p. 771–786.

Christie-Blick, N., and Biddle, K.T., 1985, Deformation and basin formation along strike-slip faults, *in* Biddle, K. T,, and Christie-Blick, N., eds., Strike-slip deformation, basin formation, and sedimentation: Society of Economic Paleontologists and Mineralogists Special Publication 37, p. 1-34

Crowell, B.W., Bock, Y., Sandwell, D.T., and Fialko, Y., 2010, Accelerated loading of the southern San Andreas fault due to transient deformation in the Salton Trough: 2010 SCEC Annual Meeting poster 1-145.

Crowley, J.L., Schoene, B., and Bowring, S.A., 2007, U–Pb dating of zircon in the Bishop Tuff at the millennial scale. Geology 35 (12), p. 1123–1126.

DeMets, C., Gordon, R.G., Argus, D.F., and Stein, S., 1994, Effects of recent revisions to the geomagnetic reversal time scale on estimates of current plate motions, Geophysical Research Letter, p. 2191-2194.

DeMets, C., 1995, Reappraisal of seafloor spreading lineations in the Gulf of California: Implications for the transfer of Baja California to the Pacific plate and estimates of Pacific-North Americ motion. Geophysical Research Letter, v. 22, p. 3545-3548.

Dibblee, T.W., Jr, 1954, Generalized Geologic Map of Imperial Valley Region California: Geology of southern California: California Division of Mines Bulletin 170, scale 1:382,550.

Dibblee, T.W., Jr., 1954, Geology of the Imperial Valley region, California, in Jahns, R. H., ed., Geology of southern California: California Division of Mines Bulletin 170, p. 21-28.

Dibblee, T.W. Jr., 1984, Stratigraphy and tectonics of the San Felipe Hills, Borrego Badlands, Superstition Hills, and vicinity. In: Rigsby, C.A., (ed.), 1984, The Imperial Basin-tectonics, sedimentation, and thermal aspects. Pacific Section S.E.P.M., p. 31-44.

Dibblee, T.W. Jr., 1986, Geology of the San Andreas fault zone near Salton Sea, War Department, U.S. Army Corps of Engineers, scale 1:62,500.

Dibblee, T.W. Jr., 1986, Geologic maps of San Andreas fault in Coachella Valley; in Geology of the Imperial Valley, California: South Coast Geological Society Annual Field Trip Guidebook no. 14, p. 10-14.

Dibblee, T. W. Jr., 1996, Stratigraphy and tectonics of the San Felipe Hills, Borrego Badlands, Superstition Hills and vicinity. Sturzstroms and Detachment Faults,

Anza-Borrego Desert State Park California. South Coast Geological Society Annual Field Trip Guide Book, (24), 45-58.

Dibblee, T.W. Jr., 1996, Stratigraphy and tectonics of the Vallecito-Fish Creek Mountains, Vallecito Badlands, Coyote Mountain, and Yuha Desert, southwestern Imperial basin, in Abbott, P.L. and Seymour, D.C., eds., 1996, Sturtzstroms and detachment faults, Anza-Borrego desert State Park, California. South Coast Geological Society Annual Field Trip Guide Book, no. 24, p. 59-79.

Dibblee, T. W. Jr., 1997, Geology of the southeastern San Andreas fault zone in the Coachella Valley. Southern San Andreas Fault Whitewater to Bombay Beach, Salton Trough, California: Annual Field Trip Guidebook, 25, 35-56.

Dibblee, T.W. Jr., and Minch, J.A., 2008a, Geologic map of the Durmid 15 minute quadrangle, Riverside and Imperial Counties, California: Dibblee Foundation Map DF-376, scale 1:62 500.

Dibblee, T.W., and Minch, J.A., 2008b, Geologic map of the Palm Desert and Coachella 15 minute quadrangles, Riverside County, California: Dibblee Foundation Map DF-373, scale 1:62,500

Dibblee, T.W. and Minch, J.A., 2008c, Geologic map of the Cottonwood Spring and Canyon Spring 15 minute quadrangles, Riverside County, California: Dibblee Geological Foundation, Dibblee Foundation Map DF-375, scale 1:62,500.

Dickinson, W.R., 1996, Kinematics of Transrotational Tectonism in the California Transverse Ranges and Its Contribution to Cumulative Slip Along the San 150

Andreas Transform Fault System: Geological Society of America Special Paper, 305, p. 1-46.

Dorsey, R. J., 2002, Stratigraphic record of Pleistocene initiation and slip on the Coyote Creek fault, lower Coyote Creek, southern California, in Contributions to Crustal Evolution of the Southwestern United States, Special Paper Geological Society of America, 365, p. 251–269.

Dorsey, R.J., and Roering, J.J., 2006, Quaternary landscape evolution in the San Jacinto fault zone, Peninsular Ranges of Southern California: transient response to strike-slip fault initiation. Geomorphology 73, p. 16–32.

Dorsey, R.J., Fluette, A., McDougall, K., Housen, B.A., Janecke, S.U., Axen, G.J., and Shirvell, C.R., 2007, Chronology of Miocene–Pliocene deposits at Split Mountain Gorge, Southern California: A record of regional tectonics and Colorado River evolution: Geology, v. 35, p. 57–60, doi: 10.1130/G23139A.1.

Dorsey, R.J., and Axen, G.J., 2009, End of detachment faulting and initiation of strike-slip faults at 1.0 Ma, western Fish Creek–Vallecito basin, southern California: Geological Society of America Abstracts with Programs, v. 41, no. 7, p. 138.

Dorsey, R.J., Housen, B.A., Janecke, S.U., Fanning, C.M., and Spears, A.L., 2011, Stratigraphic record of basin development within the San Andreas fault system: Late Cenozoic Fish Creek–Vallecito basin, southern California.Geological Society of America Bulletin, 123(5-6), p. 771-793.

Dorsey, R.J., Langenheim, V.E., and McNabb, J.C., 2012, Evidence for Active Northeast Tilting Across the Southern Coachella Valley and Santa Rosa Mountains: 2012 SCEC Annual Meeting.

Elders, W.A., R.W. Rex, T. Meidav, P.T. Robinson, and Biehler, S., 1972, Crustal spreading in southern California, Science, 178, p. 15-24.

Elders, W.A., and Sass, J.H., 1988, The Salton Sea scientific drilling project. Journal of Geophysical Research: Solid Earth (1978–2012), 93(B11), p. 12953-12968.

Fialko Y., 2006, Interseismic strain accumulation and the earthquake potential on the southern San Andreas fault system, Nature, 441, p. 968–971.

Field, E.H., Dawson. T., Felzer. K., Frankel, A., Gupta, V., Jordan, T., Parsons, T., Petersen, M., Stein, R., Weldon II, R., and Wills, C., 2009, Uniform California rupture forecast, version 2 (UCERF 2). Bulletin of the Seismological Society of America 99 (4), p. 2,053–2,107.

Frankel, A., Peterson, M., Mueller, C., Haller, K., Wheeler, R., Leyendecker, E., Wesson, R., Harmsen, S., Cramer, C., Perkins, D., and Rukstales, K., 2002, Documentation for the 2002 update of the National Seismic Hazard maps, U.S. Geol. Surv. Open File Rep. 02-420.

French, M., Wojtal, S.F., and Housen, B., 2006, Transpressional deformation style and AMS fabrics adjacent to the southernmost segment of the San Andreas fault, Durmid Hill, CA [abs.]: AGU Fall Meeting Abstracts, v. 1, p. 1598.

Fuis, G.S., and Kohler, W.M., 1984, Crustal structure and tectonics of the Imperial Valley region, California, in Rigsby, C.A., ed., The Imperial Basin—Tectonics,

sedimentation and thermal aspects: Los Angeles, Pacific Section, Society of Economic Paleontologists and Mineralogist, p. 1-13.

Fuis, G.S., Mooney, W.D., Healey, J.H., McMechan, G.A., and Lutter, W.J., 1982, Crustal structure of the Imperial Valley region. US Geol. Surv. Prof. Pap, 1254, p. 25-49.

Fuis, G.S., Mooney, W.D., Healy, J.H., McMechan, G.A., and Lutter, W.J., 1984, A seismic refraction survey of the Imperial Valley region, California. Journal of Geophysical Research, 89(B2), p. 1165-1189.

Griscom, A., and Muffler, L.J.P., 1971, Aeromagnetic map and interpretation of the Salton Sea geothernal area, California: United States Geological Survey Geophysical Investigations Map GP 754.

Harding, T.P., 1988, Petroleum traps associated with wrench faults: American Association of Petroleum Geologists Bulletin, v. 58, p. 1290-1304.

Harding, T.P., and Tuminas, A.C., 1988, Interpretation of footwall (lowside) fault traps sealed by reverse faults and convergent wrench faults: American Association of Petroleum Geologists Bulletin, v. 72 (6), p. 738-757.

Hauksson, E., 2000, Crustal structure and seismicity distribution adjacent to the Pacific and North America plate boundary in southern California. Journal of Geophysical Research, 105(B6), p. 13875-13.

Hauksson, E. and Yang, W., and Shearer, P.M., 2012, Waveform Relocated Earthquake Catalog for Southern California (1981 to 2011), Bulletin Seismology Society of America, v. 102, No. 5, p. 2239-2244, October 2012, doi: 10.1785/0120120010.

Hays, W. H., 1957, Geology of the central Mecca Hills, Riverside County, California [Ph.D.dissert.]: New Haven, Yale Univ., 324 p.

Herzig, C.T., and Elders, W.A., 1988, Nature and significance of igneous rocks cored in the State 2–14 research borehole: Salton Sea Scientific Drilling Project, California. Journal of Geophysical Research, 93(B11), p. 13069-13.

Herzig, C.T., Mehegan, J.M., and Stelting, C.E., 1988, Lithostratigraphy of the State 2–14 borehole: Salton Sea scientific drilling project. Journal of Geophysical Research, 93(B11), p. 12969-12.

Hildreth, W., 1979, The Bishop Tuff: Evidence for the origin of compositional zonation in silicic magma chambers, Geological Society of America Special Paper, 180, p. 43-75.

Hudnut, K., Seeber, L., Rockwell, T., Goodmacher, J., Klinger, R., Lindvall, S., and McElwain, R., 1989, Surface ruptures on cross-faults in the 24 November 1987 Superstition Hills,California, earthquake sequence: Bulletin of the Seismological Society of America, v. 79, p. 282–296.

Hulen, J.B., Norton, D.L., Moore, J.N., Osborn, W., Van de Putte, T., and Kaspereit, D., 2003, The Role of Sudden Dilational Fracturing in Evolution and Mineralization of the Southwestern Salton Sea Geothermal System, Imperial Valley, California, Stanford Geothermal Workshop.

Jamison, W. R. 1991. Kinematics of compressional fold development in convergent wrench terranes: Tectonophysics 190, p. 209-232.

Janecke, S.U., Dorsey, R.J., Forand, D., Steely, A.N., Kirby, S.M., Lutz, A.T., Housen, B.A., Belgarde, B., Langenheim, V.E., and Rittenour, T.M., 2010, High geologic slip rates since early Pleistocene initiation of the San Jacinto and San Felipe Fault zones in the San Andreas fault system, Southern California, USA, Geological Society of America Special Paper, 475, 1–48, doi:10.1130/2010.2475.

Janecke, S.U., and Thornock, S.J., 2011, Interactions between the Clark strand of the San Jacinto fault zone and the Extra-Elmore fault arrays: 2011 SCEC Annual Meeting poster A-149.

Janecke, S.U., and Markowski, D., 2013, New structures from the southern tip of the San Andreas fault zone near Durmid Hill: 2013 SCEC Annual Meeting poster, p. 199. http://www.scec.org/meetings/2013am/SCEC2013Proceedings.pdf

Jennings, C.W., and Bryant, W.A., 2010, Fault activity map of California: California Geological Survey Geologic Data Map No. 6, map scale 1:750,000 http://www.conservation.ca.gov/cgs/cgs_history/pages/geologicmaps.aspx#2010.

Jones, L. and Benthien, M., 2011, Preparing for the 'Big One': The great Southern Californian shakeout. Earthquake Spectra, 27(2): 575–595. (doi:10.1193/1.3586819).

Kelley, V.C., and J.L. Soske., 1936, Origin of the Salton volcanic domes, Salton Sea, California

Journal of Geology, p. 496–509.

Kell-Hills, A.M., Kent, G., Driscoll, N., Harding, A., and Baskin, R., 2010, Seismic Reflection Study of the Salton Sea. [abs]: 2010 SCEC Annual Meeting poster 2-131.

Kendrick, K., McFadden, L., Morton, D., 1994, Soils and slip rates along the northern San Jacinto Fault. In: McGill, Sally F., Ross, Timothy M. (eds.) Geological investigations of an active margin, Geol. Soc. of Am., Cordilleran Section Annual Meeting Guidebook., v. 27, p. 146-151.

Kim, Y.S, Peacock, D., and Sanderson, D., 2004, Fault damage zones, Journal of Structural Geology. v. 26, p. 502-517.

Kimbrough, D.L., Grove, M., Gehrels, G.E., Dorsey, R.J., Howard, K.A., Lovera, K.A., Aslan, A., House, P.K., Pearthree, P.A., Detrital zircon U-Pb provenance of the Colorado River: A 5 m.y. record of incision into cover strata overlying the Colorado Plateau and adjacent regions, Geosphere, December 2015, v. 11, p. 1719-1748, first published on October 2, 2015, doi:10.1130/GES00982.1

Kirby, S.M. 2005. Quaternary tectonic and structural evolution of the San Felipe Hills, California. MS thesis, Utah State University, Logan, scale, 1 : 48,000.

Kirby, S.M., Janecke, S.U., Dorsey, R.J., Housen, B.A., McDougall, K., Langenheim, V., and Steely, A., 2007, Pleistocene Brawley and Ocotillo formations: evidence for initial strike-slip deformation along the San Felipe and San Jacinto fault zones, California. Journal of Geology 115, p. 43–62.

Kopf, A.J., 2002, Significance of mud volcanism, Reviews of Geophysics, 40(2), 1005, doi:10.1029/2000RG000093.

Krantz, R. W., 1995, The transpressional strain model applied to strike-slip, oblique convergent and oblique-divergent deformation. Journal of Structural Geology, 17, p. 1125-1137.

Langenheim, V.E., Jachens, R.C., Matti, J.C., Hauksson, E. Morton, D.M., and Christensen, Allen, 2005, Geophysical evidence for wedging in the San Gorgonio Pass structural knot, southern San Andreas fault zone, southern California: Geological Society of America Bulletin, v. 117, no. 11, p. 1554–1572.

Langenheim, V.E., Biehler S., McPhee D.K., McCabe C.M., Watt J.T., Anderson M., Chuchel B.A., and Stoffer P., 2007, Preliminary isostatic gravity map of Joshua Tree National Park and vicinity, southern California: U.S. Geological Survey Open-File Report 2007–1218, scale 1:100,000.

Langenheim V.E., and Powell R.E., 2009, Basin geometry and cumulative offsets in the Eastern Transverse Ranges, Southern California: Implications for transrotational deformation along the San Andreas fault system: Geosphere, v. 5, p. 1-22, doi:10.1130/GES00177.1.

Langenheim, V.E., Scheirer, D.S., and Athens, N.D., 2011, Crustal structure of the Salton Trough and southern San Andreas fault from new gravity and magnetic data: 2011 SCEC Annual Meeting.

Langenheim, V.E., Athens, N.D., Scheirer, D.S., and Fuis, G., 2012, Width and dip of the southern San Andreas fault from modeling of magnetic and gravity data: 2012 SCEC Annual Meeting.

Langenheim, V. E., and Christensen, A. H., 2011, Gravity Survey of the Agua Caliente Spring Area in Martin, Martin, P., ed., The source, discharge, and chemical characteristics of water from Agua Caliente Spring, Palm Springs, California: U.S. Geological Survey Scientific Investigations Report 2011-5156, p. 19-26.

Langenheim, V.E., Athens, N.D., Scheirer, D.S., Fuis, G., Rymer, M., and Goldman, M., 2014, Width and dip of the southern San Andreas Fault at Salt Creek from modeling of geophysical data: 2014 Desert Symposium Volume.

Lewis, J.L., Day, S.M., Magistrale, H., Eakins, J., and Vernon, F., 2000, Regional crustal thickness variations of the Peninsular Ranges, southern California. Geology, 28(4), p. 303-306.

Lin, G., Shearer, P.M., and Hauksson, E., 2007, Applying a three-dimensional velocity model, waveform cross correlation, and cluster analysis to locate southern California seismicity from 1981 to 2005, J. Geophys. Res., 112, B12309, doi: 10.1029/2007JB004986.

Lin, G.P., 2013, Three-Dimensional Seismic Velocity Structure and Precise Earthquake Relocations in the Salton Trough, Southern California, Bulletin of the Seismological Society of America, 103(5), p. 2694-2708.

Lindsey, E.O., Fialko, Y., Bock, Y., Sandwell, D.T. & Bilham, R., 2014, Localized and distributed creep along the southern San Andreas Fault, Journal of Geophysical Research: Solid Earth, 119, 7909–7922.

Lohman, R.B., and McGuire, J. J., 2007, Earthquake swarms driven by aseismic creep in the Salton Trough, California, Journal of Geophysical Reasearch, 112, B04405, doi:10.1029/2006JB004596.

Lutz, A.T., 2005, Tectonic Controls on Pleistocene Basin Evolution in the Central San Jacinto Fault Zone, Southern California [M.S. thesis]: Eugene, Oregon, University of Oregon, 136 p.

Lutz, A. T.; Dorsey, R. J.; Housen, B. A., and Janecke, S. U. 2006, Stratigraphic record of Pleistocene faulting and basin evolution in the Borrego Badlands, San Jacinto fault zone, southern California. Geol. Soc. Am. Bull. 118, p. 1377–1397.

Lyons, S., and Sandwell, D., 2003, Fault creep along the southern San Andreas from interferometric synthetic aperture radar, permanent scatterers, and stacking, J. Geophys. Res., 108(B1), doi:10.1029/2002JB001831.

Magistrale, H., 2002, Relative contributions of crustal temperature and composition to controlling the depth of earthquakes in Southern California: Geophysical Research Letters, v. 29, no. 10, p. 1447, doi:10.1029/2001GL014375.

Mazzini, A., Svensen, H., Etiope, G., Onderdonk, N., and Banks, D., 2011, Fluid origin, gas fluxes and plumbing system in the sediment-hosted Salton Sea Geothermal System (California, USA). J. Volcanol. Geotherm. Res. 205 (3–4), p. 67–83.

McKibben, M .A., Williams, E.A., Elders, A.E., and Eldrig, C.S., 1987, Saline brines and metailogenesis in a modem sedimentfilled rift: The Salton Sea Geothermal Svstem. California. U.S.A., Applied Geochemistry, p. 2,563-578.

McNabb, J. C., 2013, Stratigraphic Record of Pliocene-Pleistocene Basin Evolution and Deformation Along the San Andreas Fault, Mecca Hills, California [M.S. thesis]: Eugene, University of Oregon, 70p.

Merriam, R., and Bischoff, J.L., 1975, Bishop Ash: a widespread volcanic ash extended to Southern California: Journal of Sedimentarty Petrology, v. 45, p. 207-211.

Morton, D. M., and Matti, J. C., 1993, Extension and contraction within an evolving divergent strike-slip fault complex; the San Andreas and San Jacinto fault zones at their convergence in Southern California. In: Powell, R. E., Weldon, R. J., and Matti, J. C. (eds), Geol. Soc. Am. Memoir 178, p. 217-230.

Muffler, L.J.P., and White, D.E., 1969, Active metamorphism of upper Cenozoic sediments in the Salton Sea geothermal field and the Salton Trough, southeastern California, Geological Society of America Bulletin, 80, p. 157–182.

Nicholson, C., Seeber, L., Williams, P., and Sykes, L., Seismic evidence for conjugate slip and block rotation within the San Andreas fault system, southern California, Tectonics, V. 5, #4, p. 629-648. 1986.

Olsen, K.B., Day, S.M., Dalguer, L.A., Mayhew, J., Cui, Y., Zhu, J., Cruz-Atienza, V.M., Roten, D., Maechling, P., Jordan, T.H. Okaya, D., and Chourasia, A., 2009, ShakeOut-D: Ground motion estimates using an ensemble of large earthquakes on the southern San Andreas fault with spontaneous rupture propagation, Geophysical Research Letter, 36, L04303, doi:10.1029/2008GL036832

Parsons, T., and McCarthy, J., 1996, Crustal and upper mantle velocity structure of the Salton Trough, southeast California. Tectonics, 15(2), p. 456-471.

Ramsay, J.G., and Huber, M.I., 1983, The techniques of modern structural geology. v. 1, Strain Analysis, Academic Press, London, 307p.

Rivera, T.A., Storey, M., Zeeden, C., Hilgen, F.J., and Kuiper. K., 2011, A refined astronomically calibrated Ar^{40}/Ar^{39} age for Fish Canyon sanidine, Earth and Planet Science Letters, 311(3–4), p. 420–426, doi:10.1016/j.epsl.2011.09.017.

Rockwell, T., Loughman, C., Merifield, P., 1990, Late Quaternary rate of slip along the San Jacinto fault zone near Anza, Southern California. Jour. Geoph. Res. B, v. 95, n. 6, p. 8593-8605.

Roten, D., Olsen, K. B., Day, S., Cui, Y, Fah, D., 2014, Expected seismic shaking in Los Angeles reduced by San Andreas Fault zone plasticity, Geophysical Research Letter, 41, 2769–2777, doi:10.1002/2014GL059411.

Rudolph, M.L., and Manga, M. 2010., Mud volcano response to the 4 April 2010 El Mayor‐Cucapah earthquake. Journal of Geophysical Research: Solid Earth (1978‐2012), 115(B12).

Rymer, M.J. and Lindvall, S.C., 2005, A Broad Holocene-Active San Andreas Fault on Durmid Hill, Southern California-A Zone of Interaction with the Brawley Seismic Zone? [abs.]: AGU Fall Meeting Abstracts, v. 1, p. 1385.

Sarna-Wojcicki, A. M., Pringle, M. S., and Wijbrans, J., 2000, New 40Ar/39Ar age of the Bishop Tuff from multiple sites and sediment rate calibration for the Matuyama-Brunhes boundary, Journal of Geophysical Research, 105, p. 431-443.

Salyards, S.L., Sieh, K.E., and Kirscbvink, L., 1987, Paleomagnetic measurement of dextral warping during the past three large earthquakes at Pallett Creek, southern California, Geological Society of America Abstract Programs, 19(7), 828.

Sanders, C.O., 1989, Fault segmentation and earthquake occurrence in the strike-slip San Jacinto fault zone, California, in Schwartz, D.P., and Sibson, R.H., eds., Proceedings of Conference XLV: A Workshop on Fault Segmentation and Controls of Rupture Initiation and Termination: United States Geological Survey Open-File Report, v. 89-0315, p. 324–349.

Schreurs, G., 1994, Experiments on strike-slip faulting and block rotation: Geology, v. 22, p. 567–570.

Sharp, R.V, 1967, San Jacinto fault zone in the Peninsular Ranges of Southern California. Geological Society of America Bulletin, v. 78, p. 705-729.

Sharp, R.V., and Clark, M.M., 1972, Geologic evidence of previous faulting neat the 1968 rupture of the Coyote Creek fault: U. S. Geological Survey Professional Paper 787, p. 131-140.

Sharp, R.V., 1981, Variable rates of late Quaternary strike slip on the San Jacinto fault zone, Southern California, Journal of Geophysical Research, v. 86, p. 1754-1762.

Sharpe, R ., Cork. G., Kogel, J.E., Trivedi, N.C., Barker , J.M., and Krukowski, S.T., 2006, Gypsum and anhydrite. In Industrial minerals & rocks, Society for Mining, Metallurgy, and Exploration, Inc., Littletown, p. 519–540.

Shaw, J. H., E. Novoa, and C. D. Connors, 2004, Structural controls on growth stratigraphy in contractional fault-related folds, in K. R. McClay, ed., Thrust

tectonics and hydrocarbon systems: American Association of Petroleum Geologists Memoir 82, p. 400–412.

Shearer, P., E. Hauksson, and G. Lin, 2005, Southern California hypocenter relocation with waveform cross-correlation. part 2: Results using source-specific station terms and cluster analysis, Bull. Seismol. Soc. Am., 95, 904 – 915

Sherill, R.E., 1929, Origin of the en echelon faults in north-central Oklahoma: American Association of Petroleum Geologists Bulletin, v. 13, p. 31-37.Salton m and tectonic evolution of the Detachment syst

Shirvell, C.R., 2006, Pliocene exhumation along the West Salton Detachment system and tectonic evolution of the Fish Creek–Vallecito supradetachment basin, Salton Trough, southern California. [M.S. thesis]: Los Angeles, University of California, 133 p.

Schmitt, A.K., and Vazquez, J.A., 2006, Alteration and remelting of nascent oceanic crust during continental rupture: Evidence from zircon geochemistry of rhyolites and xenoliths from the Salton Trough, California: Earth and Plan- etary Science Letters, v. 252, p. 260–274, doi: 10.1016/j.epsl.2006.09.041.

Schmitt, A.K., and Hulen, J.B., 2008, Buried rhyolites within the active, high-temperature Salton Sea geothermal system. Journal of Volcanology and Geothermal Research, 178(4), p. 708-718.

Schmitt, A.K., Martín, A., Stockli, D.F., Farley, K.A., and Lovera, O.M., 2013, (U-Th)/He zircon and archaeological ages for a late prehistoric eruption in the Salton Trough (California, USA). Geology, 41(1), 7-10.

Sneed, M., and Brandt, J. T., Interferometric Synthetic Aperture Radar Data in the Agua Caliente Spring Area. In The Source, Discharge, and Chemical Characteristics of Water from Agua Caliente Spring, Palm Springs, California 2011 p. 43 to 44.

Spotila, J., House, M., Niemi, N., Brady, R., Oskin, M., and Buscher, J., 2007, Patterns of bedrock uplift along the San Andreas fault and implications for mechanisms of transpression. In (Till, A., Roeske, S., Foster, D., and Sample, J., eds.), Uplift and Extension along Continental Strike-slip Faults, Geological Society of America Special Paper, 434, pp. 15–33.

Steely, A.N., 2006, The evolution from Pliocene West Salton detachment faulting to cross-cutting Pleistocene oblique strike-slip faults in the SW Salton Trough, southern California [M.S. thesis]: Logan, Utah State University, 239 p.

Steely A.N., Janecke S.U., Dorsey R.J., and Axen G.J., 2009, Early Pleistocene initiation of the San Felipe fault zone, SW Salton Trough, during reorganization of the San Andreas fault system: Geological Society of America Bulletin, v. 121, p. 663–687, doi: 10.1130/B26239.1.

Sykes, L.R., and Nishenko, S.P., 1984, Probabilities of occurrences of large plate rupturing earthquakes for the San Andreas, San Jacinto, and Imperial faults, California, 1983-2003, Journal of Geophysical Research, 89, p. 5905-5927.

Sylvester, A.G., 1988, Strike-slip faults: Geological Society of America Bulletin, v. 100, p. 1666– 1703.

Thornock, S. J., 2013, Southward Continuation of the San Jacinto Fault Zone Through and Beneath the Extra and Elmore Ranch Left-Lateral Fault Arrays, Southern California [M.S. thesis]: Logan, Utah State University, 226p.

Tong, X., Sandwell, D., and Smith-Konter, B., 2012, High-resolution interseismic velocity data along the San Andreas fault from GPS and InSAR, J. Geophys. Res., 2013.

Woodcock, N.H., and Fischer, M., 1986, Strike-slip duplexes, Journal of Structural Geology, v. 8, p. 725-735.

Weldon, R., Fumal, T., and Biasi, G., 2004, Wrightwood and the earthquake cycle: what a long recurrence record tells us about how faults work, Geological Society of America Today, 14, 4–10.

Weldon, R.J., Fumal, T.E. , Biasi, G., and Scharer., K.M., 2005, Past and future earthquakes on the San Andreas fault, Science 308, 966–967.

Wesnousky, S. G., Prentice, C. S., Sieh, K. E., 1991, An offset Holocene stream channel and the rate of slip along the northern reach of the San Jacinto fault zone, San Bernardino Valley, California. Geological Society of America Bulletin, v. 103, p. 700-709.

Wilcox, R.E., Harding, T.P., Seely, D.R., 1973. Basic wrench tectonics. American Association of Petroleum Geologists Bulletin 57, 74–96.

Winker, C. D., and Kidwell, S.M., 1996, Stratigraphy of a marine rift basin: Neogene of the western Salton Trough, California. In Abbott, P. L., and Cooper, J. D., (eds.),Field conference guidebook and volume for the annual convention, San

Diego, California, May, 1996, Bakersfield, California, Pacific Section, American Association of Petroleum Geologist, p. 295-336.

Winker, C. D., 1987, Neogene stratigraphy of the Fish Creek–Vallecito section, southern California: Implications for early history of the northern Gulf of California and Colorado Delta [Ph.D. dissertation]: Tucson, University of Arizona, 494 p.

Winker, C. D., and Kidwell, S.M., 1986, Paleocurrent evidence for lateral displacement of the Pliocene Colorado River delta by the San Andreas fault system, southeastern California: Geology, v. 14, p. 788–791.

Wisely, B. A., and D. Schmidt (2009), Aquifer system compaction rates estimated for the Coachella Valley, California, using InSAR, groundwater level data, and drillers' logs, Geol. Soc. Amer., Abstracts with Programs, Vol. 41, No. 7, p. 175.'

Wisely, B. A., and D. A. Schmidt (2006), Geodetic constraints on vertical tectonic deformation in the Coachella and San Bernardino Valleys from InSAR and well level data, EOS Trans. AGU, 87 (52), Fall Meet. Suppl., Abstract G23B-1274

Wright, H. M., J. A. Vazquez, D. E. Champion, A. T. Calvert, M. T. Mangan, M. Stelten, K. M. Cooper, C. Herzig, and A. Schriener (2015), Episodic Holocene eruption of the Salton Buttes rhyolites, California, from paleomagnetic, U-Th, and Ar/Ar dating, Geochem. Geophys. Geosyst., 16, 1198–1210, doi:10.1002/2015GC005714.

Younker, L.W., Kasameyer, P.K., and Tewhey, J.D., 1982, Geological, geophysical, and thermal characteristics of the Salton Sea geothermal field, California: Journal of Volcanology and Geothermal Research, v. 12, p. 221-258.

PLATES

Plate 1: Geologic Map and Cross Section of Durmid Hill, southern California area with False Color NAIP Basemap of Geologic Units, Faults, and Marker Units within the Brawley Formation.

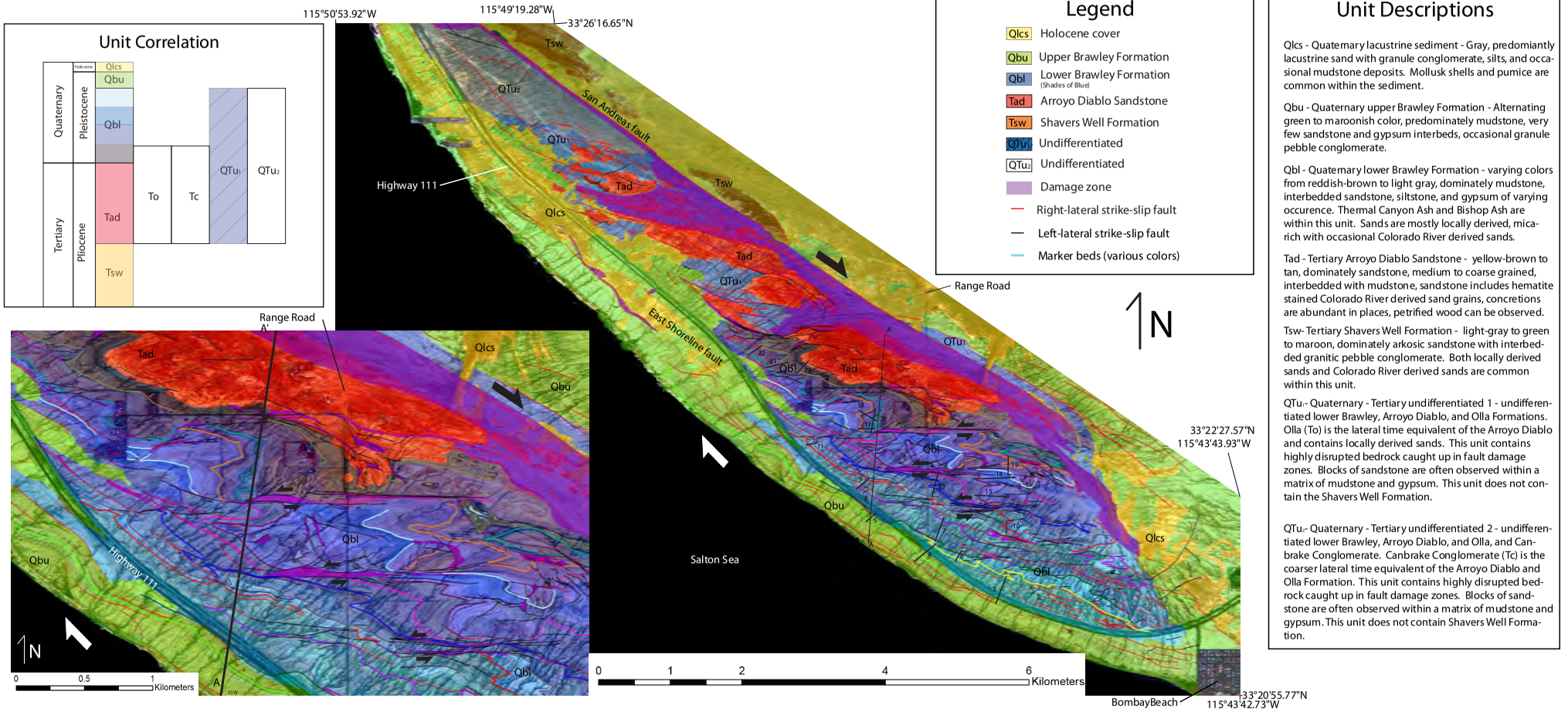

Unit Descriptions

Qlcs - Quaternary lacustrine sediment - Gray, predominantly lacustrine sand with granule conglomerate, silts, and occasional mudstone deposits. Mollusk shells and pumice are common within the sediment.

Qbu - Quaternary upper Brawley Formation - Alternating green to maroonish color, predominately mudstone, very few sandstone and gypsum interbeds, occasional granule pebble conglomerate.

Qbl - Quaternary lower Brawley Formation - varying colors from reddish-brown to light gray, dominately mudstone, interbedded sandstone, siltstone, and gypsum of varying occurence. Thermal Canyon Ash and Bishop Ash are within this unit. Sands are mostly locally derived, mica-rich with occasional Colorado River derived sands.

Tad - Tertiary Arroyo Diablo Sandstone - yellow-brown to tan, dominately sandstone, medium to coarse grained, interbedded with mudstone, sandstone includes hematite stained Colorado River derived sand grains, concretions are abundant in places, petrified wood can be observed.

Tsw- Tertiary Shavers Well Formation - light-gray to green to maroon, dominately arkosic sandstone with interbedded granitic pebble conglomerate. Both locally derived sands and Colorado River derived sands are common within this unit.

QTu_1- Quaternary - Tertiary undifferentiated 1 - undifferentiated lower Brawley, Arroyo Diablo, and Olla Formations. Olla (To) is the lateral time equivalent of the Arroyo Diablo and contains locally derived sands. This unit contains highly disrupted bedrock caught up in fault damage zones. Blocks of sandstone are often observed within a matrix of mudstone and gypsum. This unit does not contain the Shavers Well Formation.

QTu_2- Quaternary - Tertiary undifferentiated 2 - undifferentiated lower Brawley, Arroyo Diablo, and Olla, and Canbrake Conglomerate. Canbrake Conglomerate (Tc) is the coarser lateral time equivalent of the Arroyo Diablo and Olla Formation. This unit contains highly disrupted bedrock caught up in fault damage zones. Blocks of sandstone are often observed within a matrix of mudstone and gypsum. This unit does not contain Shavers Well Formation.

Notes:

1. Map is coauthored with Susanne Janecke.
2. Plate 1 includes all mapped geologic units, faults, marker beds, and cross-section lines. Plate 2 contains all geologic units and fold axial surfaces.
3. The inset map shows the area of more detailed mapping of the geologic features described above.
4. Each individual geologic feature is shown on its own figure in the thesis text.
5. For a map of the faults see Figure 27.
6. For a map of the marker units see Figure 28.
7. For the correlation of the marker units to the stratigrphic column see Figure 21.

Plate 2: Simplified Structural Map of Durmid Hill, southern California with False Color NAIP Basemap of Geologic Units, Strike and Dips, and Fold Axes.

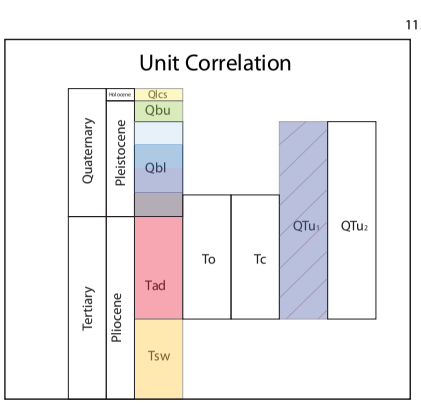

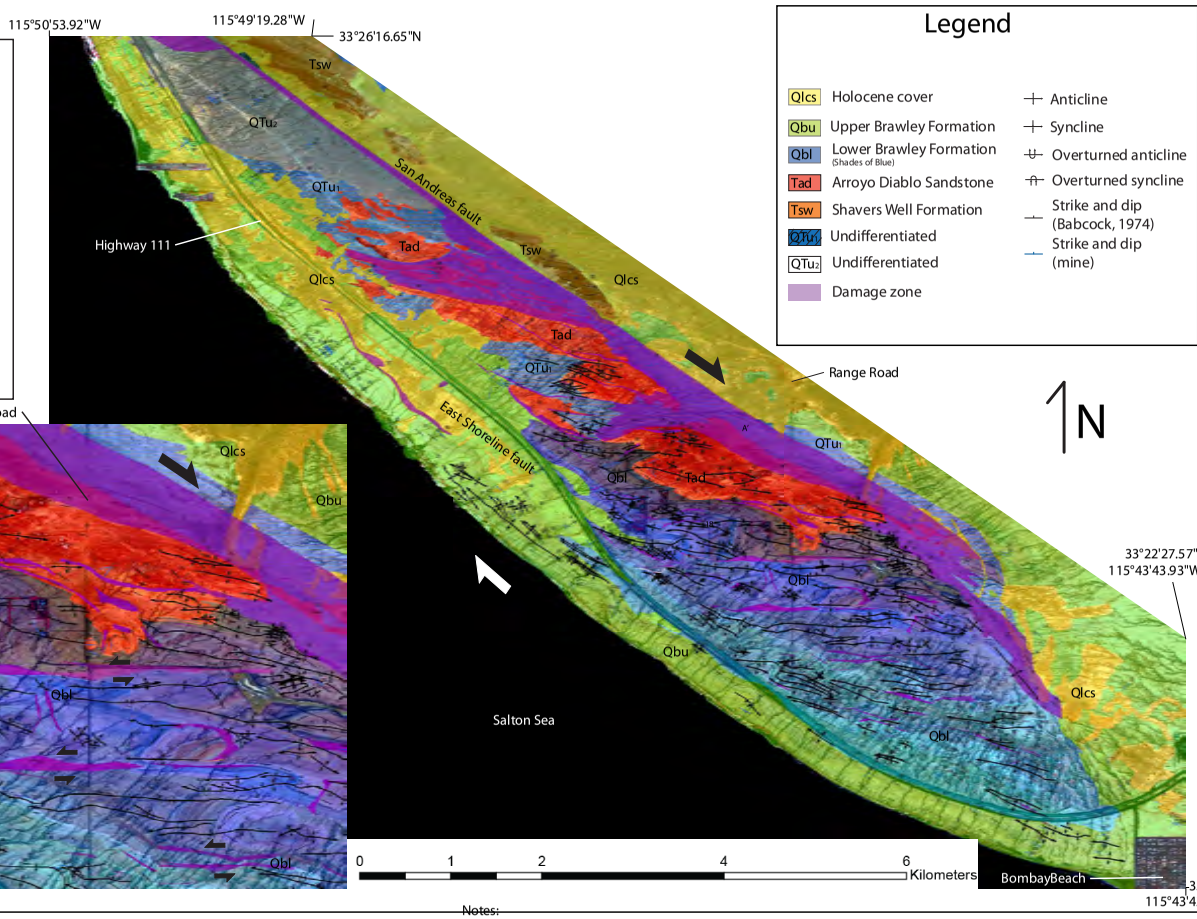

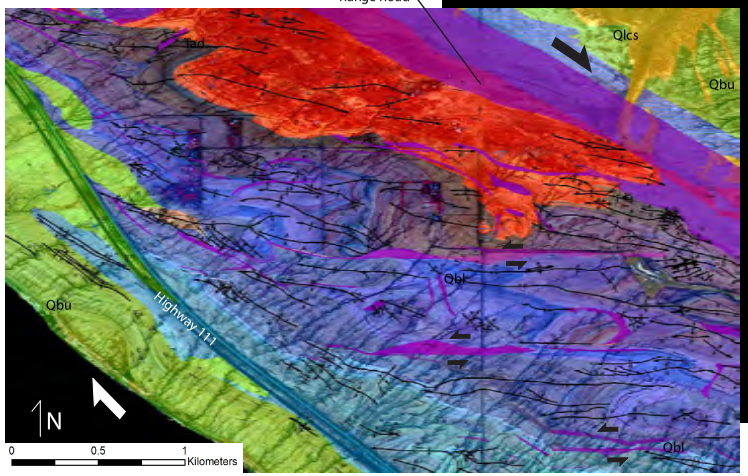

Legend

- Qlcs — Holocene cover
- Qbu — Upper Brawley Formation
- Qbl — Lower Brawley Formation (Shades of Blue)
- Tad — Arroyo Diablo Sandstone
- Tsw — Shavers Well Formation
- QTu1 — Undifferentiated
- QTu2 — Undifferentiated
- Damage zone
- Anticline
- Syncline
- Overturned anticline
- Overturned syncline
- Strike and dip (Babcock, 1974)
- Strike and dip (mine)

Unit Descriptions

Qlcs - Quaternary lacustrine sediment - Gray, predomiantly lacustrine sand with granule conglomerate, silts, and occasional mudstone deposits. Mollusk shells and pumice are common within the sediment.

Qbu - Quaternary upper Brawley Formation - Alternating green to maroonish color, predominately mudstone, very few sandstone and gypsum interbeds, occasional granule pebble conglomerate.

Qbl - Quaternary lower Brawley Formation - varying colors from reddish-brown to light gray, dominately mudstone, interbedded sandstone, siltstone, and gypsum of varying occurence. Thermal Canyon Ash and Bishop Ash are within this unit. Sands are mostly locally derived, mica-rich with occasional Colorado River derived sands.

Tad - Tertiary Arroyo Diablo Sandstone - yellow-brown to tan, dominately sandstone, medium to coarse grained, interbedded with mudstone, sandstone includes hematite stained Colorado River derived sand grains, concretions are abundant in places, petrified wood can be observed.

Tsw- Tertiary Shavers Well Formation - light-gray to green to maroon, dominately arkosic sandstone with interbedded granitic pebble conglomerate. Both locally derived sands and Colorado River derived sands are common within this unit.

QTu- Quaternary - Tertiary undifferentiated 1 - undifferentiated lower Brawley, Arroyo Diablo, and Olla Formations. Olla (To) is the lateral time equivalent of the Arroyo Diablo and contains locally derived sands. This unit contains highly disrupted bedrock caught up in fault damage zones. Blocks of sandstone are often observed within a matrix of mudstone and gypsum. This unit does not contain the Shavers Well Formation.

QTu- Quaternary - Tertiary undifferentiated 2 - undifferentiated lower Brawley, Arroyo Diablo, and Olla, and Canbrake Conglomerate. Canbrake Conglomerate (Tc) is the coarser lateral time equivalent of the Arroyo Diablo and Olla Formation. This unit contains highly disrupted bedrock caught up in fault damage zones. Blocks of sandstone are often observed within a matrix of mudstone and gypsum. This unit does not contain Shavers Well Formation.

Notes:

1. Map is coauthored with Susanne Janecke. 2. Plate 2 includes all mapped geologic units, strike and dips, and fold axial axes. 3. The inset map shows the area of more detailed mapping of the strike and dip and fold axes. 4. Each individual geologic feature is shown on its own figure in the thesis text. 5. For a map of the fold axes and distribution of their interlimb angles see Figure 29. 6. For maps of all mapped faults see Plate 1 and Figure 27. 6. For a map of the marker units see Plate 1 and Figure 28. 7. For the correlation of the marker units to the stratigrphic column see Figure 21. 8. For a map without the false colored NAIP baseimagery see Plate 2b.